SHELL MODEL STATES IN ^{138}La

by

AQUILA ISLAM

A Thesis

Submitted to the School of Graduate Studies

in Partial Fulfilment of the Requirements

for the Degree

Doctor of Philosophy

McMaster University

May 1975

© AQUILA ISLAM 1976

SHELL MODEL STATES IN ^{138}La

DOCTOR OF PHILOSOPHY (1975)
(Physics)

McMASTER UNIVERSITY
Hamilton, Ontario

TITLE: Shell Model States in ^{138}La

AUTHOR: Aquila Islam

SUPERVISOR: Professor R. G. Summers-Gill

NUMBER OF PAGES: xiv, 165

SCOPE AND CONTENTS:

A combination of particle and γ-ray spectroscopy has been utilized to elucidate the nuclear structure of ^{138}La. The single nucleon transfer reactions ^{137}Ba(^{3}He,d)^{138}La, ^{137}Ba(α,t)^{138}La and ^{139}La(d,t)^{138}La have revealed 62 levels in this odd-odd nucleus up to an excitation of 1.8 MeV, the majority of them being reported here for the first time. Parity assignments have been made and spectroscopic strengths obtained for most of these levels.

The decay modes of the levels have been studied using the ^{138}Ba(p,n)^{138}La reaction to populate the excited states. Both singles and γ-γ coincidence experiments were carried out. The life-time of the first excited state, measured by the method of n-γ delayed coincidence, demonstrates the E2 nature of this transition. For the other low-lying levels whose life-times are less than 10 ns, M1 transitions are expected to dominate and this assumption was used to obtain definite spin assignments for all the states below 650 keV.

The complementary information from the proton transfer and neutron pick-up reactions, together with their spin assignments, is used to analyze the wave functions for the twelve lowest levels. These appear to be simple shell model states arising from the coupling of a neutron hole in the $2d_{3/2}$ or $3s_{1/2}$ orbit to the j = 7/2 or 5/2 proton configurations observed at low energy in ^{139}La.

Two groups of negative parity states, predicted by the simple shell model, have also been identified. Unfortunately only tentative spin assignments, based on the 2J+1 rule for spectroscopic strengths have been possible for most of these because the (p,n) reaction does not populate the many high spin states involved.

A lowest seniority shell model calculation, employing the surface delta interaction, was carried out for the low-lying levels. Spectroscopic factors are calculated for both the proton transfer and neutron pick-up reactions. A comparison with the experimental findings shows disappointing agreement.

ACKNOWLEDGMENTS

I could probably increase the bulk of this manuscript substantially by listing the names of all those persons, whose interest, understanding, encouragement and co-operation has contributed towards the evolution of the work reported here. But even the brief acknowledgments are rarely taken seriously and a long one stands no chance of attracting anybody's attention. Hence I shall mention only a few and foremost ones I am really indebted to:

Professor R. G. Summers-Gill for helping me during the long tedious accelerator runs in the numerous experiments described in this thesis, for his valuable guidance in experimental analysis and finally for scrutinizing this script for logical and literary errors.

Dr. J. A.Cameron, for many enlightening discussions and for his easy accessibility both as a committee member and as a teacher.

Dr. W. W. Smeltzer, the other member of my committee, for his extremely co-operative attitude and his interest in the project.

Dr. M. W. Johns, for providing me with the reassurance and a few very valuable dollars in time of crisis.

Dr. J. C. Waddington, for an attentive ear, friendly attitude and many constructive suggestions.

Dr. S. Wender, for his wonders with electronics which helped to shorten my stay at McMaster.

Dr. J. S. Barret, for brightening the dark dungeon of N.R.B. B-117 with his jokes and smiles.

D. T. Kelly, for helping me out whenever 9 or 15 created problems.

P. G. Kerr, for his friendship.

Past and present members of the group:

Malcolm Macphail for guiding me in the experimental ventures during my initial stages of learning all about nuclear physics and odd-odd nuclei.

Terry Taylor, for his expertise in MSMC and T.N.T., his witty sarcasm and his comradeship.

Konrad Aniol, Don Dohan, Sherali Hussein, Dan Nir and Neil Sanderson for their assistance during the experiments.

I would also like to acknowledge the help from the accelerator staff, target technicians, and the counting girls in the process of data acquisition.

I sincerely appreciate the co-operation of Dr. J.B. Ball (O.R.N.L.) who provided the necessary wave functions for the calculation of the spectroscopic factors, from his three year old output.

Very special thanks are due to:

Avelina Bardwell-Wender, for a deft proof-reading of this manuscript.

Jaya Gosh, for a shoulder to cry upon during the most frustrating period of my research.

Maliks and Dosts, for surrounding me with a homey atmosphere 11000 miles away from home.

And my loved ones in Pakistan, who managed to keep my spirits up by a uniform flow of letters through all these four years.

The direct financial support from C.I.D.A., in the form of a Colombo Plan scholarship, and an indirect one from N.R.C. as the research grant to the group is also sincerely acknowledged.

At the very end I would like to thank my artist, Judith Balogh and my typist, Helen Kennelly, for an incredible speed in their respective fields. They instigated me to work harder and faster

To My Parents

TABLE OF CONTENTS

CHAPTER		Page
	INTRODUCTION	1
I	BASIC NUCLEAR THEORY	6
	1.1 Nuclear Models	6
	a Shell Model	7
	b Shell Model Calculations	11
	1.2 Nuclear Reactions	14
	a Stripping and Pick-up Reactions	15
	b Distorted Wave Born Approximation	17
	c Selection Rules and Spectroscopic Factors	19
	1.3 Electromagnetic Transitions	24
	a The Weisskopf Units	26
	b Internal Conversion	28
II	PARTICLE TRANSFER REACTIONS	30
	2.1 Experimental Set-up and Target Preparation	33
	a Target Preparation	34
	b Experimental Set-up	36
	c Determination of Absolute Cross-sections	37
	2.2 Energy Levels of ^{138}La	40
	a The ^{137}Ba(^{3}He,d)^{138}La Reaction	40
	b The ^{137}Ba(α,t)^{138}La Reaction	46
	c The ^{139}La(d,t)^{138}La Reaction	51
	2.3 The ^{138}Ba(^{3}He,d)^{139}La Reaction	55

CHAPTER			Page
	2.4	The Proton Transfer Results for ^{138}La	61
		a The Angular Distributions and Spectroscopic Strengths	64
		b (^{3}He,d) to (α,t) Cross-section Ratios	67
		c The Sum Rules for Proton Transfer	72
	2.5	The Neutron Transfer Results for ^{138}La	75
		a The Angular Distributions and Spectroscopic Strengths	75
		b The Sum Rules for the Neutron Pick-up Reaction	81
III	GAMMA-RAY STUDIES		84
	3.1	The ^{138}Ba(p,nγ)^{138}La Experiment	85
		a Efficiency Calibration of the Detectors	91
		b Gamma-ray Self Absorption in the Target	91
	3.2	Gamma-gamma Coincidence Experiment	97
		a Experimental Set-up	97
		b Analysis of Coincidence Data	102
	3.3	Life-time Measurement of 72 keV Level	104
IV	DISCUSSION AND INTERPRETATION OF THE RESULTS		110
	4.1	The Level Scheme of ^{138}La	111
	4.2	The Low-lying Positive Parity Levels	116
		a Spin Assignments	117
		b γ-Ray Excitation Functions and the Spins	123
		c The 2J+1 Rule and the Wave Functions	126

		Page
4.3	Higher Excited States	131
	a The Negative Parity States	132
	b The Others	137
4.4	The Energy Centroids	138
4.5	Shell Model Calculations	139
SUMMARY AND CONCLUSIONS		148
APPENDIX		153
REFERENCES		160

LIST OF FIGURES

FIGURE		Page
2.1	Deuteron spectra from $^{137}Ba(^{3}He,d)^{138}La$ and $^{138}Ba(^{3}He,d)^{139}La$.	41
2.2	Triton and deuteron spectra for $^{137}Ba(\alpha,t)^{138}La$ and $^{137}Ba(^{3}He,d)^{138}La$.	48
2.3	Triton spectra for $^{138}Ba(\alpha,t)^{139}La$, $^{137}Ba(\alpha,t)^{138}La$ and $^{136}Ba(\alpha,t)^{137}La$.	49
2.4	The $^{139}La(d,t)^{138}La$ and $^{137}Ba(^{3}He,d)^{138}La$ spectra for the region below 650 keV excitation.	52
2.5	The triton spectrum from the $^{139}La(d,t)^{138}La$ reaction.	54
2.6	Deuteron angular distributions in the $^{138}Ba(^{3}He,d)^{139}La$ reaction.	59
2.7	Theoretical and empirical ℓ-shapes for $^{137}Ba(^{3}He,d)^{138}La$.	60
2.8	Differential cross-sections for $^{137}Ba(^{3}He,d)^{138}La$.	65
2.9	The $(^{3}He,d)/(\alpha,t)$ cross-section ratios.	71
2.10	The ℓ_n = 0 and 2 differential cross-sections calculated by DWBA for $^{139}La(d,t)^{138}La$.	76
2.11	Differential cross-sections for $^{139}La(d,t)^{138}La$.	80

FIGURE		Page
3.1	The γ-ray spectrum from the $^{138}Ba(p,n\gamma)^{138}La$ reaction.	88
3.2	Excitation functions of γ-rays observed in $^{138}Ba(p,n\gamma)^{138}La$.	90
3.3	The calculated correction for γ-ray absorption in the ^{138}BaO target.	98
3.4	Block diagram of the electronics for γ-γ coincidences.	100
3.5	The Ge(Li)-Ge(Li) coincidence spectra	103
3.6	Block diagram of the electronics for n-γ delayed coincidences.	106
3.7	The shape spectrum from the plastic scintillator.	107
3.8	The n-γ time spectra	109
4.1	Proposed level scheme for the low-lying states of ^{138}La.	112
4.2	Proposed level scheme for ^{138}La.	113
4.3	A plot *versus* spin of the observed γ-ray intensity ratios.	124
4.4	The 2J+1 rule for the $\ell_p = 2$ spectroscopic strengths.	127
4.5	The 2J+1 rule for the $\ell_n = 0$ and 2 spectroscopic strengths.	128

FIGURE		Page
4.6	The 2J+1 rule for the $\ell_p = 5$ spectroscopic strengths.	133
4.7	The 2J+1 rule for the $\ell_n = 5$ spectroscopic strengths.	135
4.8	SDI shell model calculations for ^{138}La.	147

LIST OF TABLES

TABLE		Page
2.1	Isotopic Composition of the Target Materials	35
2.2	Comparison of Energy Levels Observed in Proton and Neutron Transfer	43-45
2.3	Optical Model Parameters for the $^{137}Ba(^{3}He,d)^{138}La$ Reaction	62
2.4	The ℓ_p Values and Spectroscopic Strengths for $^{138}Ba(^{3}He,d)^{139}La$	63
2.5	The ℓ_p Values and Spectroscopic Strengths for $^{137}Ba(^{3}He,d)^{138}La$	66
2.6	Optical Model Parameters for the $^{137}Ba(\alpha,t)^{138}La$ Reaction	69
2.7	The Sum Rules for Proton Transfer	73
2.8	Optical Model Parameters for $^{139}La(d,t)^{138}La$ Reaction	77
2.9	The ℓ_n Values and Spectroscopic Strengths for $^{139}La(d,t)^{138}La$	79
2.10	The Sum Rules for Neutron Transfer	82
3.1	γ-ray Energies, Intensities from $^{138}Ba(p,n\gamma)^{138}La$ and their Placement	92-95
3.2	Summary of Coincidence Data	105

TABLE		Page
4.1	The Wave Functions of the Low-Lying Group	130
4.2	A Comparison of Energy Centroids in ^{138}La and its Odd-A Neighbours	140
4.3	Calculated Spectroscopic strengths.	144
A-1	Differential Cross-sections for $^{137}Ba(^{3}He,d)^{138}La$	153
A-2	Observed Cross-sections at 45° for the Reaction $^{137}Ba(\alpha,t)^{138}La$ at 27 MeV	158
A-3	Observed Cross-sections for the $^{139}La(d,t)^{138}La$ Reaction at 16 MeV	159

INTRODUCTION

It is rather hard to decide which of the two is more complex - the atomic nucleus or human nature. More than half a century has gone by since the first definition of the nuclear force was given, and the exact nature of this force still evades complete elucidation. It is simple enough to say that any nucleus is composed of a number of neutrons and protons but the dynamical analysis of this many-body system is a formidable task. In spite of the modern advances in computational facilities, theorists are forced to find a way of reducing the many body problem to an effective two body interaction, and to hypothesize some sort of model for realistic calculations. Experimentalists are forever trying to find some detail of the nuclear structure which can be correlated to a certain nuclear model. Most of the simple models have been relatively successful in explaining the gross structure of the nucleus, though almost always the mathematical formulation is guided by the empirical findings. The shell model has enjoyed a prestigious position amongst these models mainly because it does explain the magic numbers and the ground state spins of the even-even and odd-even nuclei.

Nuclei in the vicinity of the magic numbers hold a strong attraction for the believers in the shell model because the concept of an inert core is more plausible in such cases and these nuclei can be described in a relatively simple and smaller configuration space. Odd-odd nuclei are more challenging to the experimentalists. The level density in the low-lying region is much higher for these nuclei than for the even-even or even-odd spherical nuclei and their study requires more sophisticated experimental techniques. Also these nuclei form an attractive system for studying the proton-neutronresidual interaction and hence for determining the extent to which the nuclear force is isospin independent. One hopes to find some clues by studying the nuclear structure of suitable nuclei and interpreting the experimental data to find a relevant expression for the nuclear force.

Interest in the study of odd-odd nuclei has developed considerably in the recent years with the advent of suitable particle accelerators, great technological advances in the data acquisition systems and improved computational facilities for analysis. In the light rare earth region, nuclei around N=82 have been popular with the experimentalists, 82 being a magic number. As 50 is also a magic number the nucleus $^{132}_{50}Sn_{82}$ can be treated as an inert core for the nuclei having a few more protons and neutrons. This has prompted many researchers to investigate N=83 nuclei with Z ranging from 53 to 61, i.e. ^{136}I, ^{138}Cs, ^{140}La, ^{142}Pr and ^{144}Pm. The long list of references

includes Agarwal *et al.* 1964, Aniol 1973, Burde *et al.* 1965, Carlson *et al.* 1972, Geiger *et al.* 1961, Hussein 1973, Jurney *et al.* 1970, Kern *et al.* 1967, Lucas *et al.* 1973, Macphail 1973 and Monnad *et al.* 1972. These nuclei have been assumed to be spherical and exhibit a structure which can be understood in terms of the shell model.

The N=81 nuclei should be equally interesting. So far ^{140}Pr, having 59 protons and 81 neutrons, is the only nucleus of this class for which extensive information has become available recently, (Fulmer *et al.* 1962, Krehbial *et al.* 1964, Helton *et al.* 1973, Guile *et al.* 1973 and Hussein *et al.* 1974). Some work has also been reported on ^{132}Sb (Horsch 1970), ^{144}Eu and ^{142}Pm (Funke *et al.* 1973). The nucleus ^{138}La, with 57 protons is another interesting member of this group, next down in line from ^{140}Pr. It is not unreasonable to expect that these nuclei should have some common features. Very little information was available about ^{138}La when the present work was begun. The spin of the ground state had been measured to be 5 by Sogo *et al.* (1955). The systematics of the neighbouring nuclei (e.g. ^{137}Ba and ^{139}La) suggest a positive parity for this state. This assignment is confirmed by DuBard *et al.* 1971 from their ^{138}La(d,p)^{139}La experiment. The proton group to the $7/2^+$ ground state of ^{139}La shows a pure ℓ=2 angular distribution. This contradicts the negative parity assignment by Ellis *et al.* (1970) and Lederer *et al.* (1968) which was based on the third forbidden β-decay to the 2^+ states of ^{138}Ce and ^{138}Ba. Helton *et al.* (1973) and Lasijo

et al. (1972) have reported neutron pick up reactions $^{139}La(d,t)$ and $^{139}La(p,d)^{138}La$. The pure $\ell=2$ angular distribution for both the tritons and deuterons upholds the even parity assignment for the ground state. Helton *et al.* investigated only the low-lying group of levels while Lasijo *et al.* studied levels up to an excitation of 1.54 MeV.

The shell model systematics of the neighbouring nuclei suggests that the low-lying levels of both ^{140}Pr and ^{138}La should arise from the coupling of a neutron hole in $2d_{3/2}$ or $3s_{1/2}$ to a $1g_{7/2}$ or $2d_{5/2}$ proton. In ^{140}Pr all the 12 states which could arise from such couplings have been identified. For ^{138}La only 9 levels have been reported, but the experiments of Helton *et al.* and Lasijo *et al.* suffer from insufficient resolution.

To extract further details about the wave functions of these levels, as well as to search for the missing levels, we investigated the proton transfer reactions $^{137}Ba(^{3}He,d)^{138}La$ and $^{137}Ba(\alpha,t)^{138}La$. We also improved upon the (d,t) measurements and were able to locate one more level hidden in a previously unresolved doublet. These two reactions (proton transfer and neutron pick-up) can complement each other in restricting the spin possibilities for any level. We have also studied the γ-ray decay modes of these levels by means of the $^{138}Ba(p,n\gamma)^{138}La$ reaction, observing the γ-ray spectra both in singles and in coincidence. Life-time measurements have also been carried out for the first excited state, using the (n,γ) delayed coincidences

in $^{138}Ba(p,n\gamma)^{138}La$ reaction. It is encouraging to note that the low-lying levels of ^{138}La and ^{140}Pr prefer to decay in a similar manner.

We have also investigated the higher states of ^{138}La up to an excitation of 1.8 MeV by proton transfer reactions. The group of negative parity states arising from the coupling of an $h_{11/2}$ proton to a $d_{3/2}$ neutron hole have been identified and tentative spin assignments have been made on the basis of the strengths of these transitions. Shell model systematics predict these levels to lie beyond an excitation of 1 MeV. The $11/2^-$ state in ^{139}La occurs at 1420 keV. The centroid of the negative parity states seen in our work lies at about 1.32 MeV.

The subsequent chapters (II and III) give the details of all these experiments. Interpretation of these data, for the construction of the level scheme of ^{138}La, is deferred to the last chapter (IV). The deductions made on the basis of our experimental findings are also compared with the earlier work in that chapter and the outstanding common features of ^{140}Pr and ^{138}La are discussed. A shell model calculation with a surface delta residual interaction (SDI) has also been attempted to find the appropriate T=0 strength. The spectroscopic factors for the proton transfer are also calculated and compared with the experimental findings.

CHAPTER I

BASIC NUCLEAR THEORY

Introduction

Before presenting a report of the experimental investigations about the nuclear structure of ^{138}La, we must describe the theoretical framework which shall be the testing ground for those findings. The theoretical considerations to be stated here are well documented in the volumes written by experts in the field, and any effort on our part to deal with the detailed mathematical development or to elaborate on the fine theoretical aspects will be superfluous. We shall limit our discussion to the axioms and a general description of the theoretical concepts. The relevant formulae will be quoted in this chapter so that they can be referred to in subsequent chapters. A proper appreciation of our experimental data demands a basic understanding of the nuclear shell model, the mechanism of direct reactions and the theory of the electromagnetic transitions.

1.1 Nuclear Models

At least one thing is common in all nuclear processes. Directly or indirectly they show that every nucleus has a set of unique energy levels or excited states. The study of nuclear structure is aimed at finding the physical observables for these states and delineating their wave functions. As the nucleus is a composite system of many particles, the complete wave function will contain many variables and can be written in

very many different ways. Due to practical limitations one then tries to find a representation which will give the best approximation to a physically significant feature of the nucleus under consideration. This means that one may have to resort to a different model for different types of data. For example, the collective model (Bohr 1952, Bohr and Mottelson 1953) has been very successful in explaining the rotational bands observed in many nuclei but offers no explanation for the magic numbers. The shell model, on the other hand, requires very delicate quantum mechanical handling of this problem although the magic numbers come naturally to it. The unified model attempts to bridge this gap. In such a model the single-particle motion of a few extra-core nucleons can be coupled to the collective vibrational motion of a spherical core. Heyde and Brussard (1968) have been quite successful in describing the N=82 and N=83 nuclei, using such an intermediate coupling model. Recently they have extended their calculations to N=81 hole states for the odd-A nuclei from ^{133}Te to ^{143}Sm (Heyde and Brussard 1973). Because ^{138}La will be described in the shell model framework in this thesis we shall discuss that model in a little more detail.

1.1a Shell Model

The idea for such a model is borrowed from atomic physics. In fact it was the existence of the magic numbers, e.g. the observation that nuclei with certain neutron or proton numbers show a large increase in the separation energy of their last

nucleon, which suggested that there might be something common between the electronic structure of the inert gases and these stable nuclei.[2] At first sight it is hard to hypothesize the existence of a central potential in the nuclear case, which in atomic physics is provided by the nucleus itself. But one can assume that most of the time each nucleon is moving in an average potential generated by the rest of the nucleus. This is the basis of the Hartree-Fock theory. A simplistic assumption for this potential would be a finite square well potential. An infinite square well or harmonic oscillator potential can be a more useful approximation. Quantum mechanically, such a system will be permitted to exist in discrete orbits with quantized energies. The energy of the nucleon in these orbits is defined by the shape and size of the orbit and is directly related to its principle quantum number n. Several quantum states can correspond to the same energy level if they differ from each other only in the orientation of their angular momentum. Each such state is defined by its principle quantum number n, its orbital angular momentum ℓ and its total spin quantum number j ($\vec{j}=\vec{\ell}+\vec{s}$).

There can be strong objections to the idea of a long mean free path within a nucleus. One might think that a nucleon moving in the field of all the other nucleons should experience frequent collisions due to the tremendous strength of the nuclear force and the immense density of the nucleons. Probably Weisskopf was the first person to offer the explanation - large fluctuations in the potential energy should result in the scattering of the nucleons

into other energy states, but because all the nearby states are full, the Pauli exclusion principle does not allow this scattering.

The historical shell model, which won a Nobel prize for Mayer (1949) and Jensen (1949), consisted of a spherically symmetric simple harmonic oscillator potential with a strong spin-orbit interaction added to it. Though they proposed the shell model with a view to explaining the magic numbers, it has been successful in predicting many other nuclear properties as well. The nuclear force appears to have a strong pairing component since two identical nucleons tend to pair off to produce a resultant zero angular momentum. Thus the extreme single particle shell model would predict a ground state spin of zero for all even-even nuclei, and the ground state spin, parity and magnetic moment of the odd A nuclei should be determined by the last unpaired nucleon.

Experimentally there is no known exception to the even-even rule, and the spin and parity predictions for odd A nuclei are valid for nearly all the so-called spherical nuclei. Schmidt (1937) had calculated the magnetic moment of a single nucleon with total angular momentum j long before the shell model's appearance on the horizon of nuclear theory. It is interesting to note that with a few exceptions, (^{3}He, ^{13}C, ^{15}N, ^{197}Au and ^{237}Np), the measured values of the magnetic moments of odd A nuclei lie between the Schmidt lines for $j = \ell \pm \frac{1}{2}$. An extreme single particle model appears to be an oversimplification of the real situation but it exhibits the trend that a closed shell forms an inert core and that the behaviour of a nucleus is mainly governed by its extra-

core nucleons. A vacancy in a closed shell, popularly known as a hole, also plays the same role. The well known Pandya transformation (Pandya 1956) enables one to calculate hole-core interactions and particle-hole interactions in terms of particle-core and particle-particle interactions.

Theoretically, the Hartree-Fock method is followed to generate a suitable nuclear potential. It is assumed that the many-body interactions are relatively weak at nuclear matter densities and only two-body interactions are important. The Hamiltonian of the system thus reduces to

$$H = \sum_i T_i + \frac{1}{2} \sum_{i,j} V_{ij}$$

where T_i is the familiar kinetic energy operator given by

$$T_i = -\left(\frac{\hbar^2}{2m_i}\right)\nabla_i^2.$$

The inter-nucleon potential V_{ij} is derived from the properties of the deuteron and nucleon-nucleon scattering data. This potential is then used to calculate the wave-functions for each nucleon and hence the matter distribution of the nucleus. The many-body eigenfunctions are approximated by an anti-symmetrized product of single particle wave-functions of the Hartree-Fock potential given by

(i) $$\langle\phi_i|U_{HF}|\phi_j\rangle = \sum_k \left(\langle\phi_i\phi_k|V|\phi_j\phi_k\rangle - \langle\phi_i\phi_k|V|\phi_k\phi_j\rangle\right).$$

These wave functions are then used to diagonalize the potential, i.e.

(ii) $$\langle\phi_i|T+U_{HF}|\phi_j\rangle = \varepsilon_i\delta_{ij}$$

where the eigen values ε_i are chosen to be single particle

energies. Self consistency between the assumed and calculated potential is achieved by successive approximations of the equations (i) and (ii). Very often harmonic oscillator wave functions are used as the first approximation to the basis states and the central potential is approximated to Woods-Saxon or some other theoretically acceptable potential.

Better microscopic agreement between the theory and the observation demands the presence of a residual interaction between the extra-core nucleons. The search for the nature and strength of this interaction has been the guiding force for many nuclear structure physicists for the last decade or so. In the iso-spin formalism, when the charge state of the nucleon is defined by the quantum number t_z ($t_z = +\frac{1}{2}$ for a neutron, $-\frac{1}{2}$ for a proton), the residual interaction may also depend upon the total isospin of the interacting nucleons. Thus two protons or two neutrons can only interact in the isospin T=1 state but a neutron-proton pair can be formed in either the T=0 or T=1 state. Hence an odd-odd nucleus is a very suitable system where the T=0 residual interaction may be investigated, and this was one of the incentives for undertaking the present study.

1.1b Shell Model Calculations

One aim of any shell model calculation is to find the most appropriate one-body Hamiltonian and the most suitable set of the basis states which will reproduce the experimental findings. Normally the central part of the potential is assumed to be the simple harmonic oscillator potential. The inert core

does not make any contribution except for a reference energy, and only valence nucleons need to be considered. The total wave-function for these nucleons is generated by the complete set of the single particle states, suitably anti-symmetrized, using the recipe of Slater determinants. A number of such wave-functions can be formed, each having a definite value of the total angular momentum J and iso-spin T, following de-Shalit and Talmi (1963). The mechanics of shell model calculations in the second quantization formalism of French are beautifully explained in his review article (French 1969). The single particle energies for different orbitals are adjusted to reproduce the known single particle states in the neighbouring nuclei. The many-body matrix elements can be decomposed into sums over two-body matrix elements using the coefficients of fractional parentage. Thus the only input for the shell model calculations is the two-body matrix elements and the single particle energies. The shell model calculation is facilitated by the multi-shell model computer code (MSMC) of Halbert *et al.* (1971).

The choice of the residual interaction is also a very important factor. There are three popular approaches to this problem:

(a) The free nucleon-nucleon interaction is assumed and the nuclear matrix elements are calculated by the reaction matrix method. This method is useful in calculating effective interactions for two particles outside, or two holes inside, an inert core. Kuo and Brown (1966, 1967) have carried out sizeable calculations for matrix

elements in the f-p shell. Core excitation effects are taken into account in this method for low excitations, but effects due to the partially filled shells cannot be incorporated. Hence the method loses its power for nuclei farther away from the closed shells.

(b) Talmi (1962) and Glaudemans *et al.* (1964) have initiated the method of treating the two body matrix elements as free parameters to be determined by fitting calculated eigen values to the observed level energies. The applicability of the method is sharply limited to nuclei very near to the closed shells. For more complex nuclei the matrix elements outnumber the observed energy levels.

(c) A phenomenological effective interaction is chosen, incorporating the known basic properties of the nuclear force, and having a limited number of parameters. The calculation is model dependent, of course. Two such interactions are rather popular, one of them being a surface delta interaction (SDI). SDI assumes that the effective interaction is more attractive at lower densities, i.e. at the surface of the nucleus and because of the very short range of the interaction it can be treated as a delta function. The analytic expression for this interaction is given by Green and Moszkowski (1965) as

$$V_{ij}^{SDI} = - 4\pi A_T \delta(\Omega_{ij}) \delta(r_i - R) \delta(r_j - R)$$

where Ω_{ij} is the angle between the radius vectors of the interacting nucleons and R is the nuclear radius.

The interaction strength A_T is assumed to depend only upon

the iso-spin. If we further assume that the amplitudes of the radial wave functions at the surface are independent of ℓ, then a simple analytical expression can be found for the matrix elements (Glaudemans *et al.* 1967), the two values of A_T being the only essential parameters.

Inclusion of iso-spin dependent monopole terms to V_{ij}^{SDI} can describe the binding energy systematics (Glaudemans *et al.* 1967). The modified surface delta interaction (MSDI) can thus be written as:

$$V_{ij}^{MSDI} = -4\pi A_T \delta(\Omega_{ij}) \delta(r_i - R) \delta(r_j - R) + B_T$$

The additional term does not affect the excitation energies or eigenfunctions as it alters all the diagonal matrix elements by the same amount and leaves the off-diagonal ones unchanged.

Another well known phenomenological interaction is the zero range spin-exchange interaction, essentially a combination of Wigner and Bartlett forces. It is defined as

$$V_{ij} = -V_o(\alpha + (1-\alpha)(\hat{\sigma}_i \cdot \hat{\sigma}_j)\delta(\vec{r}_i - \vec{r}_j)$$

where V_o is the strength of the interaction

and α is the spin exchange parameter

1.2 Nuclear Reactions

Nuclear reactions can be classified as direct or compound nucleus reactions. In a direct reaction mechanism the incident projectile interacts only with a few nucleons of the target nucleus, the rest of the nucleons behaving as spectators. Thus there is a high degree of correlation between the initial and final states

of the system. Also the reaction amplitude shows a smooth dependence on the incident beam energy and peaks in the forward hemisphere. The angular distributions of the differential cross-sections exhibit an oscillatory pattern, characterized by the angular momentum of the transferred nucleons. By measuring the angular distributions and identifying the ℓ-transfers the spins and parities of the final states can be restricted, due to angular momentum selection rules.

Compound nucleus reactions, on the other hand, can excite many more degrees of freedom and hence the final state may be totally uncorrelated with the initial state. The reaction can peak in both the forward and backward hemisphere, and may show violent fluctuations with the incident projectile energy.

In general, both compound and direct reaction mechanisms may contribute to the observed reaction amplitude but one will dominate over the other in suitable experimental conditions. Direct reactions, being very selective, reveal a wealth of information about the configuration of the states (single particle aspects of the wave-functions), whereas compound nuclear reactions, though sensitive to angular momentum transfer, can populate states of widely different configuration. In the present work we have used both types of reactions to investigate the nuclear structure of ^{138}La.

1.2 a Stripping and Pick-up Reactions

The most widely used, and perhaps the best understood, group of direct reactions are the stripping and pick-up reactions.

A number of good texts (e.g. Austern 1970, Brown 1972, and Jackson 1970) and many review articles (e.g. Lane 1967 and Robson 1969) discuss the mechanism of these reactions in depth and with a keen theoretical insight. Robertson (1971) has given a concise summary of the formalism employed and Taylor (1974) has documented the pertinent mathematical details in a relatively simple manner. The reader is referred to these more theoretical works for a better understanding of the reaction mechanism. We shall limit our discussion to the statement of the important definitions and to a reproduction of the principal results relevant to the analysis of our experimental data.

Generally only the stripping reactions are considered and the pick-up reaction cross-sections are extracted from the stripping cross-sections using the principle of detailed balance. A stripping reaction can be described as

$$A + a \rightarrow B+b \quad \text{or} \quad A(a,b)B$$

where a can be pictured as a composite system of two groups of nucleons b and x. The group x is stripped from a and transferred to A to form the residual nucleus B. Hence the states of B, formed in this reaction, should be described by the anti-symmetrized vector coupling of the wave-function of x to the initial wave-function of A.

The differential cross-section for the reaction is given by Fermi's Golden Rule

$$\frac{d\sigma}{d\Omega} = \frac{\mu_a \mu_b}{(2\pi\hbar^2)^2} \frac{K_b}{K_a} \left| M_{fi} \right|^2$$

where μ_a and μ_b are the reduced masses of the particles a and b and K_a and K_b are their wave numbers. The transition matrix element is

$$M_{f_i} = \langle \psi_b \psi_B e^{i\vec{K}_b \cdot \vec{r}_b} | V_{bB} | \psi_{aA}^{(+)} \rangle .$$

Here $\psi_{aA}^{(+)}$ is the solution of the Schrödinger equation with incoming waves in channel aA and outgoing waves in all open channels. The quantities ψ_B and ψ_b are the eigenfunctions of H_B and H_b, the total Hamiltonian of the system being

$$H = H_a + H_A + T_{aA} + V_{aA} = H_b + H_B + T_{bB} + V_{bB}.$$

The operators T_{aA} and T_{bB} are the relative kinetic energies in the incident and exit channels. The post interaction of b with B (i.e. V_{bB}) in the expression for M_{fi} could be replaced by the prior interaction of a with A (i.e. V_{aA}) if it happens to be simpler.

1.2b. Distorted Wave Born Approximation

The distorted wave Born Approximation (DWBA) is a reasonably reliable approximation widely used to calculate the transition amplitude M_{fi} according to the direct reaction mechanism. The validity of the argument depends on the fact that the potential, though very strong, tends mostly to scatter particles without rearrangement. In DWBA one considers only the elastic scattering parts of the incoming and outgoing waves, which are distorted by the coulomb and nuclear potentials. The interaction can be treated using perturbation theory. Thus multiple scattering processes are not taken into account.

The choice of distorting potential essentially limits

the quality of the approximation. It is generally approximated to a phenomenological two-body potential (the optical potential) given by

$$U = V+iW.$$

The imaginary term in the potential signifies the loss of flux from the elastic scattering state to the reaction channels. The analogy is taken from the dispersion of light and the optical model is also called the cloudy crystal ball model. Such a potential was first used by Feshbach *et al.* (1954) to analyze neutron scattering at low energies. For more massive particles (e.g. tritons ^{3}He or alphas) the interaction is assumed to be localized at the surface whereas for lighter particles (e.g. protons, neutrons and deuterons) the penetration inside the nucleus is taken into account by a so-called volume term. The parameters for optical potentials are usually obtained by fitting elastic scattering data (except for tritons where such data are limited). Unfortunately these fits do not determine a unique set of parameters. Ambiguities arise because the elastic scattering data are mainly sensitive to the tail of the potential (Cage *et al.* (1973)). Various discrete values of the real well depth V_o give equally good fits to the data for a fixed real well radius parameter r_o. There are also continuous ambiguities. If both V_o and r_o are varied so that $V_o r_o^2$ stays essentially constant, the quality of fit remains the same. One way out of this dilemma is to use the well depth closest to 50 MeV per nucleon.

The evaluation of the transition matrix element is simpli-

fied a great deal by using a zero range approximation, which assumes that the incident and emitted particles must be at the same point to be able to interact. Austern (1964) claims that the inclusion of a finite range does not change the angular distribution noticeably, though the magnitude of the differential cross-sections may change by a considerable amount. The distorted wave approximations should not be relied upon for large angles and usually it is sufficient to compare the calculated and observed angular distribution at relatively forward angles only. In this range the computed shapes are essentially independent of the total angular momentum of the transferred particle and characteristic of the orbital angular momentum only.

Details of the DWBA calculation are given in a number of works (e.g. Satchler (1966)) Quite a few computer codes are now available to calculate $(\frac{d\sigma}{d\Omega})^{DWBA}$. The one used in our calculation, called DWUCK, originated at the University of Colorado. We are indebted to Dr. Kunz for making it available to us at McMaster, and to J. C. Tippett for adapting it for the CDC 6400.

1.2c. Selection Rules and Spectroscopic Factors

Certain selection rules, which are useful in determining the parity of the final state and restricting the spin to some extent, should be mentioned at this stage.

(i) If the transferred particle is in s-state, which is assumed to be the case almost always, then the parity of the final state in the residual nucleus is given by

$$\Delta\pi = (-)^{\ell}$$

where ℓ is the orbital angular momentum of the transferred particle.

(ii) The total angular momentum J_B of the final state always obeys the vector sum rule

$$|J_A - j| \leq J_B \leq J_A + j$$

where j of the transferred particle is given by

$$|\ell - s| \leq j_B \leq \ell + s.$$

(iii) The transfer of a $t = \frac{1}{2}$ particle can populate states of iso-spin $T = T_o \pm \frac{1}{2}$ where T_o is the iso-spin of the target ground state.

For stripping of a single nucleon into the $n\ell j$ shell of the target (of spin J_A) to form the final state of spin J_B in the residual nucleus, the observed differential cross-section is related to the DWBA calculation by

$$\left(\frac{d\sigma}{d\Omega}\right)^{exp}_{n\ell j} = \frac{N}{2j+1} \left(\frac{d\sigma}{d\Omega}\right)^{DWBA}_{n\ell j} c^2 \left[\frac{2J_B+1}{2J_A+1} \sum_j S_{n\ell j}(J_B)\right] .$$

The sum over j is indicated because the experimental cross-sections are insensitive to j. However $\frac{1}{2j+1} \left(\frac{d\sigma}{d\Omega}\right)^{DWBA}_{n\ell j}$ can be taken out of the summation as it only counts the cross-section per magnetic sub-state.

For pick-up the expression becomes

$$\left(\frac{d\sigma}{d\Omega}\right)^{exp}_{n\ell j} = \frac{N}{2j+1} \left(\frac{d\sigma}{d\Omega}\right)^{DWBA}_{n\ell j} c^2 \left[\sum_j S_{n\ell j}(J_B)\right] .$$

Here N is a normalisation constant, which is different for different reactions. Generally accepted values of this constant, for (^{3}He,d) and (d,t) reactions are 4.42 and 3.33 respectively.

The factor c^2 accounts for the iso-spin coupling, and the $S_{n\ell j}(J_B)$ is the spectroscopic factor for the final state of the spin J_B.

The spectroscopic factor is a measure of the probability of the reaction and an index of the similarity of the nuclear structure of the states involved in the reaction. It is defined as the overlap between the final nuclear state and the initial target state, vector coupled to the transferred nucleon, the coupling satisfying the anti-symmetrization condition.

The quantity in the square bracket, which is directly related to the ratio of the experimental cross-section and to the theoretical one, is called the strength of the transition. It obeys the sum rules (Robertson and Summers-Gill (1971))

$$\sum_{J_B} \sum_{j} \frac{2J_B+1}{2J_A+1} S_{\ell j}(J_B) = N_\ell^h \quad \text{for stripping}$$

and

$$\sum_{J_B} \sum_{j} S_{\ell j}(J_B) = N_\ell^p \quad \text{for pick-up}$$

where N_ℓ^h represents the number of holes protons in (^{3}He,d), and N_ℓ^p is the number of particles, neutrons in (d,t), in the ℓ orbital of the target nucleus.

Comparison of the expressions for the sum rules and the $(\frac{d\sigma}{d\Omega})^{exp}_{n\ell}$ clearly indicates that knowledge of the spins of the initial and final states is not required for testing either sum rule. When the strength for a given spin is fragmented in many states, as is often the case for odd-odd nuclei, then the strength for all

these levels should be added before applying the sum rules, i.e.

$$S_{\ell j}(J_B) = \sum_i S_{\ell j}(i, J_B) \ .$$

French and Macfarlane (1961) have generalized the sum rules to derive an expression for the separate strength of each iso-spin component.

The sum rules are often used to verify the single particle aspects of the final states in the residual nucleus but one should not take them literally. The computed value depends largely on the cross-sections predicted by DWBA calculation, and though the shape of the angular distributions does not vary remarkably with the optical-model parameters, the magnitude is very sensitive to them. The inclusion of spin-orbit coupling or finite range correction can change the magnitude by as much as 20%. Also the absolute experimental cross-sections contain inherent uncertainties of ≈ 10% (systematic errors etc.). If one satisfies the sum rule strength to 30%, it should be considered quite good agreement.

The J dependence of the transition strengths can be utilized for tentative spin assignments; or to confirm assignments made on the basis of other data. For stripping reaction this dependence is obvious. The $(2J_B+1)$ factor simply counts the number of possible magnetic substates for a given final spin. The expression for the pick-up strength does not contain any such dependence explicitly. However it is still there, concealed in the expression for $S_{n\ell j}(J_B)$ which is in reality a stripping spectroscopic factor. If the cross-section were written in terms of a pick-up spectroscopic factor, the J dependence would become evident. We shall

discuss the application of these rules in Chapter IV.

As only relative strength is important for spin assignments, one does not worry too much about the magnitude of the theoretical cross-sections, but the shape of the angular distribution becomes very important. The angular distributions for $(\frac{d\sigma}{d\Omega})^{DWBA}$ are quite distinct for different ℓ-values, the lower ℓ peaking in a relatively more forward direction. For a target of ground state spin $J_A=0$, the final states are expected to have definite ℓ-values, and the ℓ-assignment is simple enough. The situation becomes much more complicated when $J_A \neq 0$ and the final nucleus is an odd-odd one. In this case a state of a given spin J_B may be populated by more than one ℓ-transfer. The resultant angular distribution is usually dominated by the lower ℓ-value and the extraction of the amplitude for each ℓ is no longer simple. The ratio of the amplitudes for the competing orbital angular momenta is very sensitive to the position of the maxima and minima and to the peak-to-valley ratio in the individual angular distributions. Q-values also play a part, as the whole pattern is slightly shifted towards higher angles with increasing excitation energies. Thus the choice of the optical model parameters becomes very important for extracting spectroscopic information for the levels in odd-odd nuclei. Ideally one should determine the parameters by fitting elastic scattering of the relevant particles from the desired targets but, as mentioned earlier, ambiguities can still arise. However, since the elastic scattering is not overly sensitive to slight variation in Z and A, it is usual to select the parameters from the available

compilations used in the same mass region for a similar range of energy. The best approach, which we have utilized in our (^{3}He,d) analysis, is to derive the empirical ℓ-shapes from the angular distributions of well known single particle states.

1.3 Electromagnetic Transitions

Nuclear structure physics could have suffered quite a setback if the nucleus had not included photon emission or ejection of an extra nuclear electron in its modes of de-excitation. At least the theory of electromagnetic interactions is well understood and the matrix elements of the electromagnetic operators governing the decay of the nuclear states can provide a testing ground for the nuclear structure theories. While particle transfer reactions do provide ℓ-values of the levels, and hence their parities, spin assignments deduced from the spectroscopic strength are regarded as only tentative. The study of decay modes of these levels allows one to put more definitive constraints on the possible spins.

There are two types of radiative transitions in a nucleus, electric and magnetic. Changes in the charge distribution inside the nucleus give rise to electric multipoles. Magnetic multipoles are formulated in terms of the orbital motion of the protons and the intrinsic magnetic moments of all the nucleons. A number of good texts and review articles (e.g. Siegbahn 1965, Yoshida and Zamick 1972 and Preston 1962) discuss the theory of these transitions in great detail so we shall limit our discussion to a description of the phenomena and the documentation of the more important formulae.

It is convenient to discuss the transition rates in terms of a reduced transition probability $B(\sigma L, J_i \to J_f)$ which is given by

$$B(\sigma L, J_i \to J_f) = \frac{1}{2J_i+1} \sum_{M_i M_f \mu} |\langle J_f M_f | Q^{\sigma}_{L\mu} | J_i M_i \rangle|^2 .$$

Here L is the multipolarity of the transition,

σ is the type of radiation, i.e. electric or magnetic,

$Q^{\sigma}_{L\mu}$ is the electromagnetic operator of the relevant type,

and $|i\rangle$ and $|f\rangle$ are the initial and final states involved in the transition.

The operator $Q^{\sigma}_{L\mu}$ can be easily expressed in terms of spherical harmonics and the matrix element can be further simplified using the Wigner-Eckart theorem to introduce a reduced matrix element. It is this which contains all the nuclear structure information. The transition probabilities between the states $|i\rangle$ and $|f\rangle$, for a photon of energy $\hbar\omega$, multipolarity L and type σ can now be written as

$$T_{ij}(\sigma, L) = \frac{8\pi(L+1)}{L[(2L+1)!!]^2} \frac{1}{\hbar} \left(\frac{\omega}{c}\right)^{2L+1} B(\sigma L, J_i \to J_f)$$

provided the wave-length of the photon is much larger than the nuclear dimension, which is true for all observed γ-rays.

The decay mode of any state can involve several electric and magnetic multipoles which should obey the following selection rules:

(i) Conservation of parity demands that

$(\pi_i \pi_f) = (-)^L$ for electric transitions,

$(\pi_i \pi_f) = (-)^{L+1}$ for magnetic transitions.

(ii) Conservation of angular momentum demands that

$$|J_i - J_f| \leq L \leq J_i + J_f .$$

Thus electric and magnetic multipoles of the same order never compete with each other. As the photon carries an intrinsic angular momentum of one unit, L=0 multipoles do not contribute to γ-transitions. Hence 0 to 0 transition can only occur by internal conversion, internal pair creation or two photon emission.

1.3a The Weisskopf Units

Single particle estimates of the transition probabilities can be obtained by making some simplifying assumptions:

(i) The nucleus consists of an inert core with one active proton.

(ii) The orbital angular momentum of the final and initial states differs by L the final state having $\ell=0$.

(iii) The transition does not affect the spin wave functions of the particle undergoing the transition.

(iv) The radial wave functions are constant over the volume of the nucleus, i.e.

$$U(r) = \text{constant} \quad r < R$$

$$U(r) = 0 \qquad\quad r > R.$$

Under these assumptions the matrix elements become,

$$B_W(E_L) = \frac{e^2}{4\pi} \left(\frac{3}{L+3}\right)^2 R^{2L}$$

$$B_W(M_L) = \frac{10e^2}{4\pi} \left(\frac{3}{L+3}\right)^2 \frac{\hbar^2}{M_p^2 c^2} R^{2L-2}$$

where R is the nuclear radius,

and M_p is the mass of the proton.

The partial radiative width $\Gamma(L)$ of a state is related to the transition probability by the uncertainty principle

$$\Gamma(L) = \hbar T(L).$$

Using $R = 1.2\ A^{1/3}$ fm, the Weisskopf estimates for the radiative widths can be stated in terms of E_γ (MeV) and A (Preston 1962):

$$\Gamma_W(E1) = 0.068\ A^{2/3}\ E_\gamma^3 \text{ eV}$$

$$\Gamma_W(M1) = 0.021\ E_\gamma^3 \text{ eV}$$

$$\Gamma_W(E2) = 4.9\times10^{-8}\ A^{4/3}\ E_\gamma^5 \text{ eV}$$

$$\Gamma_W(M2) = 1.5\times10^{-8}\ A^{2/3}\ E_\gamma^5 \text{ eV}.$$

These estimates have acquired the status of basic units in nuclear physics. The transition probabilities are generally expressed as a multiple of single particle estimates, and one talks about the enhancement or the retardation of the actual rates observed. It is obvious from the above expressions that the transition probabilities of the same type of radiation rapidly diminish with the increasing multipolarity. Hence they can hardly compete with each other and generally it is sufficient to consider the lowest order of multipole for a given type. In the case of mixed electric and magnetic multipoles the situation is more complex. Apparently the lower multipole should dominate, but electric transitions (particularly E2) are often greatly enhanced and may favourably compete with, or even dominate, the lower order magnetic transition.

Some model dependent rules may impose a further restriction on the allowed transitions. For example, the ground and first ex-

cited states of ^{139}La have J^{π} of $7/2^+$ and $5/2^+$ respectively. In terms of the simple shell model these are single proton states in the $g_{7/2}$ and $d_{5/2}$ orbitals. The J^{π} values would suggest an M1 transition, but this is ℓ forbidden ($\Delta\ell=2$) and hence it is not surprising that this is observed to be greatly retarded. The M1 retardation ($\sim$ 300 times) has been observed in all the d→g transitions, i.e. in the odd-A isotopes of Cs, Pr, La, Pm and Eu (Bäcklin and Malmskog 1967). In an odd-odd isotope, like ^{138}La, this situation does not arise as each level will generally have both $g_{7/2}$ and $d_{5/2}$ components due to configuration mixing. The form of the M1 operator suggests that M1 transitions only occur between states of the same configuration and hence low-lying levels of ^{138}La are expected to decay mostly by M1 transitions.

1.3b Internal Conversion

Internal conversion is an additional mode of decay for the excited states of nuclei. The excess energy is transferred to an extra-nuclear electron, which is then ejected from the atom. This process is called internal conversion and the ejected electron is said to be a conversion electron. The conversion probability depends directly on the electron density at the nucleus, and hence is greater the higher the Z of the atom. It also depends upon the angular momentum change in the nucleus, and the angular momentum and the binding energy of the electrons involved (Rose 1965). In the point nucleus approximation the nuclear matrix elements for the internal conversion and radiative processes are identical. The conversion coefficient, defined as the ratio of the number of conversion electrons to the number of photons, is thus essentially

independent of the nuclear structure and hence can serve as an important tool in determining the multipolarity of transitions. The experimental values of these co-efficients have been tabulated by Hamilton *et al.* (1966). Hager and Seltzer (1968,1969) have compiled an extensive table of computed values.

Internal conversion is sometimes the only available mode of decay for states where single photon emission is forbidden. A classic example of such a case is the decay of the 0^+ first excited state of ^{72}Ge to the 0^+ ground state.

CHAPTER II

PARTICLE TRANSFER REACTIONS

Introduction

By virtue of its position in the chart of the nuclides, ^{138}La should be a relatively simple spherical nucleus conforming to the norms of the shell model. With 7 protons beyond the major shell closure at 50 and one neutron less than the magic number 82, its low-lying states can be described in a small configuration space. The systematics of the neighbouring odd-A nuclei (^{137}Ba and ^{139}La) suggest that the 7 active protons occupy $1g_{7/2}$ or $2d_{5/2}$ orbits at lowest excitations while the neutron hole may exist in either $2d_{3/2}$ or $3s_{1/2}$ state orbits. In the lowest seniority scheme, levels of ^{138}La should then arise from the various possible couplings of the odd proton and the neutron hole. The spins of these low-lying levels can be easily computed in the j-j coupling scheme where $|j_p - j_n| \leq J \leq j_p + j_n$ holds true. The four configurations thus lead to 12 levels given by

(a) $(\pi 1g_{7/2}, \nu 2d_{3/2}^{-1}) \rightarrow 2^+, 3^+, 4^+, 5^+$

(b) $(\pi 1g_{7/2}, \nu 3s_{1/2}^{-1}) \rightarrow 3^+, 4^+$

(c) $(\pi 2d_{5/2}, \nu 3s_{1/2}^{-1}) \rightarrow 2^+, 3^+$

(d) $(\pi 2d_{5/2}, \nu 2d_{3/2}^{-1}) \rightarrow 1^+, 2^+, 3^+, 4^+$.

Proton states of the $1h_{11/2}$, $2d_{3/2}$ and $3s_{1/2}$ along with the neutron hole states of $1h_{11/2}$, $2d_{5/2}$, and $1g_{7/2}$ should contribute at higher excitations. The only negative parity states at reasonable excitation (i.e. below $\sim$ 2 MeV) will arise from $h_{11/2}$ orbits. These can be counted as follows:

(e) $(\pi 1g_{7/2}, \nu 1h_{11/2}^{-1}) \rightarrow 2^-, 3^-, 4^-, 5^-, 6^-, 7^-, 8^-, 9^-$

(f) $(\pi 2d_{5/2}, \nu 1h_{11/2}^{-1}) \rightarrow 3^-, 4^-, 5^-, 6^-, 7^-, 8^-$

(g) $(\pi 1h_{11/2}, \nu 2d_{3/2}^{-1}) \rightarrow 4^-, 5^-, 6^-, 7^-$

(h) $(\pi 1h_{11/2}, \nu 3s_{1/2}^{-1}) \rightarrow 5^-, 6^-$.

Particle transfer reactions can provide information about the excitation energies of at least some of these levels. If the reactions occur in one step and can be classified as direct, then it must be possible to describe the observed levels by the coupling of the transferred particle to the ground state configuration of the target. Helton *et al.* (1973) and Lasijo *et al.* (1972) must have been thinking along these lines when they decided, independently, to investigate the neutron pick-up reactions $^{139}La(p,d)^{138}La$ and $^{139}La(d,t)^{138}La$. The ground state of ^{139}La is $7/2^+$ (i.e. the odd proton is occupying the $1g_{7/2}$ orbit). Thus they should observe at least six low-lying positive parity states arising from the configurations (a) and (b). All but the 1^+ state would be populated if the four configurations are mixed to an appreciable extent.

Both of these investigations report 9 members of the low-lying group and their deductions about the ℓ-transfers and spectro-

scopic factors are very similar. Whenever a state was populated by a mixed ℓ-transfer ($\ell_n = 0$ and $\ell_n = 2$) Lasijo *et al.* divided the strength of the transition equally. Helton *et al.* give more quantitative values of ℓ-admixtures based on the best fit to the observed angular distributions. The resolution was comparable in both these works so if one group missed a level because of this limitation, the other could not find it either. Helton *et al.* limited their study to only the low-lying group of levels whereas Lasijo *et al.* have investigated levels up to an excitation of 1.6 MeV.

In order to obtain a more complete understanding of the levels in ^{138}La we decided to carry out some other experiments. Our first choice was to investigate the proton transfer reactions ^{137}Ba(^{3}He,d)^{138}La and ^{137}Ba(α,t)^{138}La. Since the ground state spin of ^{137}Ba is $3/2^+$, due to a neutron hole in the $2d_{3/2}$ orbit, a proton transferred into the $1g_{7/2}$ or $2d_{5/2}$ orbits can form levels with spins from 1 to 5. Thus these reactions should populate the 1^+ state and possibly the other two missing positive parity states as well. The spectroscopic factors will measure the amounts of configurations (a) and (d) in each state to complement the neutron pick-up strengths which are sensitive to configurations (a) and (b). In the same way we hoped to learn more about the negative parity states because proton transfer will detect configuration (g) and neutron transfer probes for (e).

Because the enriched targets of ^{137}Ba still contained an

appreciable amount of ^{138}Ba and a less serious percentage of ^{136}Ba, which could produce contaminant peaks in the ^{138}La spectra, the reactions ^{136,138}Ba(α,t)^{137,139}La and ^{138}Ba(^{3}He,d)^{139}La were also examined. Since the ℓ_p values of the levels in ^{139}La had been obtained previously by Wildenthal *et al.* (1971), the data provided checks on the validity of our DWBA calculations and the $(^{3}He,d)/(\alpha,t)$ ratio method for determining ℓ_p values. As the experimental study progressed we also found it necessary to re-investigate the neutron pick-up reaction ^{139}La(d,t)^{138}La at more forward angles and with better resolution than reported by Lasijo *et al.* (1972). The subsequent sections of this chapter present a detailed account of all these experiments.

2.1 Experimental Set-up and Target Preparation

There are two prerequisites for the experiments mentioned above:

(i) A projectile of high enough energy so that the reaction can be classified as a direct reaction and has a reasonable cross-section.

(ii) Suitable facilities for high-resolution studies of the closely spaced levels in an odd-odd nucleus.

The existence at McMaster University of an FN Tandem Van de Graaff accelerator and a split-pole magnetic spectrograph (popularly known as the Enge) provides these requirements and fulfills the means for undertaking such experimental studies. Notwithstanding its nominal voltage rating, the McMaster accelerator can be operated with up to 9, or even 9.5 MV on the terminal. This means that beams

of 27 MeV ^{3}He and α-particles are available for reaction studies on high Z nuclei. The spread in the beam energy is usually less than 0.01% as a result of the stabilization system developed by Cairns (1972). If the reaction products analyzed in the spectrograph are detected using nuclear emulsions, a spatial resolution in the focal plane as good as 0.5 mm is possible. The dispersion is such that this translates into a ΔE/E of 0.0005 in the event that the energy loss and straggling in the target and the kinematic broadening make negligible contributions. These laboratory facilities have been described previously in quite a few works (e.g. Robertson (1971), O'Neil (1972) and Macphail (1973)).

2.1a Target Preparation

For the proton transfer reactions the targets consisted of BaO on carbon backings. The enriched isotopes of barium obtained from Oak Ridge National Laboratory were in the form of $Ba(NO_3)_2$. The isotopic analysis of these materials is given in Table 2.1 along with the composition of naturally occurring barium for comparison. The compound was heated to ~ 800°C in a platinum crucible. At this temperature the $Ba(NO_3)_2$ dissociates evolving nitric oxide and leaving BaO behind. A platinum crucible was chosen after a few trials with tungsten and tantalum crucibles revealed that both those metals will oxidize somewhat giving rise to heavy metal impurity in the targets. The BaO thus obtained was then vacuum evaporated onto 30 μg/cm^2 thick carbon slides. The targets were acquired by floating these foils off their glass backings in de-ionized water and catching them on aluminum frames. Targets

Table 2.1

Isotopic Composition of the Target Materials

	Abundance of Isotope (percentage)						
	^{130}Ba	^{132}Ba	^{134}Ba	^{135}Ba	^{136}Ba	^{137}Ba	^{138}Ba
^{136}Ba	<0.02	<0.02	0.34	1.39	78.2	10.4	9.7
$^{137}Ba(I)$	<0.02	<0.02	0.05	0.16	0.58	89.6	9.6
$^{137}BA(II)$	<0.02	<0.02	0.06	0.23	1.55	64.0	34.1
^{138}Ba	<0.01	<0.01	<0.01	<0.02	<0.02	0.2	99.8
Natural	0.10	0.10	2.42	6.59	7.81	11.3	71.7

containing enriched ^{136}Ba, ^{137}Ba and ^{138}Ba were prepared in this manner, the typical target thickness being $\sim$ 40 $\mu g/cm^2$.

For the neutron pick-up experiments lanthanum metal of 99.5% purity, supplied by Alfa Inorganics, was used. The natural abundance of ^{139}La is virtually 100%. Targets were again prepared by vacuum evaporation onto carbon backings. A tantalum crucible was used for this purpose. Typical target thicknesses were $\sim$ 40 $\mu g/cm^2$ in this case as well.

2.1b Experimental Set-up

The set-up was almost identical for all the particle transfer experiments. The Enge spectrograph has been described in detail by Spencer and Enge (1967). A 1 mm entrance slit was used for the scattering chamber. The beam was focussed onto the target, 10 cm away from this slit, by means of a magnetic quadrupole lens. The unscattered beam was collected in a tantalum faraday cup mounted at the back of the scattering chamber. The entrance to the spectrograph was well shielded from the slit- and faraday cup-scattering by thick aluminum blocks. The faraday cup mount limited the smallest angle for the spectrograph to 7.5°. Also at relatively forward angles ($\theta \leq 20°$) the aluminum blocks shielding the spectrograph aperture from the faraday cup had to be removed. A small Si(Li) surface barrier detector, placed at 30° to the beam direction and subtending a solid angle of 0.08 msr, constantly monitored the beam by counting the elastically scattered particles. A Nuclear Data 3300 multi-channel analyzer was used to accumulate the spectra.

The spectrograph solid angle was consistently maintained at 13 msr for all the reaction exposures. For elastic exposures this was reduced to 0.026 msr. The reaction products were detected by 50 micron thick nuclear emulsions (Kodak NTB-50 plates) placed in the focal plane of the spectrograph. The kinematic broadening was compensated, at least to first order, by adjusting the kinematic shift settings on the plate holder. These settings were calculated along with the appropriate n.m.r. frequencies as a function of angle using a computer programme MAGGIE (Nelson 1970). For the Ba(^{3}He,d)La experiments, particles heavier than the deuterons were prevented from reaching the plates by a 0.033 inch aluminum absorber covering the emulsion. As the plates were beyond the magnetic field region the absorber should not appreciably affect the resolution. In fact it does slow down the deuterons somewhat so that they produce thicker tracks in the emulsion. For the Ba(α,t)La and ^{139}La(d,t)^{138}La experiments only a thin aluminum foil, about 0.004 inches thick, was used as an absorber to stop the recoil carbon nuclei. The plates were developed in Kodak D-19 and fixed using standard techniques. The spectra were obtained by counting the tracks along the length of the plate in 0.25 mm strips under a high-powered travelling microscope. The peak areas and their centroids were extracted using the computer code SPECTR originally written by Von Egidy (1968) and modified by O'Neil (1970).

2.1c Determination of Absolute Cross-sections

The normalization constant, N, for determining the absolute cross-sections was derived from the number of elastically scattered

particles recorded by the Si(Li) detector during a given exposure and the solid angles of the spectrograph and the monitor. As the kinematic factors are essentially the same for the elastic cross-section and the reaction cross-section, the ratio of the scattered particles recorded per unit solid angle is proportional to the respective differential cross-section, i.e.,

$$\frac{\left(\frac{d\sigma(\theta)}{d\Omega}\right)_R \left(\frac{\Delta\Omega_{sp}}{\Delta\Omega_M}\right)}{\left(\frac{d\sigma(\theta)}{d\Omega}\right)_E} = \frac{N_{sp}}{N_E}$$

or

$$\left(\frac{d\sigma(\theta)}{d\Omega}\right)_R = N_{sp} \times \left[\left(\frac{d\sigma(\theta)}{d\Omega}\right)_E \times \left(\frac{\Delta\Omega_M}{\Delta\Omega_{sp}}\right) \times N_E^{-1}\right] \equiv N_{sp} \times N$$

where

$\left(\frac{d\sigma(\theta)}{d\Omega}\right)_R$ and $\left(\frac{d\sigma(\theta)}{d\Omega}\right)_E$ are the differential cross-sections (center of mass) for the reaction and elastic scattering respectively,

$\Delta\Omega_M$ and $\Delta\Omega_{sp}$ are the solid angles subtended at the target by the monitor and the spectrograph respectively,

N_E and N_{sp} are the number of scattered particles detected by the monitor and the spectrograph respectively

and N is the normalization constant.

The elastic scattering cross-sections were taken from appropriate DWBA calculations. For this mass region and at $\theta = 30°$ these cross-

sections are essentially the same as the Rutherford cross-sections. The absolute cross-sections determined in this manner can generally be relied upon to 10%. This mode of normalization is independent of the target thickness and hence is not affected by the deterioration of the target or wandering of the beam spot during a given exposure.

We were compelled to modify this normalization procedure for the $^{139}La(d,t)^{138}La$ experiments as the monitor detectors rapidly deteriorated from the high neutron flux produced by the 16 MeV deuterons. Initially the beam was monitored both with the faraday cup and the monitor. Later only the faraday cup was used. Short elastic exposures were also made on the plates at the spectrograph angle of 30° before and after the run. A Brookhaven current digitizer converted the charge accumulated by the faraday cup into logic pulses which could be counted by a scaler throughout the duration of each plate exposure. The beam dumps (as they are usually called) are directly related to the total number of incident particles, the constant of proportionality depending upon the scale of the current digitizer. The ratio of the beam dumps and the number of tracks in the elastic peak was found to be consistent within 3% for the exposures made at the beginning and the end of the run. The normalization constant was then readily evaluated as

$$N = \frac{R}{B} \left(\frac{d\sigma(\theta)}{d\Omega}\right)_E \frac{\Delta\Omega_E}{\Delta\Omega_{sp}}$$

where

R is the ratio of the beam dumps and elastic peak intensity for the elastic

exposure,

B is the total number of beam dumps for a given exposure,

$\Delta\Omega_E$ and $\Delta\Omega_{sp}$ are the spectrograph solid angles for the elastic and reaction exposure respectively

and $\left(\frac{d\sigma(\theta)}{d\Omega}\right)_E$ has already been defined.

The $^{139}La(d,t)^{138}La$ differential cross-section, so determined at 25°, agrees within 5% with the cross-sections reported by Lasijo *et al.*

2.2 Energy Levels of ^{138}La

Direct reactions involving single nucleon transfer were extensively used to probe ^{138}La. Both proton transfer and neutron pick-up reactions were employed to locate the excited states of this nucleus.

2.2a The $^{137}Ba(^3He,d)^{138}La$ Reaction

A beam of 24 MeV ^3He was used in the study of the $^{137}Ba(^3He,d)^{138}La$ reaction. The isotopic analysis of the target is given in Table 2.1 (^{137}Ba(I)). The average current was ~ 500 nA, the limitation being set by the helium-3 source only. For the purpose of obtaining an angular distribution, data were taken at 11 angles ranging from 10° to 55°. The energy resolution was about 16 keV. A typical deuteron spectrum taken at the laboratory angle of 25° is shown in Fig. 2.1, where it is compared with a

Fig. 2.1

Deuteron spectra from the $^{137}Ba(^{3}He,d)^{138}La$ and $^{138}Ba(^{3}He,d)^{139}La$ reactions. The (i) indicates an unknown light impurity peak.

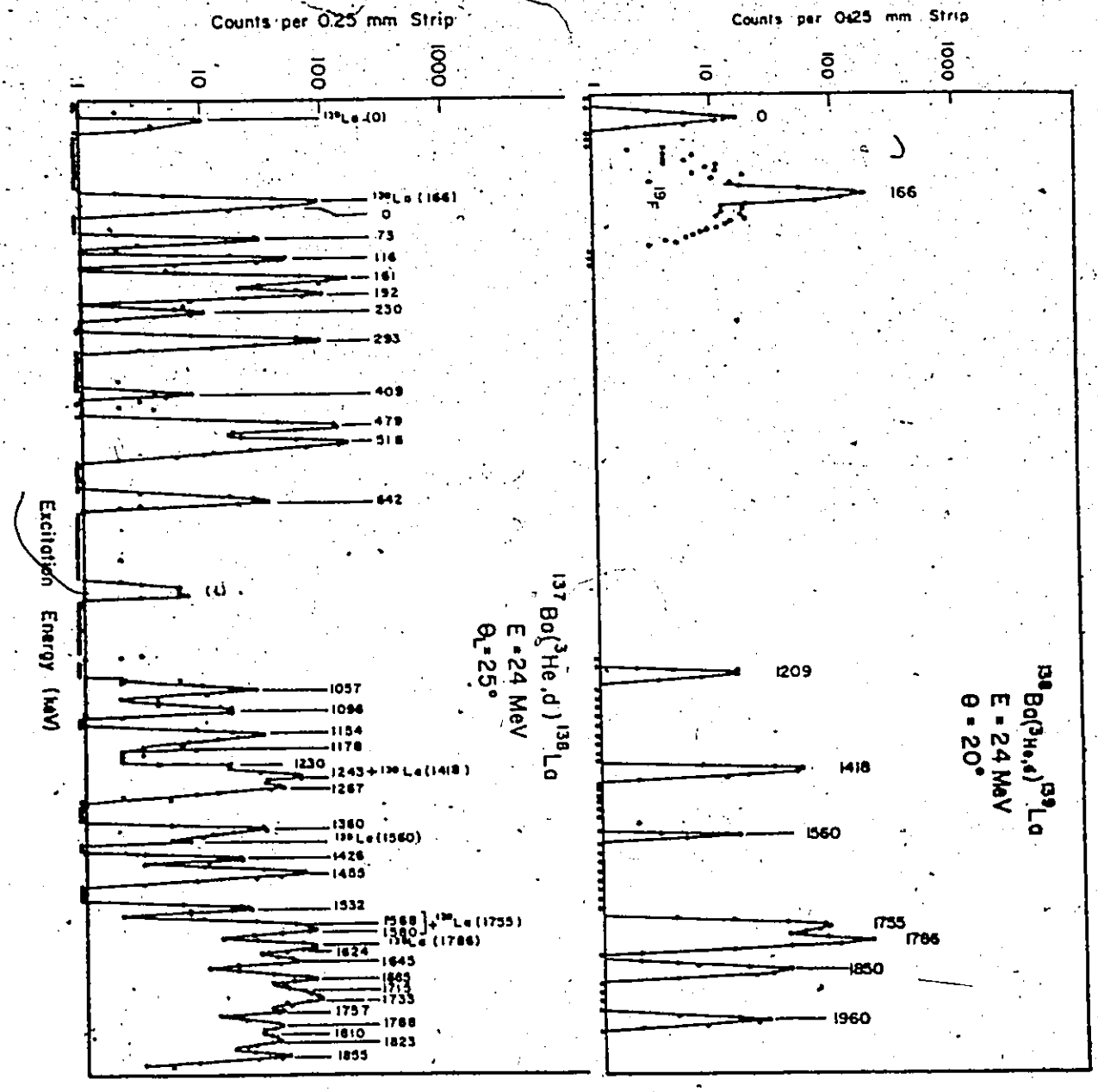
Counts per 0.25 mm Strip
1
10
100
1000
Excitation Energy (keV)
137 Ba(3He,d) 138 La
E = 24 MeV
θL = 25°
138 Ba(3He,d) 139 La
E = 24 MeV
θ = 20°
138La (0)
138La (166)
0
73
116
161
192
230
293
409
479
518
642
1057
1096
1154
1178
1230
1243 + 138La (1418)
1267
1360
138La (1560)
1426
1485
1532
1568
1580
+ 138La (1755)
138La (1786)
1624
1643
1665
1713
1735
1757
1788
1810
1823
1855
0
166
1209
1418
1560
1755
1786
1850
1960

$^{138}Ba(^{3}He,d)^{139}La$ spectrum taken at 20°. Besides the obvious isotopic impurity (^{138}Ba), other known impurities interfering with the ^{138}La spectrum are carbon, oxygen and silicon. The carbon and oxygen are inherently present in the target, it being an oxide on a carbon backing, and the silicon has turned out to be an inevitable impurity in the commercially available carbon foils. These light impurities produce wide peaks, due to the kinematic broadening, which change their relative positions with a change in angle and hence do not always interfere with the same part of the spectrum. When it was necessary to subtract the background due to one of these impurities the relevant peak intensities for ^{138}La were assigned larger uncertainties.

The Q-value of the reaction is known fairly accurately to be 0.541±0.014 MeV (Gove and Wapstra 1972) and no attempt was made to improve on it by measuring absolute energies. Since the ground state is not resolved from the 166 keV state of ^{139}La, excitation energies were determined for every exposure relative to the first excited state of ^{138}La. Its energy (72.6 keV) was obtained from the γ-ray data (see Chapter III). Levels up to an excitation of 1.8 MeV were analyzed. The adopted excitation energies are given in Table 2.2. In most cases these values are an average of six different measurements and none of the individual values lie beyond the quoted uncertainties, which are somewhat larger than those predicted by the SPECTR analysis to allow for systematic errors in the plate scanning. The observed cross-sections at the various lab angles are listed in Table A-1 of

Table 2.2

Comparison of Energy Levels Observed in Proton and Neutron Transfer

(^{3}He,d) This work[a]	(α,t) This work[a]	(p,d) and (d,t) Helton *et al.*[b]	(d,t) Lasijo *et al.*[c]	(d,t) This Work[a]
0.3(30)	0.2(10)	0	0	0
72.6	72.6	70	72.4	72.0(5)
115.7(8)	116.2(3)	114	115.1	115.3(5)
160.9(9)	161.3(4)	160	159.8	160.4(5)
192.3(9)	192.4(4)	194	190.8	192.0(7)
230 (2)	230.8(6)	232	230.5	229.6(5)
293 (1)	292.9(5)			
409 (5)[d]	409 (3)	424	413.7	412.5(5)
479.2(5)	479.1(4)	493	479.3	478.4(5)
		530	515.2	510 (2)
517.9(5)	518.1(5)			518.1(10)
642 (1)	641 (1)			
			737	737 (1)
			833	823 (1)
				836 (1)
				888 (2)
			900	900 (1)
				929 (3)
			938	937 (1)
			962	962 (1)
				1033 (2)
1057 (2)	1058 (2)			

(continued next page)

Table 2.2 (continued)

(^{3}He,d) This work[a]	(α,t) This work[a]	(p,d) and (d,t) Helton *et al.*[b]	(d,t) Lasijo *et al.*[c]	(d,t) This work[a]
			1069	1067(2)
				1095(3)
1096(2)			1102	1102(3)
			1156	1150(3)
				1155(5)
1154(2)	1160(4)			
1178(5)				
			1206	1200(2)
				1228(3)
1230(2)[d]				
1243(2)	1243(1)			
			1258	1255(1)
1267(1)	1268(1)			
			1307	1302(2)
				1344(3)
1360(3)	1360(4)			
			1384	1375(2)
				1386(3)
				1425(2)
1426(3)	1426(4)			
1455(2)	1456(2)			
			1474	1466(2)
				1490(2)
				1520(3)
1532(2)	1530(2)			
			1548	1545(3)

(continued next page)

Table 2.2 (continued

(^{3}He,d) This work[a]	(α,t) This work[a]	(p,d) and (d,t) Helton *et al.*[b]	(d,t) Lasijo *et al.*[c]	(d,t) This work[a]
1568(3)	1565(5)			1571(2)
1580(3)	1579(3)			1583(2)
			~1600	1599(2)
1624(4)	1624(4)			
1645(2)	1644(2)			1646(2)
			~1650	1656(3)
				1676(3)
1685(3)	1686(2)			1690(2)
				1707(2)
1715(4)	1713(2)			
	1728(2)			1726(2)
1733(3)				1739(2)
1757(4)	1755(4)			
1788(4)	1786(2)			1783(2)

[a]The numbers in parentheses indicate the uncertainty in the last digits.

[b]The uncertainties are 5 keV for each level.

[c]The uncertainties are 0.5 keV for the first excited state, 1-2 keV for levels up to 515 keV and 4 keV beyond.

[d]The average of three observations only.

the appendix.

Besides identifying all the low lying levels reported in the earlier work, we also see a fairly strong level at 293 keV. Our excitation energies for this group of levels are in good agreement with the measurement of Lasijo *et al.* None of the negative parity states seen in the neutron transfer work (Lasijo *et al.* 1972) are populated in the present experiment. In fact at 25° the monotony of the long stretch from 642 keV to 1057 keV is broken only by an impurity peak. Beyond this excitation there is hardly any correspondence between the levels populated in the (^{3}He,d) reaction and the earlier results.

2.2b The ^{137}Ba(α,t)^{138}La Reaction

The Q-value for the ^{137}Ba(α,t)^{138}La reaction is -13.780±0.014 MeV (Gove and Wapstra 1972) and the Coulomb barrier for the outgoing tritons is ∿ 10 MeV. Hence the maximum available beam energy of 27 MeV was chosen. Even so, the cross-sections for the (α,t) reaction are about an order of magnitude lower than the (^{3}He,d) cross-sections. Also, DWBA calculations predict relatively featureless angular distributions for this reaction and hence the measurement of complete angular distributions would be an ambitious and not very useful undertaking. However, because of the low energy of the outgoing tritons, much better energy resolution can be obtained in the (α,t) reaction than in the case of (^{3}He,d) and this was a good enough reason for studying it. Another very important reason will become apparent shortly.

Spectra were recorded at only three angles — 15°, 30° and 45°. The exposures varied from 7000 to 17000 μ coulomb. The spectrum obtained at 45° is shown in Fig. 2.2 along with a (^{3}He,d) spectrum for comparison. The energy resolution was ∿ 12 keV. We had expected to do better than this but unfortunately the beam energy drifted to some extent during the long runs because of a malfunction in the terminal stabilizer. The excitation energies, averaged over the three angles, are given in Table 2.2 and the cross-sections at 45° are listed in Table A-2 of the appendix. In general there is very good agreement between the excitation energies derived from the two types of proton transfer reaction.

A close look at Fig. 2.2 makes it very evident why it is desirable to investigate the proton transfer reactions by (α,t) as well as (^{3}He,d). Although the lower parts of the two spectra look alike, the higher regions are by no means identical. Because of the very negative Q-value, and the consequent momentum mismatch, the (α,t) does not favour low values of the angular momentum transfer. Above 1057 keV the (α,t) spectrum is less complex and levels which are relatively weaker than in (^{3}He,d), or totally absent, can be assigned a low ℓ_p value. A more quantitative discussion of this aspect will be presented in section 2.4b.

The presence of 9.6% ^{138}Ba and a trace of ^{136}Ba as isotopic impurities in the target necessitated the investigation of the (α,t) reaction on these two materials also for the purpose of eliminating any extraneous peaks from the ^{138}La spectrum. Spectra obtained at 45° are shown in Fig. 2.3, along with that from ^{137}Ba

Fig. 2.2

Comparison of the triton and deuteron spectra for the $^{137}Ba(\alpha,t)^{138}La$ and $^{137}Ba(^{3}He,d)^{138}La$ reactions.

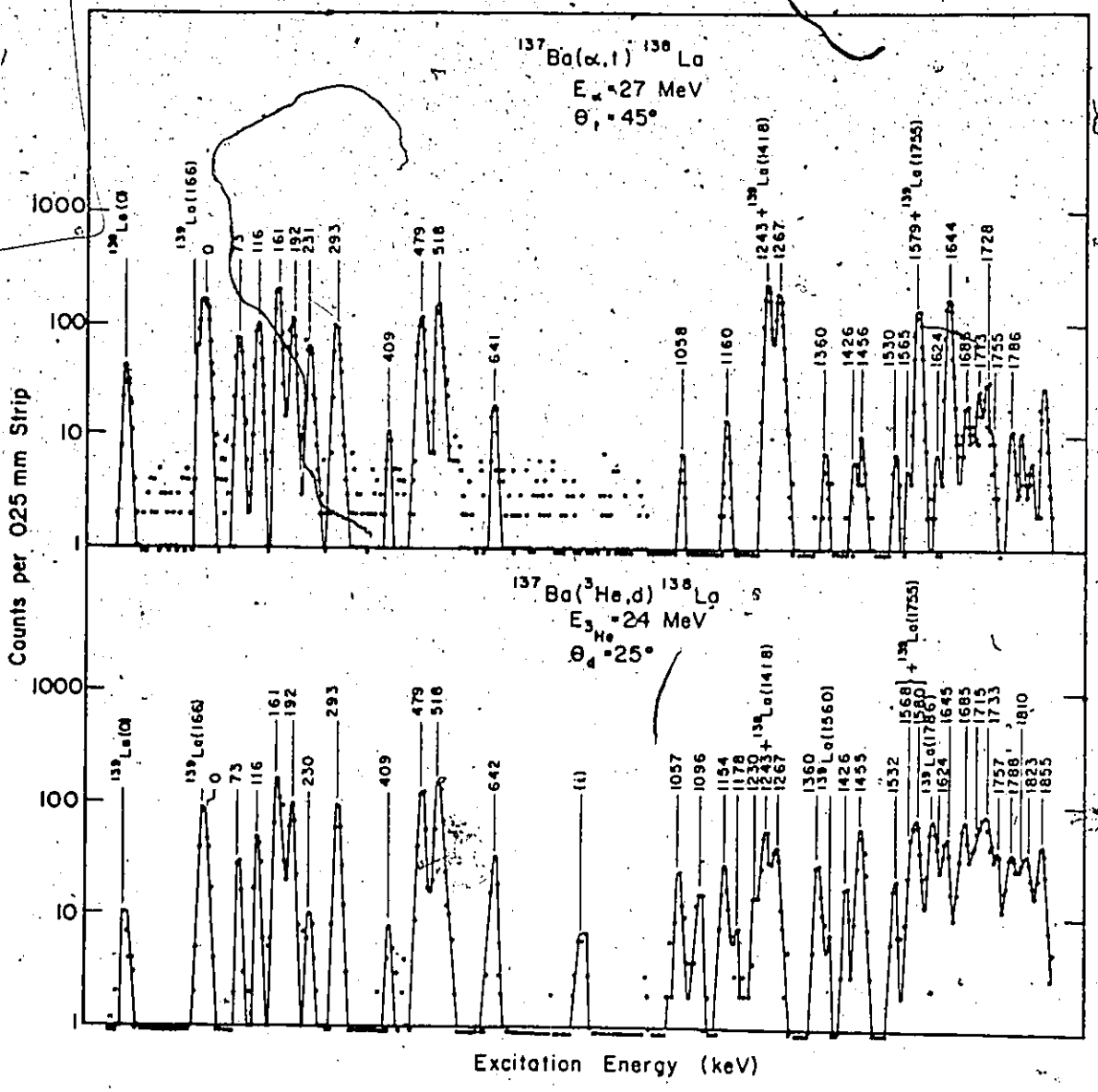
^{137}Ba(α,t) ^{138}La
E_α = 27 MeV
θ_t = 45°
^{137}Ba(^{3}He,d) ^{138}La
$E_{^3He}$ = 24 MeV
θ_d = 25°
Counts per 025 mm Strip
Excitation Energy (keV)

Fig. 2.3

A comparison of the triton spectra for the reactions (a) $^{138}Ba(\alpha,t)^{139}La$, (b) $^{137}Ba(\alpha,t)^{138}La$ and (c) $^{136}Ba(\alpha,t)^{137}La$. The peaks due to the isotopic impurities are suitably labelled.

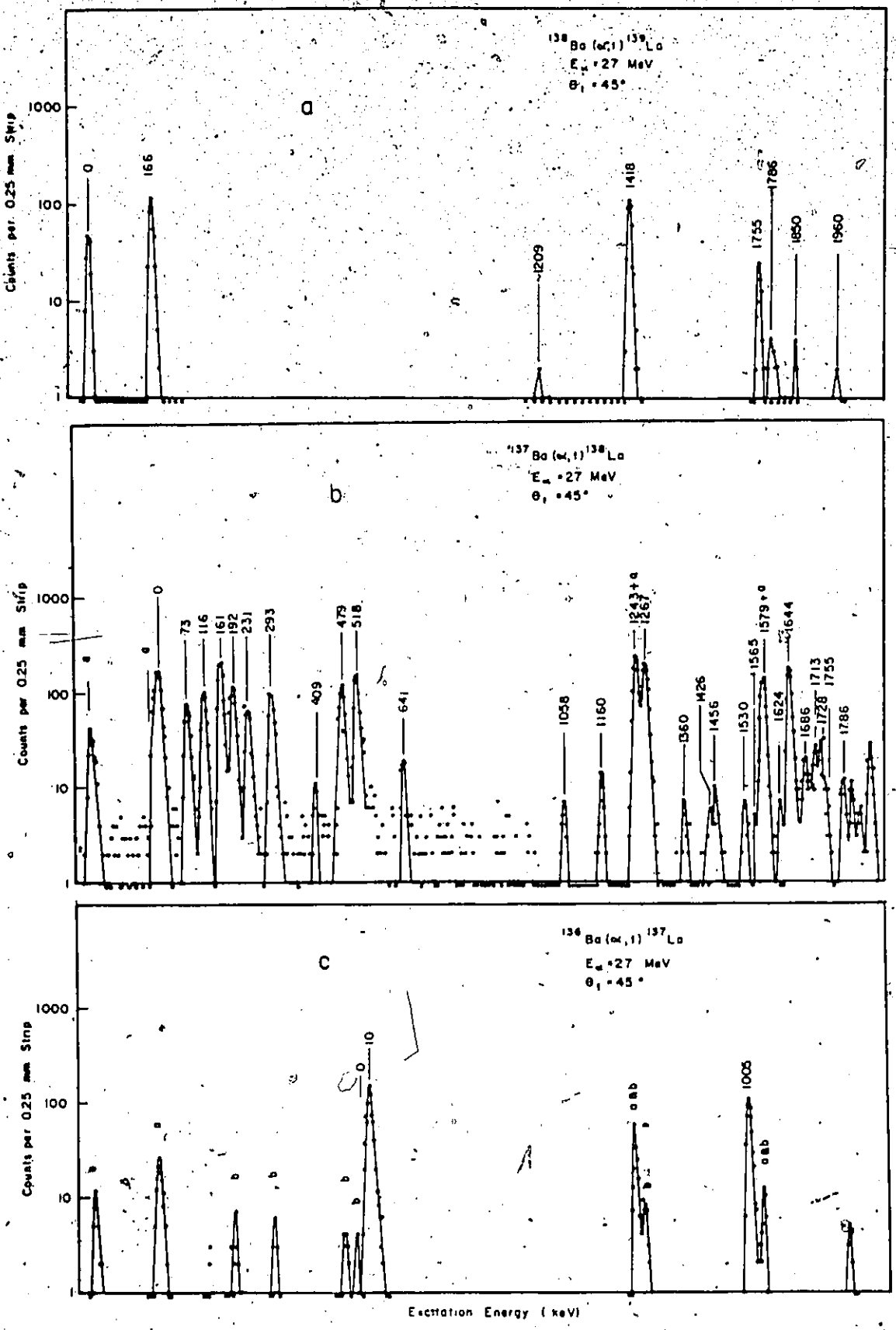
a
^{138}Ba (α,t) ^{139}La
E_α = 27 MeV
θ_t = 45°
Counts per 0.25 mm Strip
0
166
1209
1418
1755
1786
1850
1960
b
^{137}Ba (α,t) ^{138}La
E_α = 27 MeV
θ_t = 45°
Counts per 0.25 mm Strip
0
73
116
161
192
231
293
409
479
518
641
1058
1160
1243+a
1267
1360
1426
1456
1530
1565
1579+a
1624
1644
1686
1713
1728
1755
1786
c
^{136}Ba (α,t) ^{137}La
E_α = 27 MeV
θ_t = 45°
Counts per 0.25 mm Strip
0
10
1005
Excitation Energy (keV)

for comparison. The ^{136}Ba target contains ~ 10% each of ^{137}Ba and ^{138}Ba isotopes and so the stronger levels in ^{138,139}La also appear in the ^{137}La spectrum. In the course of this work we were able to determine the relative Q-values for the three (α,t) reactions using the ^{139}La peaks present in both the ^{137}La and ^{138}La spectra. The differences in the Q-values come out to be:

$$(^{137}\text{Ba} \rightarrow {}^{138}\text{La}) - (^{138}\text{Ba} \rightarrow {}^{139}\text{La}) = -178 \pm 2 \text{ keV}$$

$$(^{138}\text{Ba} \rightarrow {}^{139}\text{La}) - (^{136}\text{Ba} \rightarrow {}^{137}\text{La}) = +713 \pm 3 \text{ keV}.$$

The first result would seem to agree with the difference in the published Q-values (Gove and Wapstra 1972), both of which are uncertain by 14 keV. However our measurement should be sensitive only to the neutron separation energies in the relevant barium and lanthanum isotopes while the 14 keV uncertainty arises from the ^{138}La → ^{138}Ba positron end-point energy. The isotopic mass differences have been measured by a variety of techniques, i.e. (n,γ) (γ,n) and (d,p), and do not agree amongst themselves. Our measurement is inconsistent by 11 keV with the adopted values (Gove and Wapstra 1971).

If the published Q-value for ^{138}Ba(α,t)^{139}La is accepted as the correct one, then the ^{136}Ba(α,t)^{137}La Q-value becomes -14.326±0.017 MeV. Previously the mass of ^{137}La was available only from systematics. The quoted estimate of the above Q-value is -14.190 MeV.

2.2c The $^{139}La(d,t)^{138}La$ Reaction

As the analysis of the proton transfer studies progressed, it became evident that a better evaluation of the ℓ_n-admixtures was desired than that quoted by the earlier workers. The DWBA calculations for the $\ell_n = 0$ and $\ell_n = 2$ angular distributions at $E_d = 16$ MeV (given in Fig. 2.10) show that these curves are quite similar beyond 25° and forward angle data are necessary to extract reliable amplitudes for the mixed ℓ-values. The lowest angle in the work of Lasijo *et al.* was 22°. Thus it seemed reasonable to extend the observations to more forward angles. At the same time we hoped to improve on the 18 keV resolution of the earlier experiments.

Accordingly, a limited study of $^{139}La(d,t)^{138}La$ reaction was carried out at 16 MeV beam energy. Relatively short exposures (varying between 2000 and 5000 μ coulomb) were made at six angles between 7.5° and 25°. The resolution in these exposures was ∿ 11 keV. The spectrum of the low-lying levels taken at 18° is compared with the same region of a (^{3}He,d) spectrum in Fig. 2.4. In the (d,t) spectra one is able to see that the 518 keV peak is broader than the others. When that region of each plate was rescanned in $\frac{1}{8}$ mm strips, a definite doublet made its appearance. The peak fitting programme SPECTR gives levels at 510 and 518 keV, which is extremely reassuring as the γ-ray coincidence data (to be discussed in Chapter III) requires levels at 510.5 and 518.7 keV. The other point of difference between these results and the previous work is the extremely weak peak at ∿ 642 keV. This is

Fig. 2.4

A comparison of the $^{139}La(d,t)^{138}La$ and $^{137}Ba(^{3}He,d)^{138}La$ spectra for the region of ^{138}La below 650 keV excitation.

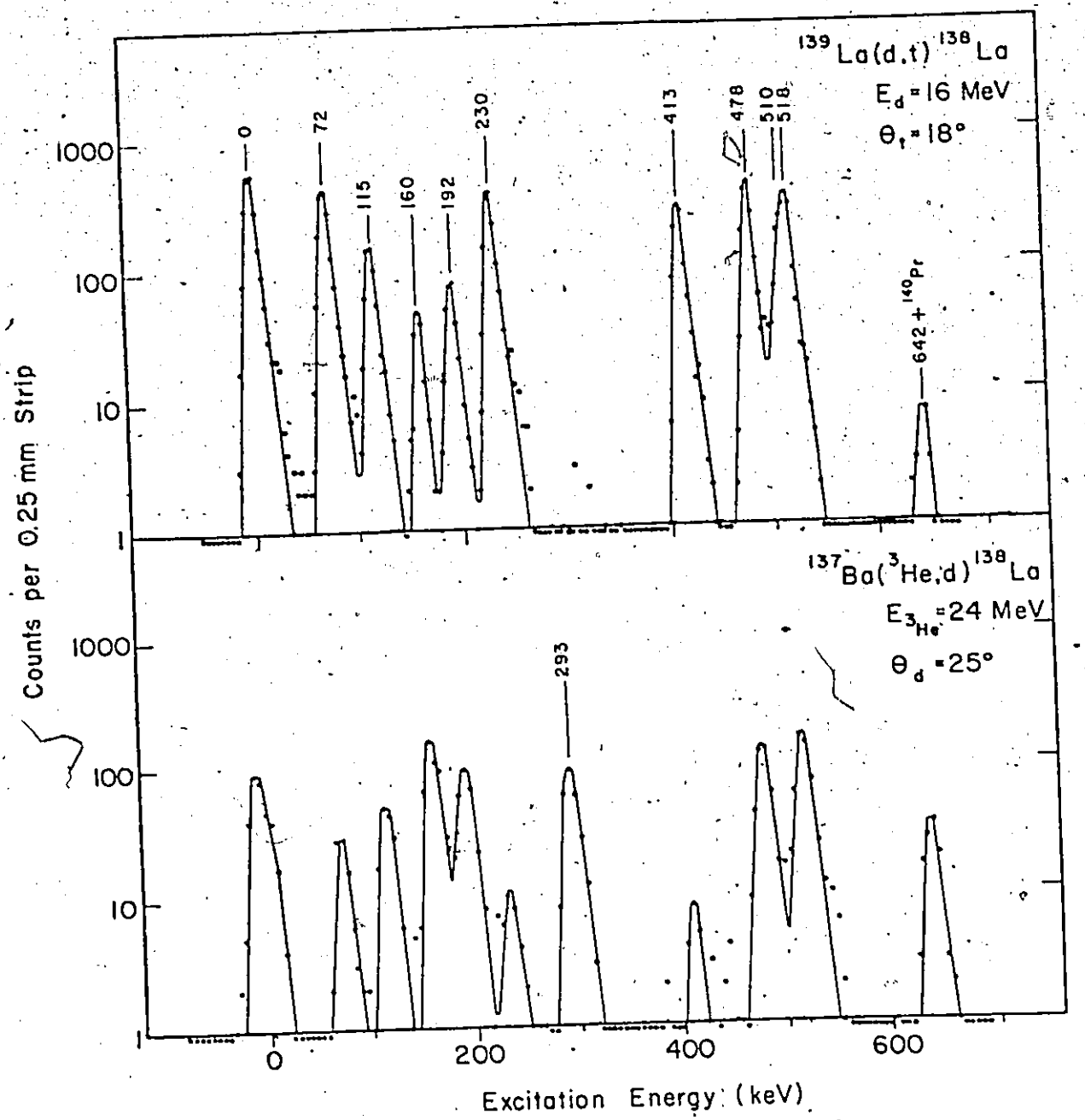
^{139}La(d,t)^{138}La
E_d = 16 MeV
θ_t = 18°
0
72
115
160
192
230
413
478
510
518
642 + ^{140}Pr
^{137}Ba(^{3}He,d)^{138}La
$E_{^3He}$ = 24 MeV
θ_d = 25°
293
Counts per 0.25 mm Strip
1000
100
10
1
0
200
400
600
Excitation Energy (keV)

discussed in the next paragraph.

In addition to these short exposures, two relatively long exposures (∿ 11000 μ coulomb) were made at 40° and 55°. The spectrum taken at 55° is shown in Fig. 2.5. The peaks at 0, 72,115, 230, 478 and 518 keV were too strong to be counted. The resolution was comparable to the shorter exposures. The peak at 642 keV is still very weak and may correspond in fact to the first excited state of ^{140}Pr since we expect some ^{141}Pr impurity in the target. Similarly, other strongly populated states in ^{140}Pr (Hussein *et al.* 1974) at 287 and 331 keV could be present under the levels at 900 and 937 keV. If this is true, then the new level (not reported by Lasijo *et al.*) seen at 1033 keV could be due, at least in part, to the 420 keV state of ^{140}Pr. Unfortunately, in the (^{3}He,d) data (Fig. 2.1), an extremely weak peak at ∿ 1033 keV has to be regarded as the 1209 keV state of ^{139}La. In addition to ^{141}Pr there may be another trace impurity in the ^{139}La target which produces weak peaks seen at 303, 587, 798 keV, etc. Their Q-values are such that ^{133}Cs(d,t)^{132}Cs could be responsible but unfortunately no information is available about the excited states of ^{132}Cs to the present date. Of course, one cannot rule out the possibility that the peaks actually belong to ^{138}La. They are weaker by almost two orders of magnitude than the strong peaks and neither Lasijo *et al.* nor Helton *et al.* would have been able to see them.

The energies of all the levels populated in (d,t) are given in Table 2-2, where they are also compared with the earlier data. The low-lying levels show very good agreement with our proton

Fig. 2.5

The triton spectrum from the $^{139}La(d,t)^{138}La$ reaction. Several of the peaks at low excitation were too strong to be counted in this long exposure. Impurity peaks are suitably labelled.

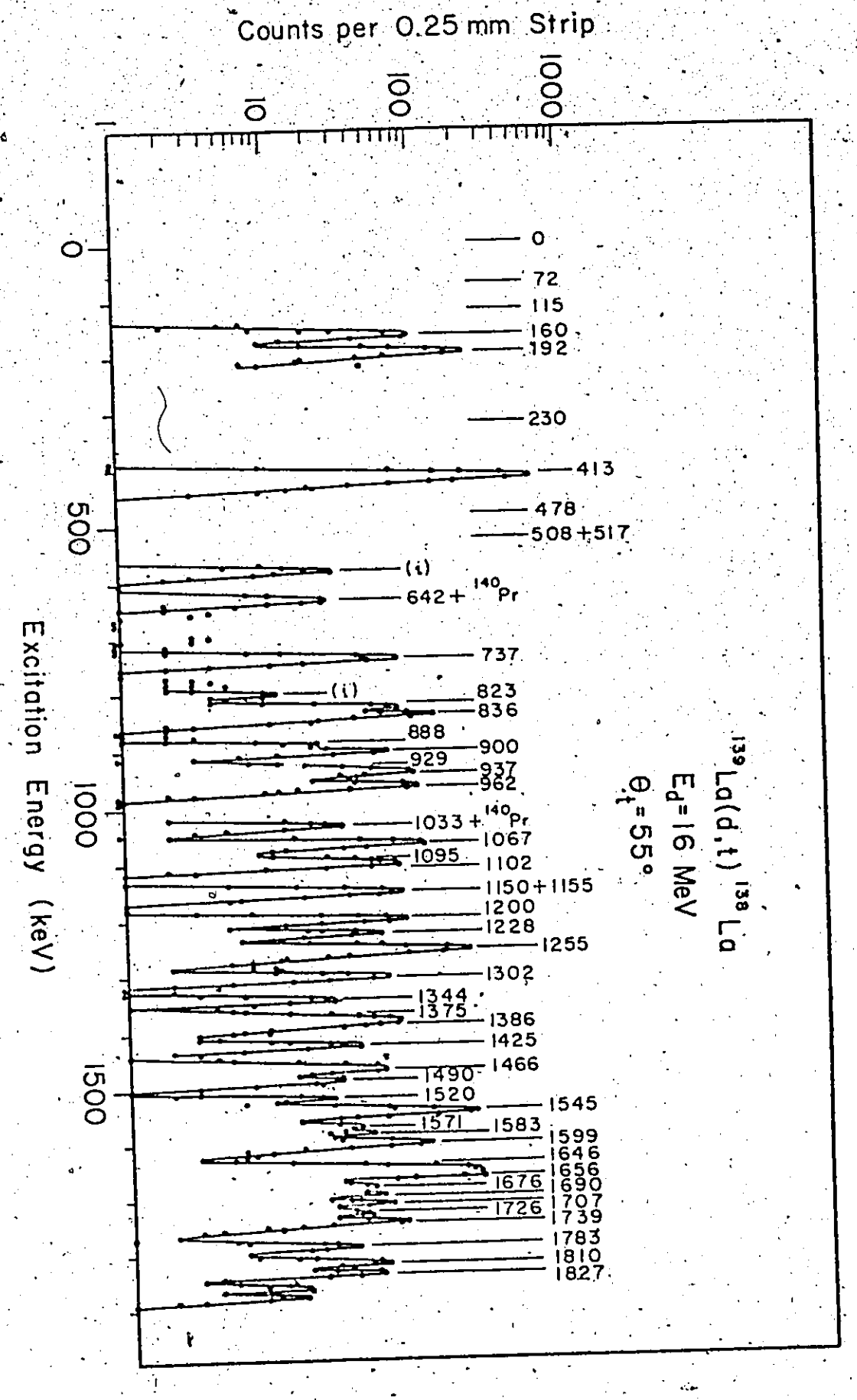
Counts per 0.25 mm Strip
1
10
100
1000
Excitation Energy (keV)
0
500
1000
1500
0
72
115
160
192
230
413
478
508+517
(i)
642+ 140Pr
737
(i)
823
836
888
900
929
937
962
1033+ 140Pr
1067
1095
1102
1150+1155
1200
1228
1255
1302
1344
1375
1386
1425
1466
1490
1520
1545
1571
1583
1599
1646
1656
1676
1690
1707
1726
1739
1783
1810
1827
139La(d,t)138La
Ed=16 MeV
θlab=55°

transfer data and the data of Lasijo *et al.*. Above 400 keV the values quoted by Helton *et al.* become systematically high. The level reported by Lasijo *et al.* at 833 keV turns out to be a doublet at 823 and 836 keV. A closer look at the relevant columns in Table 2.2 will reveal that some other levels in the higher region were also resolved as doublets in our (d,t) studies. It is difficult to correlate the levels above 1 MeV with those seen in the proton transfer reactions because of the high level density but it does appear that the agreement between the excitation energies is good. The two sets of (d,t) values are quite consistent.

The differential cross-sections observed in the (d,t) reaction are given in Table A3 of the appendix. Data for the low-lying levels are taken from the 25° exposure and the 55° exposure is used for the higher excited states. The absolute cross-sections agree, within the limits of experimental uncertainty, with the values reported by Lasijo *et al.*

2.3 The $^{138}Ba(^{3}He,d)^{139}La$ Reaction

As already mentioned in section 2.2a, it was necessary to carry out a $^{138}Ba(^{3}He,d)^{139}La$ exposure in order to identify the ^{139}La impurity peaks in the ^{138}La spectra. In fact, inspection of Fig. 2.1 reveals that the regions near 0, 1245, 1380, 1575, 1610 and 1785 keV excitation are seriously contaminated by peaks due to ^{139}La and the seemingly strong level at $\sim$ 1610 keV is entirely due to the ^{138}Ba impurity. This observation drives home an important cautionary note about the study of odd-odd-nuclei. Since

the single particle strength in such a nucleus is fragmented into many states of different J, which is not the case in the neighbouring odd-even nuclei, even a small degree of isotopic contamination represents a serious problem. In the present instance, the ^{138}Ba content would have to be reduced to less than 1% (i.e. a tenth of the present abundance) before its effect on the ^{138}La spectrum could be safely ignored.

Since it was not possible to obtain more highly enriched ^{137}Ba the only way to extract reliably the angular distributions for the ^{138}La levels (at the excitation energies mentioned in the last paragraph) was first to obtain the angular distributions for ^{139}La so that the impurity peaks could be properly subtracted at each angle. The levels of ^{139}La have been investigated by various researchers (Hill *et al.* 1968, Bouley *et al.* 1969, and Wildenthal *et al.* 1971) employing different modes and techniques. All these experimenters agree about the ground state and first excited state being $7/2^+$ and $5/2^+$ respectively. Wildenthal *et al.* have determined ℓ_p values and spectroscopic strengths of the states up to 2300 keV excitation by investigating the $^{138}Ba(^3He,d)^{139}La$ and $^{140}Ce(d,^3He)^{139}La$ reactions. States with ℓ_p = 0, 2, 4 and 5 have been clearly identified.

In an odd-odd nucleus, states can be populated with mixed ℓ-values. Thus in ^{138}La, the simple shell model leads one to expect admixtures of ℓ_p = 2 and 4 for the low-lying levels. Since a lower ℓ tends to have a dominant effect on the shape of the observed angular distribution, the extraction of reliable spectro-

scopic strengths for the higher ℓ demands that the shapes assumed for the individual ℓ-values be correct (especially for the lower ℓ, of course). The DWBA calculations cannot be trusted to this accuracy and so it is always better to use an empirical shape whenever possible. Obviously, the $^{138}Ba(^{3}He,d)^{139}La$ reaction provides an ideal means of deriving such empirical shapes to be used in the analysis. Not only does ^{139}La have known states with the required ℓ_p values but also the ground state Q-values for the two reactions differ only by 178 keV so the observed angular distributions need not be modified for a possible Q-value dependence. Of course to get these shapes we had to re-investigate the $^{138}Ba(^{3}He,d)^{139}La$ reaction at 24 MeV as Wildenthal *et al.* used a bombarding energy of 40 MeV.

There were two reasons, then, for carrying out a complete investigation of proton transfer on ^{138}Ba. As the analysis progressed it became clear that our superior resolution, compared to the 40 MeV data, also meant that we were able to improve on the existing information about ^{139}La. Although the experimental set-up and the method of data analysis were identical to the earlier experiments, more care was necessary in planning the exposures. The ratio of the $\ell_p = 2$ and $\ell_p = 4$ cross-sections can be estimated from the intensities of the ground state ($\ell_p = 4$) and 166 keV ($\ell_p = 2$) state of ^{139}La appearing in the ^{138}La spectra. As a function of angle this ratio varies between 8 and 11. To obtain reasonable statistics in the ground state peak without over-exposing

the stronger peak, it was necessary to make both long and short exposures at each angle. Only at 22.5°, the first minimum in the $\ell_p = 2$ angular distribution, was this practice abandoned by carrying out a medium length exposure of 3000 μ coulombs. The rest of the exposures varied from 420 μ coulomb for the shortest to 10,000 μ coulomb for the longest. Data were taken at 15 lab angles ranging from 7.5° to 65°. Since the highest resolution was not necessary in this study, a fairly thick target was used for these exposures. However some exposures were carried out with a thinner target in order to identify the levels with greater precision and it is one of those spectra which is shown in Fig. 2:1.

Except for the two levels near 1780 keV, there is generally good agreement between our precise energies and those quoted by Wildenthal *et al*. With only 35 keV resolution, they reported a single peak at 1780±14 keV, its angular distribution being a mixture of $\ell_p = 0$ and 2. Our spectra show this resolved into two distinct levels at 1755 and 1786 keV. In Fig. 2.6 we present the observed angular distributions for most of the ^{139}La levels up to 2 MeV. It is clear that the differential cross-section for the 1755 keV state has essentially the same shape as the 166 and 1960 keV levels, for which ℓ_p is known to be 2. Similarly, the 1786 keV level must have $\ell_p = 0$ since its angular distribution is consistent with the known $\ell_p = 0$ state at 1209 keV.

Figure 2.7 presents the angular distributions obtained from the DWBA calculations for the four relevant ℓ-values. The set of

Fig. 2.6

The deuteron angular distributions for most of the levels observed in the $^{138}Ba(^{3}He,d)^{139}La$ reaction. The solid curves are a compromise between the observed differential cross-sections and those obtained from a DWBA calculation.

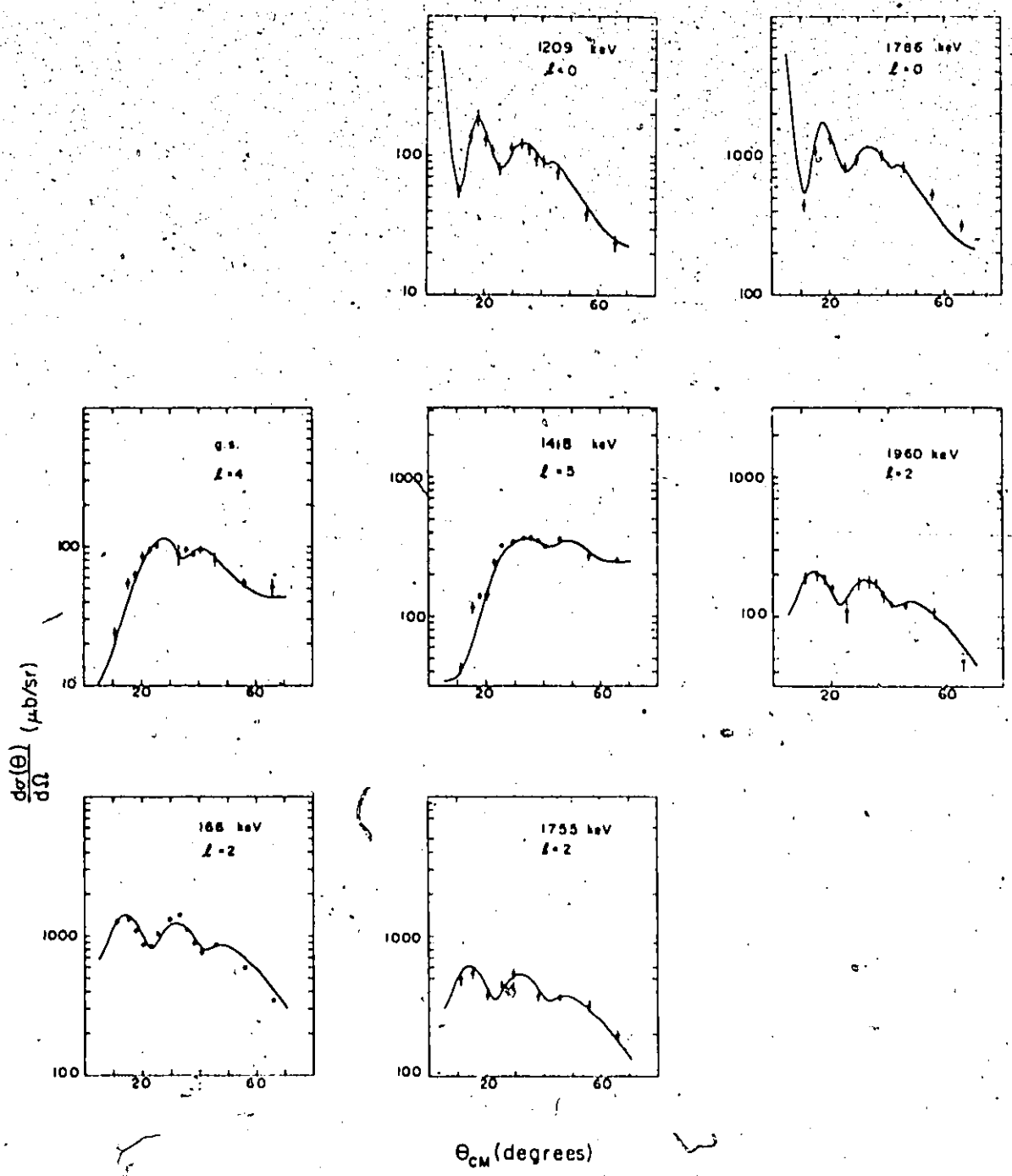
1209 keV
ℓ = 0
1786 keV
ℓ = 0
g.s.
ℓ = 4
1418 keV
ℓ = 5
1960 keV
ℓ = 2
166 keV
ℓ = 2
1755 keV
ℓ = 2
dσ(Θ)/dΩ (μb/sr)
Θ_CM (degrees)

Fig. 2.7

The angular distributions calculated from DWBA for the $^{137}Ba(^{3}He,d)^{138}La$ reaction are compared with the adopted ℓ-shapes.

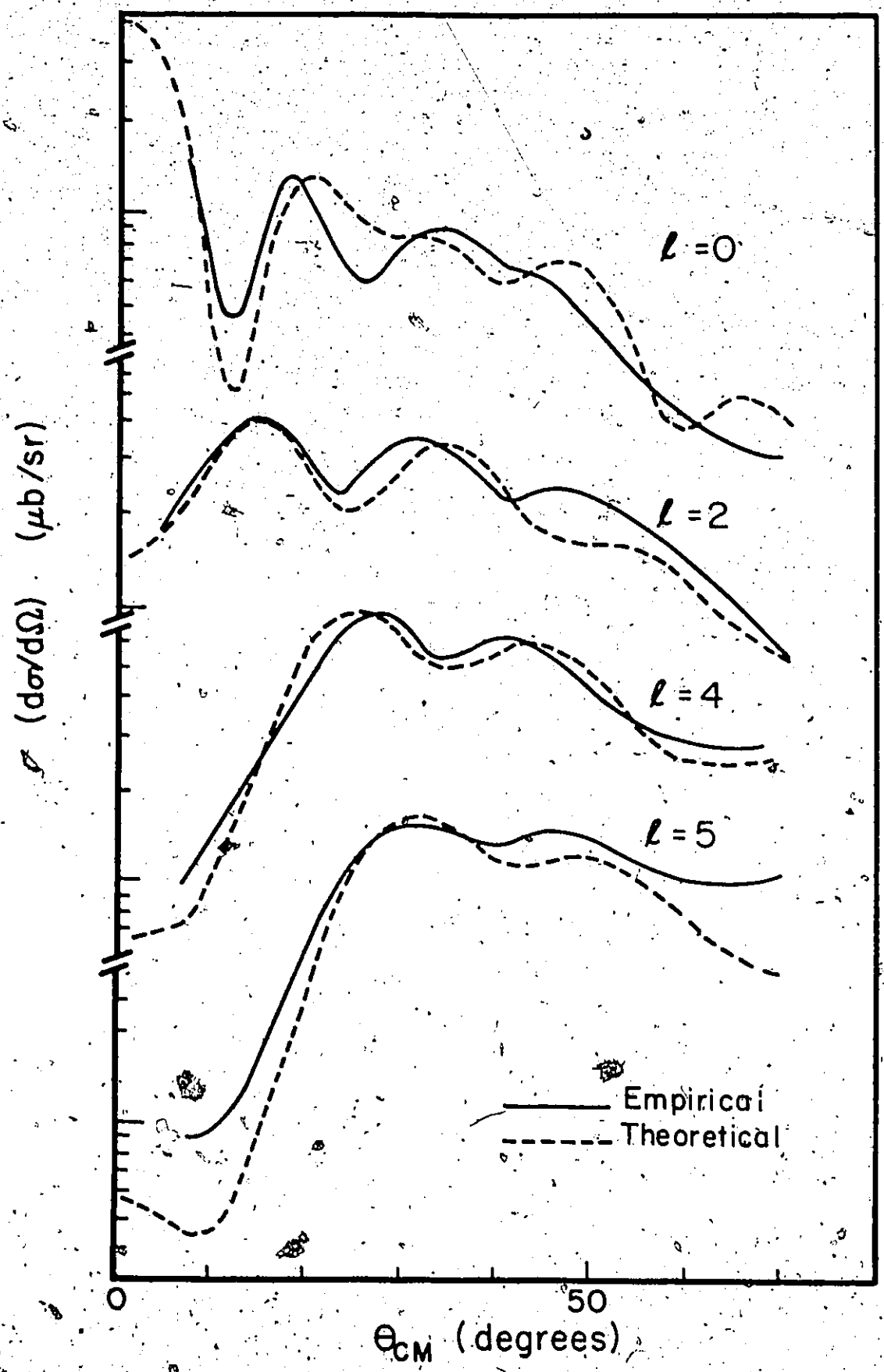
ℓ =0
ℓ =2
ℓ =4
ℓ =5
Empirical
Theoretical
0
50
θCM (degrees)
σ (dσ/dΩ) (μb/sr)

optical model parameters employed is given in Table 2.3. They are the same as used by Macphail (1973) in his calculations of the $^{143}Nd(^{3}He,d)^{144}Pm$ reaction at the same beam energy. He adopted them from Ishimatsu *et al.* (1969). The empirical ℓ-shapes, also shown in the figure, are a compromise between the theoretical curves and the observed angular distributions. They essentially agree but the first minimum of the empirical distributions is shifted towards somewhat smaller angles, indicating that one actually needs a deeper well.

Spectroscopic factors for the ^{139}La levels were obtained by comparing the empirical cross-sections at their first observed maxima to the values predicted by the DWBA calculations. The results are given in Table 2.4 which also lists the corresponding data of Wildenthal *et al.*. Except for the 1755 and 1786 keV levels, the agreement is reassuring. Most probably they divided the total strength of their 1780 keV peak equally into $\ell_p = 0$ and 2. We find that the $\ell_p = 0$ level is much stronger than the other one.

2.4 The Proton Transfer Results for ^{138}La

We return now to a discussion of the further analysis of the ^{138}La proton transfer data. The $^{137}Ba(^{3}He,d)^{138}La$ angular distributions provide ℓ_p values and spectroscopic strengths for most of the levels observed in this reaction. The $^{137}Ba(\alpha,t)^{138}La$ data were used in conjunction with $(^{3}He,d)$ data to show that consistent ℓ_p values can also be derived by the ratio method.

Table 2.3

Optical Model Parameters for the $^{137}Ba(^{3}He,d)^{138}La$ Reaction

Particle	V (MeV)	r_{oc} (fm)	r_o (fm)	a (fm)	W_S (MeV)	W_D (MeV)	r'_o (fm)	a' (fm)	V_{SO} factor	Non-local Correction Parameter
^{3}He	-172.0	1.40	1.14	0.70	-16.0	0	1.54	0.80	0	0.25
d	-101.4	1.30	1.085	0.857	0	61.0	1.29	0.788	0	0.54
p	*	1.20	1.20	0.65	0	0	0	0	8.0	0.85

$U(r) = U_c(r) + V(e^{x} + 1)^{-1} + iW_S(e^{x'} + 1)^{-1} + iW_D \frac{d}{dx'}(e^{x'} + 1)^{-1}$, where

$x = (r - r_o A^{1/3})/a$ and $x' = (r - r_o' A^{1/3})/a'$. $U_c(r)$ corresponds to the potential due to a uniformly charged sphere, radius $r_{oc}A^{1/3}$, charge $Z_A e$.

Finite range correction parameter = 0.770.

No radial cut-off was employed.

*Adjusted to reproduce separation energy.

Table 2.4

The ℓ_p Values and Spectroscopic Strengths for $^{138}Ba(^3He,d)^{139}La$

This Work			Wildenthal *et al.*		
E_x (keV)	ℓ_p	$S_{\ell j}$	E_x (keV)	ℓ_p	$S_{\ell j}$
0	4	0.39(4)	0	4	0.43
165.6(5)	2	0.92(3)	166 (1)	2	0.94
1209 (2)	0	0.096(5)	1210 (9)	0	0.09
1418 (2)	5	0.96(3)	1420 (11)	5	0.84
1755 (3)	2	0.46(5)	1780 (14)	0	0.65
1786 (3)	0	0.90(18)		2	0.73
1960 (2)	2	0.16(3)	1960 (15)	2	0.16

2.4a The Angular Distributions and Spectroscopic Strengths

The excitation energies and differential cross-sections of the levels excited in $^{137}Ba(^{3}He,d)^{138}La$ reaction have already been listed in Tables 2.2 and A-1. Levels for which the cross-sections are missing at some angles were obliterated by impurity peaks. The angular distributions, presented in Fig. 2.8, have been fitted using the appropriately normalized empirical ℓ-shapes obtained from the $^{138}Ba(^{3}He,d)^{139}La$ experiment. As the levels of an odd-odd nucleus can be populated by mixed ℓ-values, the fitting procedure (except for $\ell = 5$) allowed an incoherent mixture of either $\ell_p = 0$ and 2 or $\ell_p = 2$ and 4. It turned out that only six of them (all from the low-lying group) showed pronounced admixtures. For the rest of the levels the amplitude of the competing ℓ was either negative or had too large an error to be statistically significant. Table 2.5 lists the ℓ_p values and the spectroscopic strengths. As already discussed, the shape of a mixed ℓ-transfer is generally dominated by the lower ℓ-value. Thus the strengths for $\ell_p = 4$ admixtures are uncertain by more than 50%. For the same reason appreciable contributions of $\ell_p = 2$ might have been missed from the apparently pure $\ell_p = 0$ distributions.

Definite ℓ-assignments have been made for all but four levels observed in the $(^{3}He,d)$ reaction. The 409 keV state was not fitted as it is very weakly populated at all angles. The 510 and 518 keV levels had to be treated as a composite peak. The cross-sections for the 1154 keV peak are quite erratic. Perhaps it is a doublet or even a triplet.

Fig. 2.8

The differential cross-sections for the levels observed in the $^{137}Ba(^{3}He,d)^{138}La$ reaction. The solid curves are the best fits to the data using the empirical ℓ-shapes.

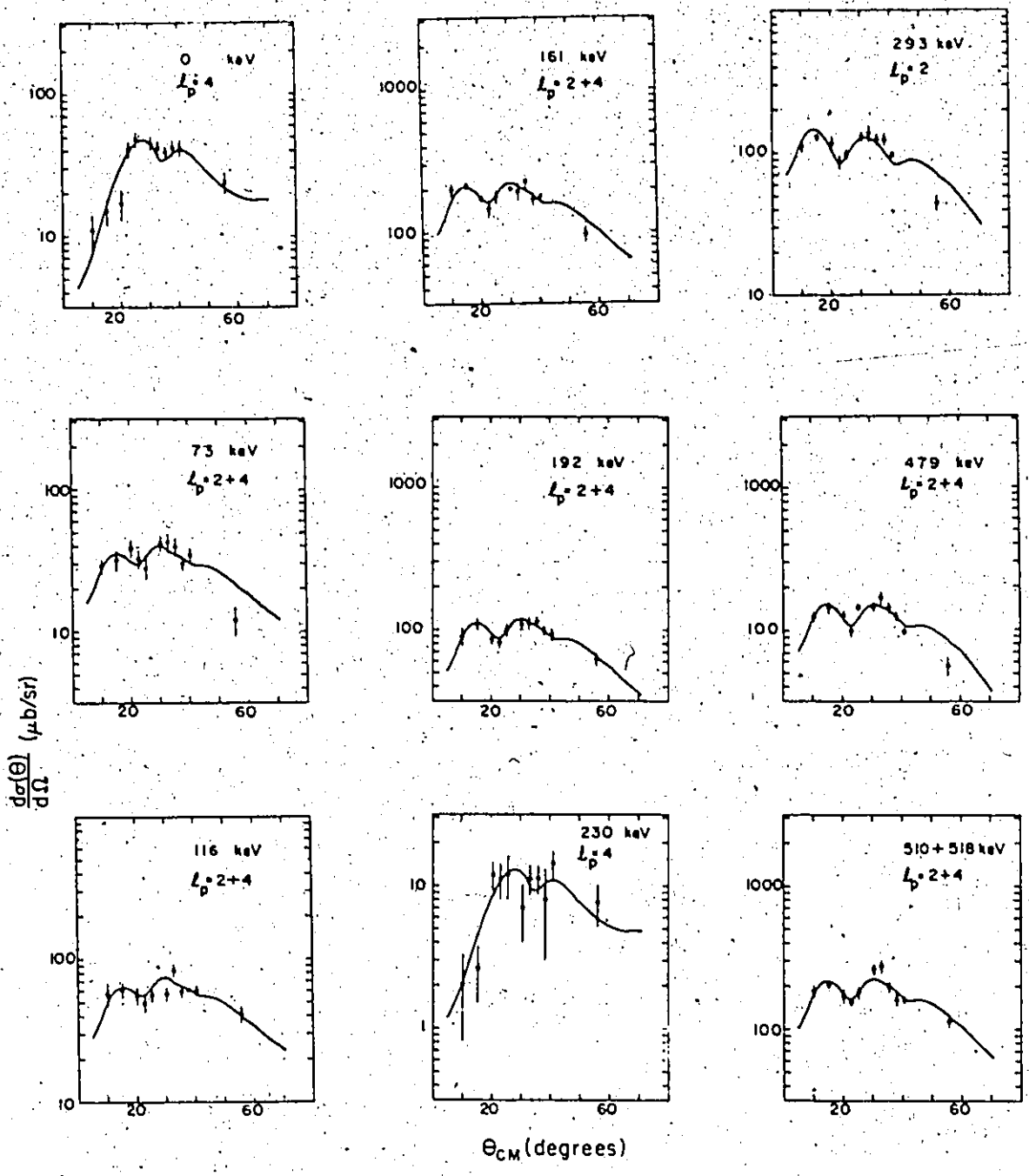
0 keV
L_p=4
161 keV
L_p=2+4
293 keV
L_p=2
73 keV
L_p=2+4
192 keV
L_p=2+4
479 keV
L_p=2+4
116 keV
L_p=2+4
230 keV
L_p=4
510+518 keV
L_p=2+4
$\frac{d\sigma(\Theta)}{d\Omega}$ (μb/sr)
Θ_{CM} (degrees)

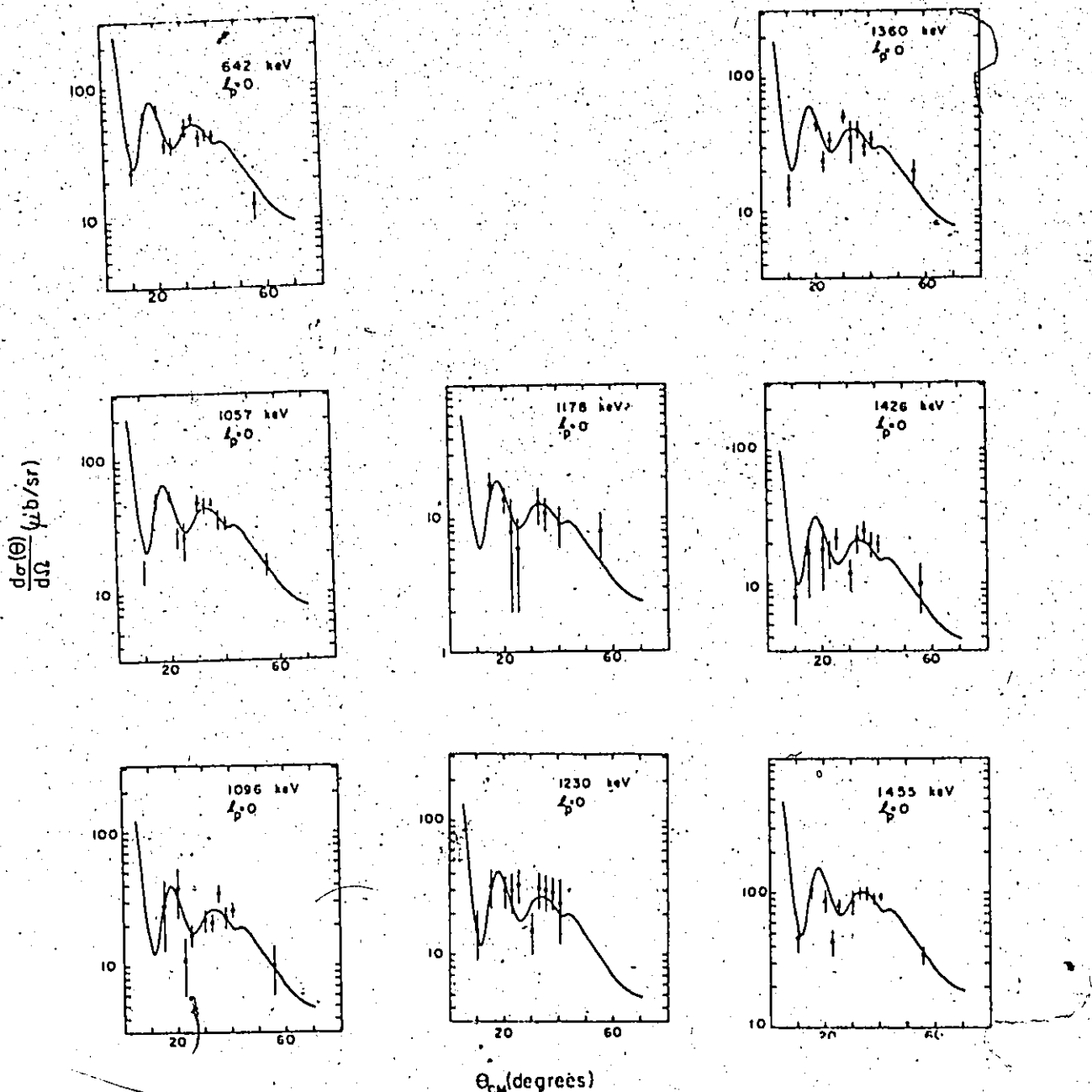
642 keV
l_p=0
1360 keV
l_p=0
1057 keV
l_p=0
1178 keV
l_p=0
1426 keV
l_p=0
1096 keV
l_p=0
1230 keV
l_p=0
1455 keV
l_p=0
100
10
20
60
$\frac{d\sigma(\theta)}{d\Omega}$ (μb/sr)
θ_{CM}(degrees)

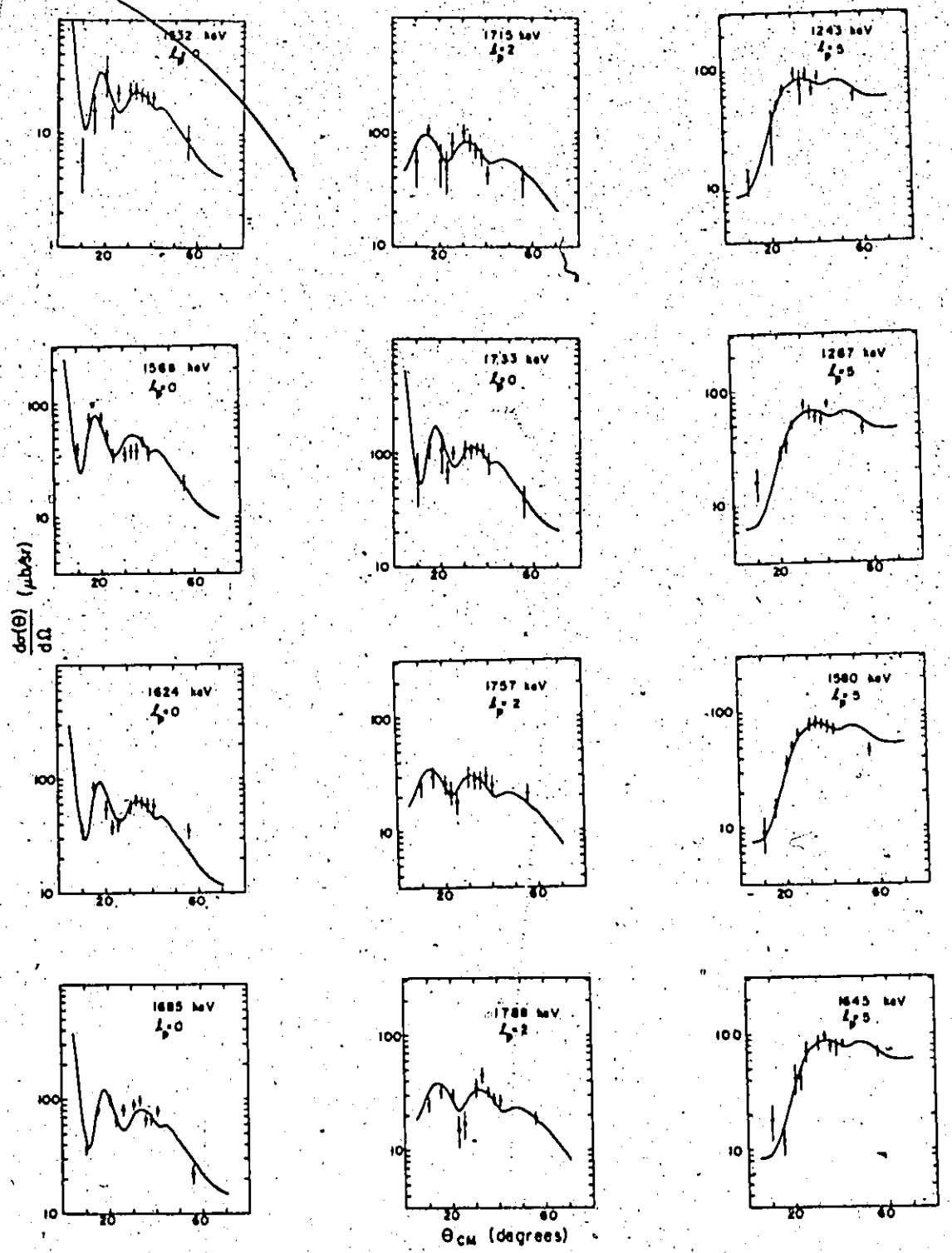
1532 keV
L_p=0
1715 keV
L_p=2
1243 keV
L_p=5
1568 keV
L_p=0
1733 keV
L_p=0
1267 keV
L_p=5
1624 keV
L_p=0
1757 keV
L_p=2
1580 keV
L_p=5
1685 keV
L_p=0
1788 keV
L_p=2
1645 keV
L_p=5
$\frac{d\sigma(\theta)}{d\Omega}$ (μb/sr)
θ_{CM} (degrees)

Table 2.5

The ℓ_p Values and Spectroscopic Strengths $C^2(\frac{2J_B+1}{2J_A+1})S$ for $^{137}Ba(^3He,d)^{138}La$

E_x(keV)	$\ell_p = 0$	$\ell_p = 2$	$\ell_p = 4$	$\ell_p = 5$
0			1.3(1)	
73		0.13(4)	0.4(3)	
116		0.24(7)	0.8(6)	
161		0.84(14)	1.7(13)	
192		0.45(5)	1.0(5)	
230			0.4(1)	
293		0.65(5)		
479		0.77(8)	<0.1	
510, 518		0.89(9)	1.5(11)	
642	0.12(3)			
1057	0.10(1)			
1096	0.05(1)			
1178	0.03(1)			
1230	0.05(2)			
1243				2.0(2)
1267				2.4(3)
1360	0.08(2)			
1426	0.03(1)			
1455	0.16(5)			
1532	0.04(1)			
1568	0.09(2)			
1580				2.7(9)
1624	0.11(2)			
1645				3.2(4)
1685	0.14(3)			
1715		0.31(6)		
1733	0.20(4)			
1757		0.11(2)		
1788		0.12(2)		

Besides providing the empirical ℓ-shapes the $^{138}Ba(^{3}He,d)^{139}La$ experiment proved to be essential in unravelling the angular distributions of the 1568 and 1580 keV levels of ^{138}La. From the ORNL analysis of the target composition and our determination of the precise excitation energies and ℓ_p-values for the interfering levels of ^{139}La we were able to extract the angular distributions for these two levels. The 1580 keV state turns out to be the fourth member of the quartet of $\ell_p = 5$ states expected to be seen in the proton transfer reactions. The other state (1568 keV) conforms to an $\ell_p = 0$ angular distribution.

2.4b $(^{3}He,d)$ to (α,t) Cross-section Ratios

The assignment of ℓ values by fitting angular distribution data is generally very reliable but it involves a lot of work. Spectra have to be taken at many angles maintaining consistent experimental conditions throughout. If the cross-sections are small, exposures are long and the complete experiment becomes very tedious. It would be worthwhile to look for some other simpler method.

As we have already mentioned, the $(^{3}He,d)$ and (α,t) reactions populate states of different ℓ_p values with widely different cross-sections. Only a few peaks stand out in the (α,t) spectrum for $E_x > 1000$ keV and these are $\ell_p = 5$ transitions as the $(^{3}He,d)$ angular distributions verify. In the low-lying group the pure $\ell_p = 4$ level at 230 keV is relatively much stronger in (α,t) than in $(^{3}He,d)$. Thus a naive ℓ-assignment can be made by just comparing the two spectra.

A more quantitative deduction is based on the ratio of the cross-sections in the two reactions (Lu and Alford, 1971). For odd-A nuclei, where one is only interested in assigning a pure ℓ-value, this method has been widely used. Its success depends upon the fact that, for any given ℓ, both cross sections involve the same spectroscopic factor which cancels out in the ratio. Macphail (1973) was the first one to apply this method to an odd-odd nucleus. He used it to determine the ℓ-values of the levels populated in ^{144}Pm by the proton transfer reactions. In his case this was the only information available. Here we shall test the method to see how reliable it is by comparing the ℓ-assignments derived from the two different methods.

The selection of appropriate angles can be tricky. It is best to choose angles in the slowly varying regions of the angular distributions, but this condition is hard to satisfy when a number of levels with different ℓ-values are involved. The ones used in our calculations are 35° for (^{3}He,d) and 45° for (α,t) at which most of the low-lying levels are uncontaminated by impurity peaks.

A theoretical estimate of the (^{3}He,d) to (α,t) cross-section ratios, for various ℓ-values, can be obtained directly from the DWBA calculations. As the ratios also depend upon the Q-values, the calculations were performed for (^{3}He,d) Q-values ranging from -1.0 to 1.0 MeV, in 0.5 MeV steps, and the corresponding Q-values for (α,t). The optical model parameters employed for (^{3}He,d) have been given already in Table 2.3 and those for (α,t) (Burke and Waddington, 1972) are listed in Table 2.6.

Table 2.6

Optical Model Parameters for the $^{137}Ba(\alpha,t)^{138}La$ Reaction

Particle	V MeV	r_{oc} (fm)	r_o (fm)	a (fm)	W_S (MeV)	W_D (MeV)	r_o' (fm)	a' (fm)	V_{SO} factor	Non-local Correction Parameter
n	-200	1.30	1.40	0.60	-20		1.40	0.60	0	0.20
p	-200	1.30	1.40	0.60	-50		1.40	0.60	0	0.25
α	*	1.25	1.25	0.65	0	0	0	0	0	0.85

The expression for the potential is the same as that used for (^{3}He,d) reactions.

No radial cut-off or finite range correction was employed.

*Adjusted to reproduce separation energy

The comparison of theory and experiment is shown in Fig. 2.9. Because of the uncertainty in the absolute normalization of DWBA calculations (especially for the (α,t) reaction) the theoretical ratios are renormalized, as a family, to fit the ratio measured for the 166 keV (ℓ_p = 2) level of ^{139}La. Ratios for other ℓ-values obtained from the known levels of ^{139}La, are also shown. As the ^{138}La levels can be populated by mixed ℓ-transfers, many of those points fall, appropriately, between the theoretical curves. The various symbols in the figure indicate the ℓ_p values deduced from the angular distribution data.

There are four levels for which the ℓ-assignments from the two different methods do not agree, and in addition the 230 keV data point lies slightly beyond the ℓ=4 line. The ratio method would suggest ℓ_p=2 or possibly ℓ_p=0+2 for the 642, 1532, 1568 and 1685 keV levels whereas their angular distributions are fitted by pure ℓ_p=0.

The ratio method employed here has not been used as the primary source of information about the nature of the ℓ-transfers, and hence it was not perfected. The slope of the theoretical curves depends to a large extent on the choice of the optical model parameters. Confidence in the method would be improved a great deal if more normalizing points were available from the states of known ℓ in the neighbouring odd-A nuclei and over a wide range of Q-values. For unambiguous ℓ-assignments one should

Fig. 2.9

The $(^3He,d)/(\alpha,t)$ cross-section ratios. Cross-sections for $^{137}Ba(^3He,d)^{138}La$ are taken from the 35° data while those for $^{137}Ba(\alpha,t)^{138}La$ were measured at 45°. The curves are obtained from DWBA calculations, renormalized as a family to fit the observed $\ell_p = 2$ ratio for the 166 keV level of ^{139}La. Other ^{139}La points are indicated by the stars. The designation of the ^{138}La points is explained in the figure.

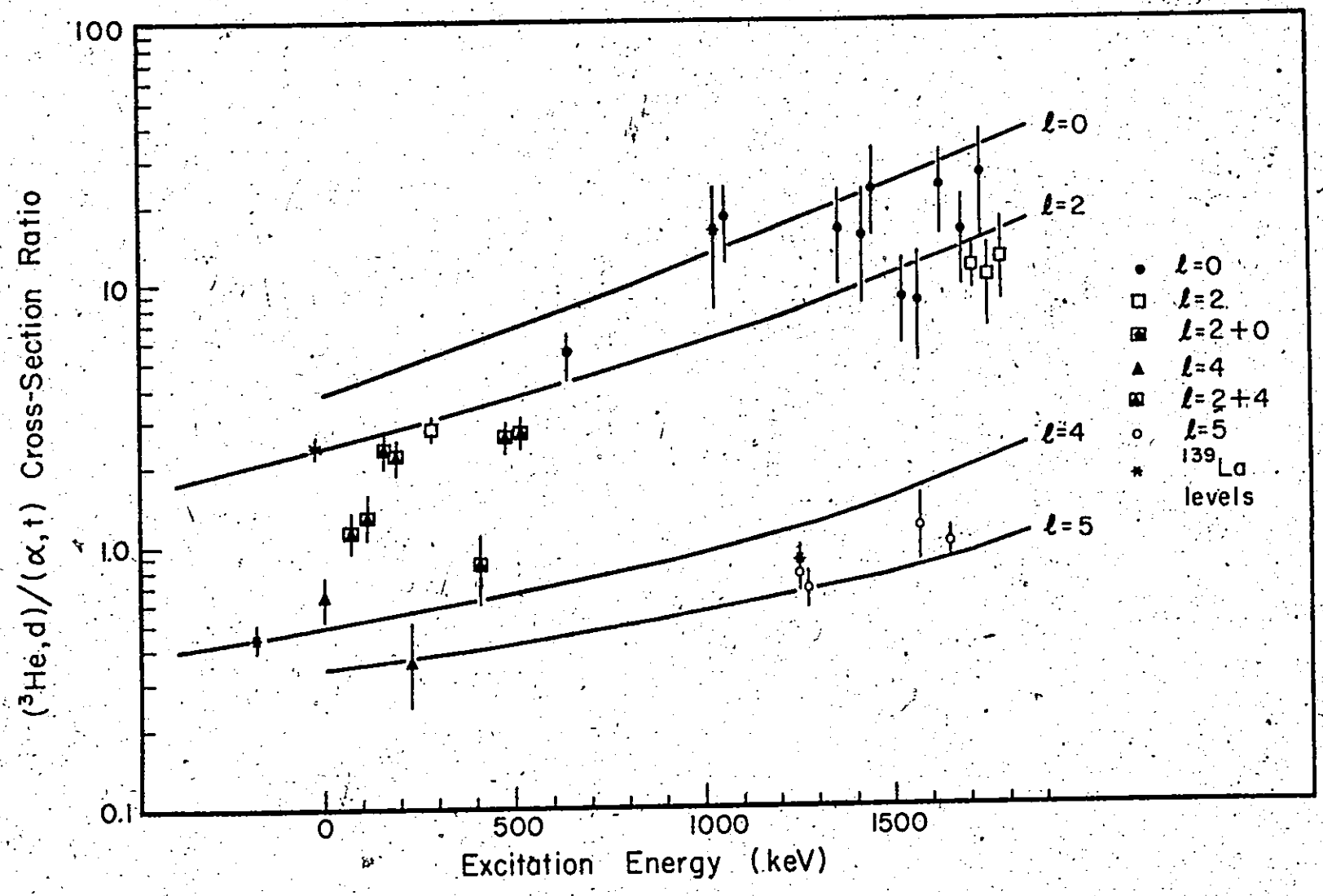
100
10
1.0
0.1
0
500
1000
1500
Excitation Energy (keV)
(³He, d)/(α, t) Cross-Section Ratio
ℓ=0
ℓ=2
ℓ=4
ℓ=5
ℓ=0
ℓ=2
ℓ=2+0
ℓ=4
ℓ=2+4
ℓ=5
¹³⁹La levels

have at least two very good exposures for each reaction. Our $\ell_p = 0$ points suffer from poor statistics in the (α,t) reaction. Briefly speaking, with a little more sophisticated calculations and careful experimentation, the ratio method can be considered an easy and fairly reliable alternative to the tedium of measuring the complete angular distributions.

2.4c The Sum Rules for Proton Transfer

As already discussed in Chapter I, the spectroscopic factors should satisfy certain sum rules. From shell model systematics the 6 protons in ^{137}Ba are expected to reside in the $1g_{7/2}$ and $2d_{5/2}$ orbits and so there should be a total of 8 vacancies in these orbits. The observed spectroscopic strengths for $\ell_p = 2$ and 4 in the low-lying levels of ^{138}La should sum to this number, i.e.

$$\sum_{J_B} \frac{2J_B+1}{2J_A+1} S_{\ell=4}^{j=7/2}(J_B) + \sum_{J_B} \frac{2J_B+1}{2J_A+1} S_{\ell=2}^{j=5/2}(J_B) = 8.$$

The total observed strength is compared with the sum rule limit in Table 2.7. We have taken the iso-spin coupling coefficient C^2 to be unity as the neutrons and protons are filling entirely different shells. It is not possible to compare $g_{7/2}$ and $d_{5/2}$ vacancies separately as the distribution of the protons between these two orbits is not self-evident. Our total observed strength, however, shows reasonable agreement. The basic cross-sections for $\ell_p = 4$ are small and so any cross-section allotted incorrectly to this configuration shows up as a large increase in the $\ell_p = 4$ spectroscopic strength.

Table 2.7

The Sum Rules for Proton Transfer

ℓ	j	Observed strength	Sum rule limit
2	5/2	4.0	8
4	7/2	~7	
5	11/2	10.3	12
0	1/2	1.1[a]	2
2	3/2	0.5[a]	4

[a] Below 1.8 MeV excitation.

To eliminate the uncertainties arising from the DWBA calculations and the absolute normalization of the experimental cross-sections, we have also used the impurity peaks of ^{139}La which appear in the ^{138}La spectrum to make a direct comparison of the ℓ_p = 2 and 4 spectroscopic strength seen in ^{138}Ba(^{3}He,d)^{139}La and ^{137}Ba(^{3}He,d)^{138}La. To do this, one only needs the areas of the two relevant ^{139}La peaks (g.s. and 166 keV) and the ten ^{139}La peaks (g.s. to 517) at any desired angle. In practice the process is somewhat complicated because the 166 keV state in ^{139}La and the ^{138}La ground state are not resolved. The intensity of the former can be obtained from the ^{139}La ground state peak since we know the ratio of these two peaks accurately from the ^{138}Ba(^{3}He,d)^{139}La experiment described in section 2.3. This means, however, that the statistical accuracy hinges on the weak ℓ_p = 4 peak. To make it as strong as possible relative to the other peaks in the spectrum it is desirable to have a relatively high abundance of ^{138}Ba in the target. The measurements were made at both 45° and 50° (where the ℓ_p = 4 cross-sections are relatively large and the appropriate region of the spectrum is entirely free from contaminating peaks) using a target made from ^{137}Ba (II) (see Table 2.1). The ratio of the combined ℓ_p = 2 and 4 cross-sections in ^{138}La and ^{139}La was observed to be 1.04±0.14 and 1.04±0.15 at 55° and 45° respectively. This confirms that the neutron hole in ^{137}Ba does not affect the configuration of the six valence protons. The hint that the total cross-section is larger

for $^{138}Ba(^{3}He,d)^{139}La$ is also understandable because the DWBA calculations predict that the $\ell_p = 2$ cross-section should increase by $\sim$ 5% for a Q-value increase of 250 keV. Since the centre of gravity of the $\ell_p = 2$ strength in ^{138}La is at 322 keV relative to its ground state, the average Q-value for the $^{137}Ba(^{3}He,d)^{138}La$ reaction is 334 keV higher than for the $\ell_p = 2$ state in ^{139}La.

The gap of $\sim$ 1.5 MeV between the $5/2^+$ and $3/2^+$ levels of ^{139}La leads us to believe that the second region of $\ell_p = 2$ strength near 1700 keV in ^{138}La arises from $d_{3/2}$ proton transfer. The other ℓ_p-values seen at high excitation obviously correspond to $s_{1/2}$ and $h_{11/2}$ transfer. Table 2.7 gives their summed spectroscopic strengths. It is encouraging to note that all the $h_{11/2}$ strength seen in ^{139}La is accounted for by the observed $\ell^\circ = 5$ levels in ^{138}La. One would not expect to exhaust all the $s_{1/2}$ and $d_{3/2}$ strength up to an excitation of only 1.8 MeV.

2.5 The Neutron Transfer Results for ^{138}La

In section 2.2c we have discussed in some detail the reasons for re-investigating the $^{139}La(d,t)^{138}La$ reaction at the forward angles. These data were needed to clarify the status of the low-lying levels. So most of our discussion for the neutron pick-up work will be limited to these low-lying levels. For higher-excited states we shall still rely upon the interpretation of Lasijo *et al.*

2.5a The Angular Distributions and Spectroscopic Strengths

Our DWBA calculations for $\ell_n = 0$ and 2 are presented in Fig. 2.10. The optical model parameters used for these calculations (Table 2.8) are the same as those employed by Hussein *et al.* (1973) for the $^{141}Pr(d,t)^{149}Pr$ reaction. The deuteron parameters are

Fig. 2.10

The ℓ_n = 0 and 2 differential cross-sections calculated by DWBA for the $^{139}La(d,t)^{138}La$ reaction at 16 MeV.

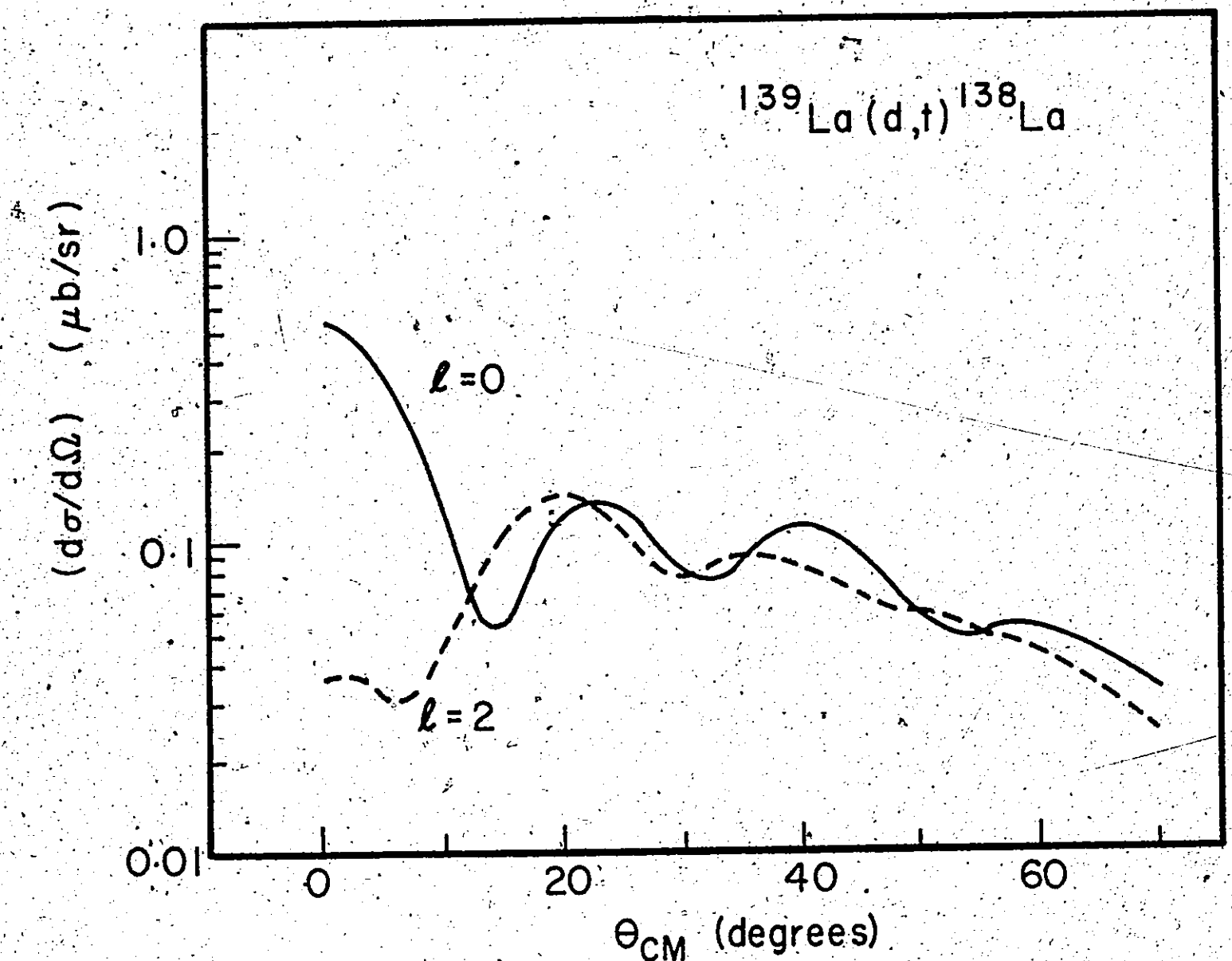
$^{139}La(d,t)^{138}La$
$(d\sigma/d\Omega)$ $(\mu b/sr)$
1·0
0·1
0·01
$\ell=0$
$\ell=2$
0
20
40
60
θ_{CM} (degrees)

Table 2.8

Optical Model Parameters for $^{139}La(d,t)^{138}La$ Reaction

Particle	V	r_{oc}	r_o	a	W_S	W_D	r_o'	a'	V_{SO}
d	-100	1.15	1.15	0.81	0	73.0	1.34	0.68	0
t	-166	1.15	1.16	0.75	-15.2		1.45	0.86	0
n	*	1.15	0.81	-	-	-	-	-	-

The expression for the potential is the same as that given in Table 2.3

The local, zero range approximation was used. No radial cut-off was employed.

*Adjusted to reproduce separation energy.

originally derived from Perey and Perey (1963) while those for the tritons come from Lasijo *et al.* (1972). The calculations clearly demonstrate the desirability of studying the angular distributions of the low-lying levels at smaller angles. Our data, taken at angles ranging from 7.5° to 25°, were augmented by the data from Lasijo *et al.* for $\theta \geq 22°$ to provide the angular distributions shown in Fig. 2.11. This joining posed no problems because the two sets of 25° cross-sections agree in absolute value to within 10%. The circles distinguish our data points from the triangles of the earlier work. To improve upon the reliability of extracting the spectroscopic factors we adopted an empirical ℓ-shape for $\ell_n = 2$ based on the observed angular distribution of the ground state. This state is known to be 5^+ and hence can have no $\ell_n = 0$ admixture. In actual fact, the results are the same if the analysis is carried out entirely with the DWBA ℓ-shapes, however the χ^2 is larger. The fitting procedure was completely analogous to the one described in section 2.4.

The ℓ_n-values and spectroscopic factors for the low-lying levels are listed in Table 2.9. Two of our ℓ_n assignments disagree, at least in part, with the earlier work. The 160 keV level shows an appreciable $\ell_n=0$ admixture in our measurements whereas it was assigned as pure $\ell_n = 2$ previously. On the other hand, the 192 keV level appears to be purely $\ell_n = 2$. This result is the same as Lasijo *et al.* found but Helton *et al.* reported a small $\ell_n = 0$ admixture. The cross-sections for each member of the 510 and 518 keV doublet seem to follow almost pure $\ell_n = 0$ angular distributions

Table 2.9

The ℓ_n Values and Spectroscopic Strengths C^2S for $^{139}La(d,t)^{138}La$

E_x (keV)	$\ell_n = 0$	$\ell_n = 2$	$\ell_n = 5$
0		1.18(5)	
72	0.26(9)	0.45(22)	
116		0.33(2)	
161	0.03(1)	0.035(21)	
192		0.16(2)	
230		0.85(8)	
413	0.26(12)	0.16(8)	
478	0.49(7)	<0.03	
510	≈0.2 } 0.60(11)	<0.01	
518	≈0.4 }		
737			1.12(11)
823			0.81(8)
836			1.65(12)
900			0.79(9)
937			1.43(15)
962			1.42(15)
1067			1.61(11)
1255			2.66(22)

Fig. 2.11

The differential cross-sections for the low-lying levels observed in the $^{139}La(d,t)^{138}La$ reaction. The dots represent the data obtained in the present investigation while the triangles are from Lasijo *et al*. The curves are least squares fitted to the data. For $\ell_n = 0$ the DWBA angular distribution was used. The smoothed ground state angular distribution was utilized as an empirical $\ell_n = 2$ shape.

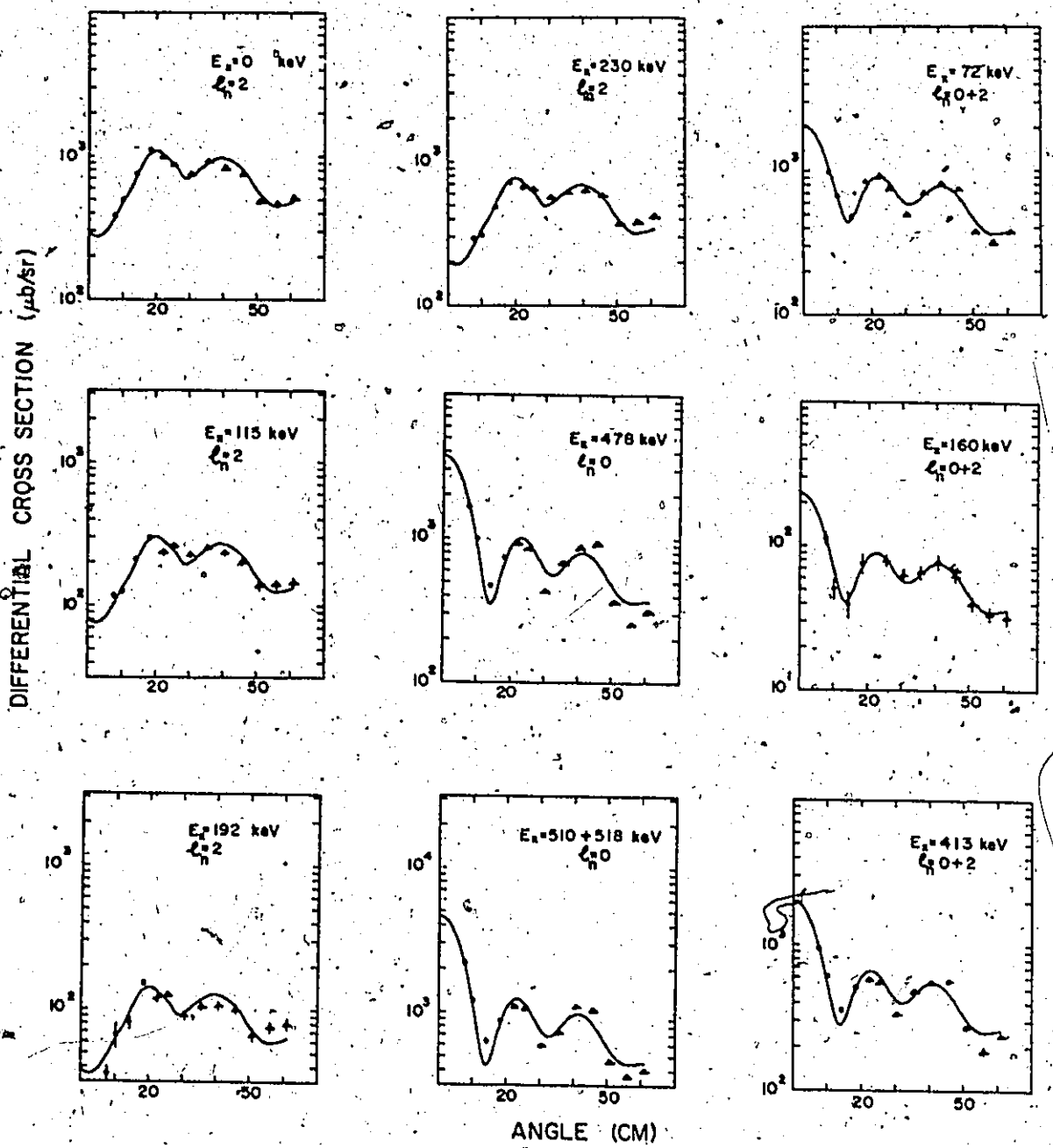
E_x=0 keV
ℓ_n=2
E_x=230 keV
ℓ_n=2
E_x=72 keV
ℓ_n=0+2
E_x=115 keV
ℓ_n=2
E_x=478 keV
ℓ_n=0
E_x=160 keV
ℓ_n=0+2
E_x=192 keV
ℓ_n=2
E_x=510+518 keV
ℓ_n=0
E_x=413 keV
ℓ_n=0+2
DIFFERENTIAL CROSS SECTION (μb/sr)
ANGLE (CM)

for $7.5° \leq \theta \leq 25°$. However, since the individual cross-sections were not available for $\theta > 25°$, only the angular distribution for the composite peak is reported.

Also listed in Table 2.9 are the results for the $\ell_n = 5$ states. The assignments for the stronger levels are borrowed from Lasijo *et al.* . The strengths, however, are calculated from the cross-sections observed in our long exposure at $\theta = 40°$. The state at 823 keV was resolved in the present work from the somewhat stronger level at 836 keV. It has been tentatively assigned $\ell_n = 5$ because the 823+836 peak (listed as 833 keV by Lasijo *et al.*) follows the $\ell_n = 5$ angular distributions very faithfully.

2.5b The Sum Rules for the Neutron Pick-up Reaction

As the neutron orbits in ^{139}La are all supposed to be completely filled, the number of particles available for pick-up from the $3s_{1/2}$, $2d_{3/2}$ and $1h_{11/2}$ shells should be 2, 4 and 12 respectively. In Table 2.10 we compare the sums of the observed strengths for $\ell_n = 0$, 2 and 5 with these expectations. As one can see, the eight observed $\ell_n = 5$ states do appear to exhaust the sum rule limit. For the low-lying levels we see $\sim 80\%$ of the expected strengths, which is not bad agreement at all considering the inherent uncertainties in DWBA calculations and absolute normalization. It is interesting to note that both the earlier works report spectroscopic strengths that fail by almost a factor of 2 to fulfill the sum rule limit. This is all the more surprising in view of the fact that our observed cross-sections agree so well with the

Table 2.10

The Sum Rules for Neutron Transfer

ℓ	j	Observed Strength	Sum rule limit
0	1/2	1.6	2
		0.94[a]	
		1.12[b]	
2	3/2	3.2	4
		2.14[a]	
		2.07[b]	
5	11/2	11.5	12

[a] From Lasiq *et al.* (1972)

[b] From Helton *et al.* (1973).

quoted values of Lasijo *et al.* The difference between our strengths and theirs must arise therefore from the DWBA calculations. We note particularly that their value of $4W_D$ in the deuteron potential was only 55 MeV, which is much too small.

Chaumeaux *et al.* (1971) report occupation probabilities of 4 and 1.6 for the $d_{3/2}$ and $s_{1/2}$ orbits respectively in their study of the $^{138}Ba(p,d)^{137}Ba$ reaction. If one assumes that an extra proton in ^{138}La does not affect the neutron configuration then our spectroscopic strengths should agree with their results. For the $s_{1/2}$ orbit this is the case but we do not see as much $\ell_n = 2$ strength.

CHAPTER III

GAMMA-RAY STUDIES

Introduction

Even the relatively simple nuclei are too complicated to be fully understood by just one set of experiments and one has to employ different modes to investigate its various moods. The particle transfer reactions, though very useful in revealing a partial level scheme and providing some nuclear structure information about these levels, are too selective to populate all the existing levels. For example, the reactions discussed in the last chapter would totally discriminate against any level of ^{138}La arising from a pure $(\pi 2d_{5/2} \nu 3s_{1/2}^{-1})$ configuration, except to the extent that one might see a weak 2-step process. Compound nucleus reactions are much more broad-minded in this respect and an $(x,n\gamma)$ reaction can be expected to populate levels of radically different configurations. Even for the levels already identified in some other reactions, the mode of de-excitation can confirm or reveal additional nuclear structure information.

Thus to complement and augment the information discussed in the preceding chapter, the $^{138}Ba(p,n\gamma)^{138}La$ studies were undertaken. The γ-rays were observed both in singles and in coincidence experiments. Such γ-ray data are particularly useful in testing the spin

assignments made on the basis of particle transfer reactions. The (p,nγ) reaction, chosen in this case, is not an ideal one as it is very inefficient in populating the high spin states. But we were limited by target considerations. The reaction $^{134}Xe(^{7}Li,3n\gamma)^{138}La$ should populate high spin states, but a gas target is not easy to work with and such experiments lead to very complex spectra. We have also measured the life-time of the 72 keV level using the n-γ delayed coincidence in the $^{138}Ba(p,n\gamma)^{138}La$ reaction.

3.1 The $^{138}Ba(p,n\gamma)^{138}La$ Experiment

The threshold for the $^{138}Ba(p,n)^{138}La$ reaction is 2.57 MeV while for (p,2n) it is 9.89 MeV. The beam energy employed in the experiment varied from 4.5 MeV to 7.5 MeV in steps of 1 MeV. Preliminary runs were made with thin targets of natural BaO containing 71.9% of ^{138}Ba, and enriched isotope (99.8% enrichment). The main experiments were carried out on an enriched target thick enough (∿ 200 mg /cm^2) to stop the beam. This target was also in the form of BaO. The enriched isotope was supplied by ORNL in the form of $Ba(NO_3)_2$. Nitric oxide was boiled off by heating the compound to ∿ 800°C in a platinum crucible. The leftover BaO was then pressed into a pellet and glued to the target holder, which was mounted in a thin glass chamber (1.2 cm in diameter with ∿ 0.15 cm thick walls).

To obtain the maximum possible resolution a 1 c.c. Ge(Li) detector was used for the lower part of the spectrum (up to 500 keV). The resolution of this detector was 800 eV at 122 keV. For higher energy gamma-rays, a 14 c.c. planar detector was employed, which had

a resolution of 1.8 keV at 661 keV. As the efficiency of this detector is very low for E_γ > 1 MeV, the data for this part of the spectrum were later complemented by recording a spectrum at 7.5 MeV proton energy with a 37 c.c. detector. The resolution of this detector was ~ 3 keV at 1332 keV. The detectors were placed at an angle of 125° with respect to the beam direction. At this angle $P_2(\cos\theta) = 0$ and hence the γ-ray intensities should be virtually independent of possible anisotropies. For a heavy target like Ba one does not expect a significant Doppler shift, so the gamma-ray energies arrived at from these exposures are expected to be the same as would have been obtained from a 90° spectrum. Graded absorbers of cadmium, molybdenum and copper were used to shield the detectors from Ba and Ta x-rays. In an effort to improve the signal-to-noise ratio, the detectors were placed quite close to the target, the 1 c.c. and 14 c.c. being at a distance of 4.8 cm and 7 cm respectively. As $^{181}Ta(p,n\gamma)$ gives rise to some lines which could interfere with the gamma-rays observed in $^{138}Ba(p,n\gamma)$ reaction, the chamber apertures of Ta were later replaced with the carbon apertures. The presence of 85.6 keV and 88.5 keV γ-rays in the ^{138}La spectrum necessitated the removal of any lead from the vicinity of the detectors and the target chamber. For a decent count rate, i.e. maintaining ≤ 20% dead time for a 14 c.c. detector, the current on the target was varied from 14 nA at 4.15 MeV to 1.6 nA at E_p = 7.5 MeV. The count rate was limited by the annihilation radiation from $^{16}O(p,\alpha\gamma)^{13}N$. The residual nucleus ^{13}N decays to ^{13}C with a half

life of 9 minutes.

The data acquisition process in these experiments was a fairly standard one. The pre-amp pulses from the two detectors were shaped and amplified by Tennelec TC203 linear amplifiers which have built-in base line restoration. In some runs, the inclusion of a linear gate and stretcher after the linear amplifier improved the resolution by rejecting the pile ups. These analog pulses were then fed into the Northern Scientific analog-to-digital converters, interfaced with a PDP-9. The programme for the data storage, written by D.T. Kelly, enabled the collection of data in any integral multiple of 1024 channels, up to a maximum of 8K. The 4K spectra so acquired were stored on Dectapes. The spectrum taken at a proton energy of 7.5 MeV is shown in Fig. 3.1.

After a rough initial calibration, the in-beam calibration was achieved by using a ^{182}Ta source. The energies of the strong and well defined gamma-rays derived from the calibrated spectra were later used to calibrate the other spectra. The energies for ^{182}W (decay of ^{182}Ta) were taken from White *et al.* (1970).

The peak areas and their centroids were extracted by using D.T. Kelly's program TFMUCH on the off-line PDP-15. The programme is very efficient for a relatively clean spectrum as it sums up the counts in a given number of channels after fitting to a linear background. Errors in the peak intensity and centroid position arise mainly from statistical uncertainties. The more complex part of the spectrum, near 230 keV, was analyzed separately by hand. The

Fig. 3.1

The γ-ray spectrum from the $^{138}Ba(p,n\gamma)^{138}La$ reaction at E_p = 7.5 MeV. The topmost section was recorded with a 1 c.c. Ge(Li) detector while the lower two segments show the data taken with a 14 c.c. detector.

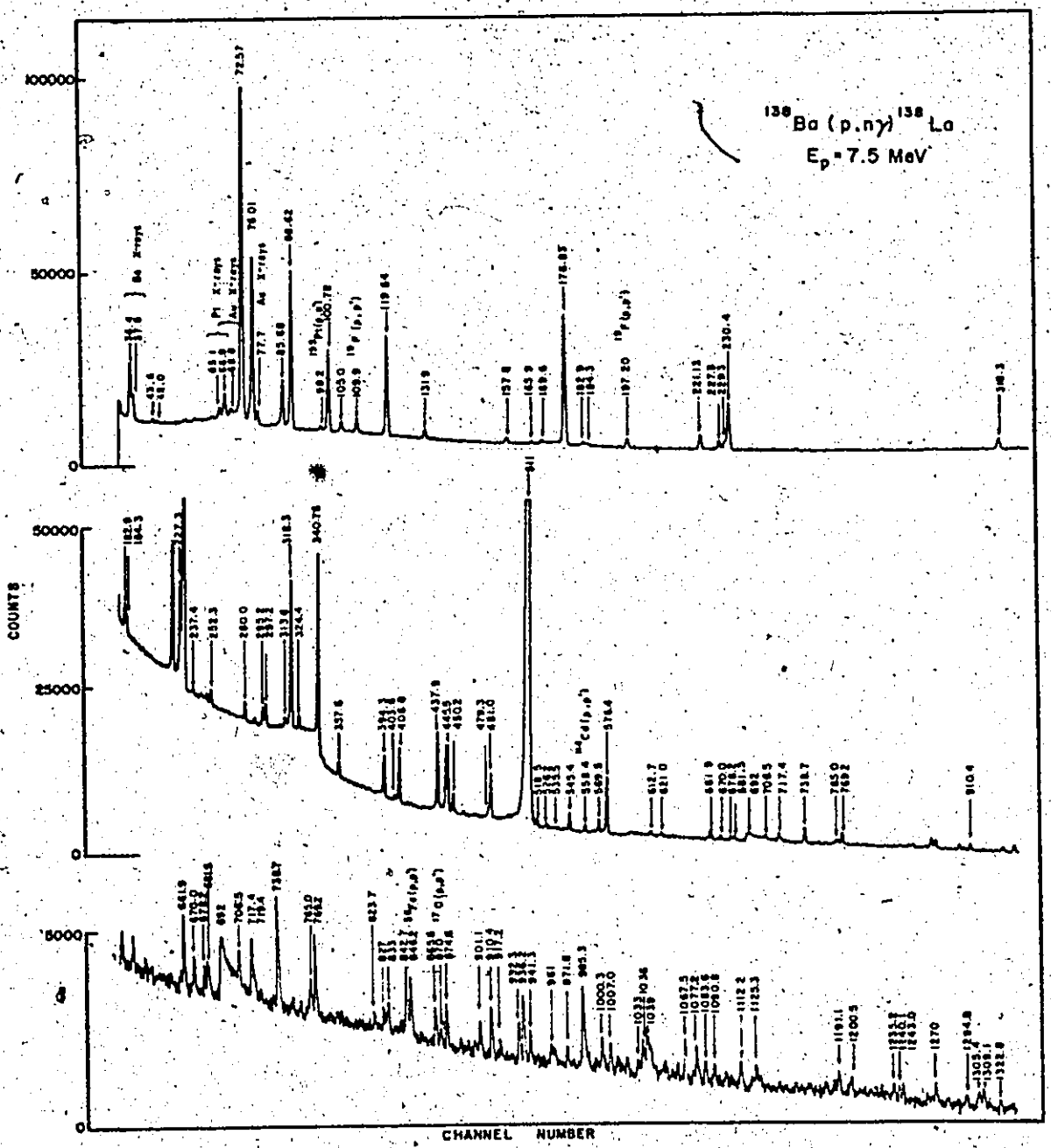
^{138}Ba (p,nγ) ^{138}La
E_p = 7.5 MeV
COUNTS
CHANNEL NUMBER

absolute gamma-ray energies were subsequently derived by both a linear and a quadratic least-squares fitting of the centroid positions, using the centroids of the strong peaks as calibrating points. In fact both these fits agree within the limits of the quoted errors.

The reaction was carried out on three different targets, natural on carbon backing, enriched thin on Ta backing, and an enriched thick one. The isotopic composition of the enriched target has already been given (table 2.I). The gamma-rays common to all these runs and of similar relative intensities (with respect to the 176.8 keV line) were tentatively assigned to ^{138}La. With the thick target, the gamma-ray yields at four different beam energies were used for a more reliable assignment. The excitation functions of some of the more prominent gamma-rays are given in Fig. 3.2. Gamma-rays which showed a significantly different trend were rejected. Also rejected were the gamma-rays seen in the background spectrum (recorded for 2 hours at the end of the run), which mostly emanate from the decay of some impurities in the target and the beam transport system. The evident contaminants are carbon, oxygen, flourine, iron and platinum and most of the rejected γ-rays can be assigned to one or other of these impurities. Though not giving rise to any interfering gamma-rays, carbon is a major source of Compton background. Oxygen is inherently present in the target as the target is BaO. Except for a weak gamma-ray at 870 keV arising from $^{17}O(p,p')^{17}O^*$, oxygen also contributes to the Compton background only. The annihilation radiation from $^{16}O(p,\alpha)^{13}N$ also adds to this background. Iron cannot be avoided because of the beam pipes and platinum owes its presence

Fig. 3.2

Excitation functions of some of the more prominent γ-rays observed in the $^{138}Ba(p,n\gamma)^{138}La$ reaction. The plotted intensities are normalized to the apparent density of the 177 keV γ-ray but have not been corrected for the variation in detector efficiency or for self-absorption in the target.

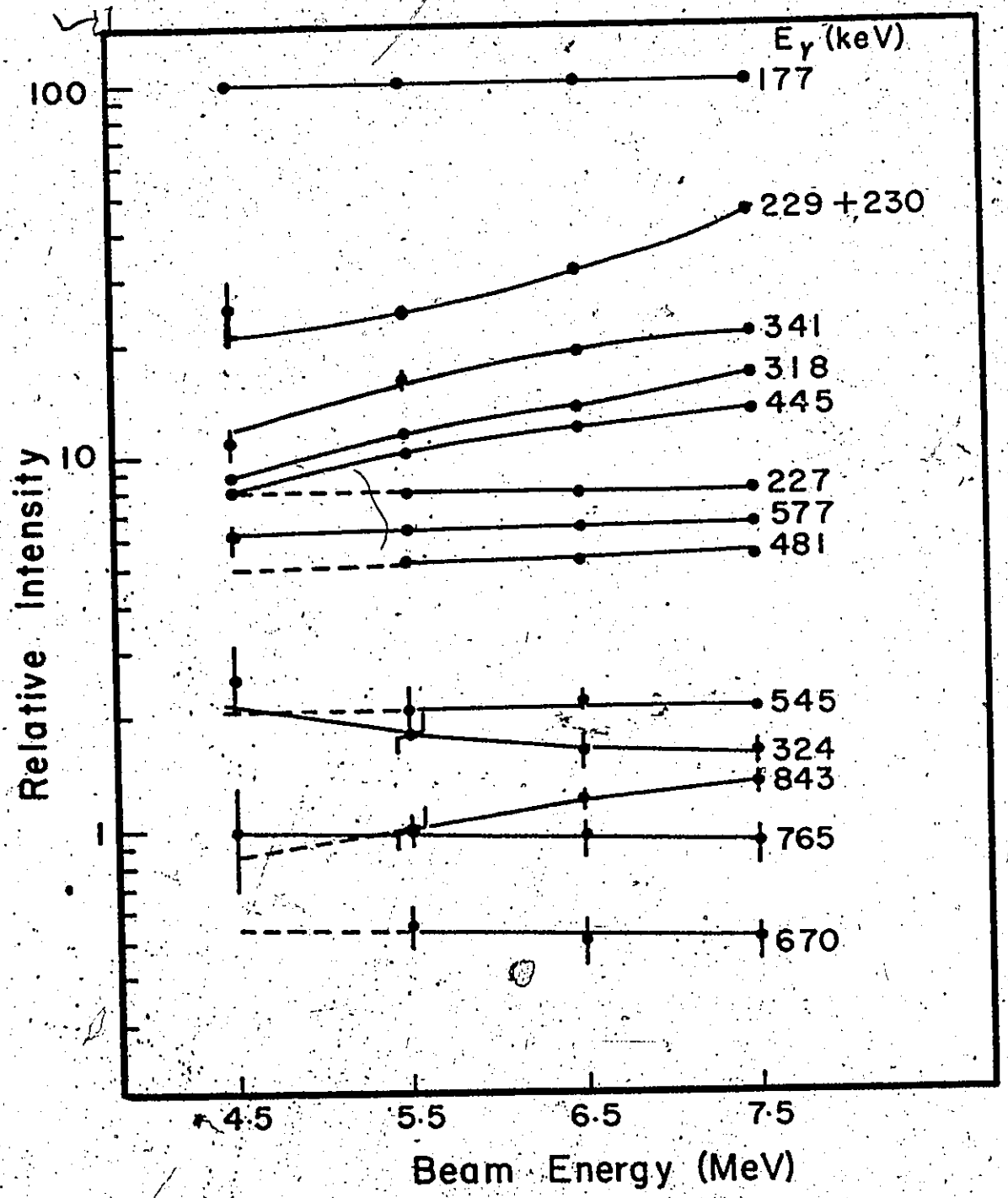
E_γ (keV)
177
229 + 230
341
318
445
227
577
481
545
324
843
765
670
100
10
1
Relative Intensity
4·5
5·5
6·5
7·5
Beam Energy (MeV)

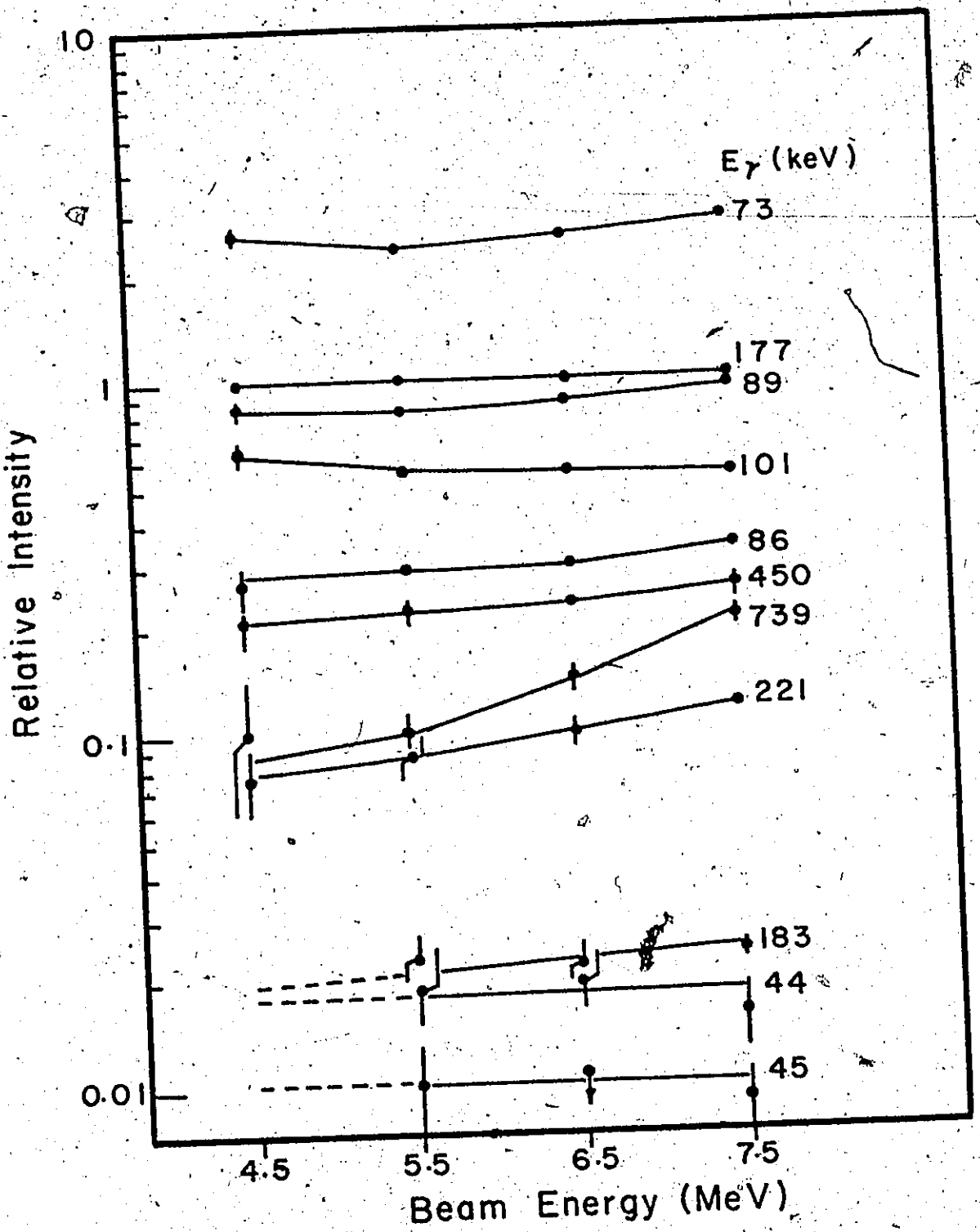
10
1
0·1
0·01
Relative Intensity
Eγ (keV)
73
177
89
101
86
450
739
221
183
44
45
4·5
5·5
6·5
7·5
Beam Energy (MeV)

to the platinum crucible used for heating the $Ba(NO_3)_2$. Fluorine has been the distinctive feature of most of the reactions conducted at this lab. Probably it comes from something in the beam transport system.

The energies and relative intensities assigned to ^{138}La are given in Table 3.1. The intensities are corrected for the detector efficiency and self-absorption in the target. These are discussed in the next sections. The placements of these γ-rays in the level scheme, also given in Table 3.1, are discussed in Chapter IV.

3.1a Efficiency Calibration of the Detectors

The relative efficiencies of the detectors, as a function of γ-ray energy, were determined at the end of each run by placing a ^{182}Ta source at the target position inside the target chamber. The correction for the absorption in the graded absorbers was thus automatically included. The relative intensities for ^{182}Ta decay lines were also taken from White *et al.* Another very useful source for such calibration was made available by the work of Cook *et al.* (1973) on the decay of ^{151}Pm to the levels in ^{151}Sm. This decay provides a wealth of lines of known absolute intensities covering an energy range of 25 keV to 1 MeV. It is not a very convenient source though, because the half life of ^{151}Pm is just 28 hours. The source was prepared by irradiating ^{150}Nd in the reactor, always one or two days before the run. The half life of ^{151}Nd is 12 minutes.

3.1b Gamma-ray Self Absorption in the Target

As the targets used for the $^{138}Ba(p,n\gamma)$ experiments were thick enough to stop the beam, it was important to correct the inten-

Table 3.1

γ-Ray Energies, Intensities from $^{138}Ba(p,n\gamma)^{138}La$ and their Placement

E_γ (keV)	I_γ	E_i (keV)	E_f (keV)
43.6 (1)	22 (8)[a]	116.2	72.6
45.0 (1)	6.4(26)	161.2	116.2
72.57(3)	201 (17)	72.6	0.0
76.01(8)	71 (6)	292.2	116.2
85.68(8)	18.0(15)	823.4	737.7
88.62(5)	50 (4)	161.2	72.6
100.78(6)	21.5(18)	293.0	192.2
105.0 (1)	3.1(3)	947.7	842.8
119.64(5)	29 (2)	192.2	72.6
131.9 (1)	3.2(3)	642.4	510.5
157.8 (1)	3.3(4)	230.4	72.6
176.83(6)	100	293.0	116.2
182.9 (1)	2.7(3)	413.3	230.4
221.13(5)	21.0(17)	413.3	192.2
227.3 (1)	16.4(14)	737.7	479.4
229.3 (2)	14.2(12)	642.4	413.3
230.4 (2)	71 (6)	230.4	0.0
248.7 (3)	2.0(2)	479.4	230.4
280.0 (1)	3.3(7)	510.5	230.4
295.2 (3)	4.4(4)	1243.0	947.7
297.2 (3)	5.2(5)	413.3	116.2
313.6 (3)	4.4(5)		
318.3 (1)	42 (3)	510.5	192.2
324.4 (2)	3.9(4)	737.7	413.3
340.78(20)	62 (5)	413.3	72.6
357.6 (2)	5.4(6)	518.7	161.2
394.3 (1)	18.6(15)	510.5	116.2
403.6 (3)	3.8(5)		
406.8 (2)	26 (2)	479.4	72.6
437.9 (1)	43 (4)	510.5	72.6

(continued next page)

Table 3.1 (continued)

E_γ (keV)	I_γ	E_i (keV)	E_f (keV)
444.7 (3)	32 (3)	737.7	293.0
445.9 (3)	32 (3)	518.7	72.6
450.2 (2)	11 (1)	642.4	192.2
479.3 (3)	5.4(8)	479.4	0.0
481.0 (3)	32.5(44)	642.4	161.2
518.5 (4)	4.9(6)	518.7	0.0
526.2 (3)	3.9(3)	642.4	116.2
535.3 (3)	1.5(4)	1358.7	823.4
545.4 (2)	15.2(13)	737.7	192.2
569.5 (2)	19 (2)	642.4	72.6
576.4 (2)	65 (5)	737.7	161.2
612.7 (4)	4.0(7)	842.8	230.4
621.0 (4)	4.4(8)	1358.7	737.7
661.9 (2)	13 (1)		
670.0 (3)	6.6(8)	900.6	230.4
678.2 (3)	6.0(8)	(1578.8)[b]	(900.6)
681.5 (3)	10.6(11)	1200.5	518.7
706.5 (5)	10.9(11)	936.7	230.4
717.4 (3)	10.9(11)	947.7	230.4
719.4 (3)	3.7(7)		
738.7 (2)	24.3(21)	738.7	0.0
765.0 (3)	11.6(12)	1058.0	293.0
823.7 (4)	5.1(8)		
827.0 (6)	5.9(9)	1788.5	961.4
833.0 (8)	7.1(12)		
842.7 (2)	20.7(18)	842.8	0.0
865.6 (3)	10.6(11)	1058.0	192.2
874.6 (3)	9.4(10)	1358.1	510.5
901.1 (5)	11.7(12)	900.6	0.0
910.4 (3)	15.5(15)	1102.6	192.2
		1733.3[c]	293.0
917.2 (4)	5.5(9)		

(continued next page)

Table 3.1 (continued)

E_γ (keV)	I_γ	E_i (keV)	E_f (keV)
932.3 (3)	13.6(13)		
936.2 (2)	22.2(19)	936.7	0.0
		1228.8	293.0
		(1097.4)[b]	(161.4)[b]
941.3 (3)	13.1(14)	1058.0	116.2
		1102.6[c]	161.2[c]
961.4 (5)	5.2(9)	961.4	0.0
971.8 (5)	4.4(9)	1358.1	413.3
		1490.5[c]	518.7[c]
985.3 (3)	32 (3)	1058.0	72.6
1000.3 (3)	11.6(13)		
1007.0 (4)	9.6(11)	(1302.)[b]	(293.0)[b]
1033 (1)	∿16		
1037 (1)	∿20		
1040 (1)	∿16		
1067.5 (3)	17.6(17)	1228.8	161.2
1077.2 (3)	19.9(19)	(1150)[b]	(72.6)[b]
		1490.5	413.3
1083.6 (3)	13.4(14)	1156	72.6
1090.8 (3)	14.0(14)	1733.3	642.4
1112.2 (3)	19.1(18)		
1125.3 (3)	16.3(15)	(1645)[b]	(518.7)[b]
1191.1 (4)	9.6(12)	(1707)	(518.7)
1200.5 (5)	8.3(14)	1200.5	0.0
1235.2 (8)	6.2(13)	(1426)[b]	(192.2)[b]
		(1715) [b]	(479.4)[b]
1240.1 (5)	3.9(8)		
1243.0 (5)	3.9(9)	1243.0	0.0
1270 (1)	6.5(11)	1788.5	518.7

(continued next page)

Table 3.1 (continued)

E_γ (keV)	I_γ	E_i (keV)	E_f (keV)
1294.8 (5)	3.7(9)		
1305.4 (5)	7.8(11)		
1309.1 (5)	7.1(10)	1722.6	413.3
		1788.5 [c]	479.4 [c]
1322.8 (5)	3.4(8)		

(a) Numbers in parentheses indicate error in the last digit.

(b) Possible placement but not supported by any other γ-ray from the same level.

(c) Alternate placement.

sities of the low energy gamma-rays for attenuation in the target. When the target is perpendicular to the beam direction the fraction of any gamma-ray absorbed in the target is given by

$$f_\gamma = \frac{\int_0^x \sigma(E)dx - \int_0^x \sigma(E)e^{-\mu x/\cos\theta}\,dx}{\int_0^x \sigma(E)dx}$$

where $\sigma(E)$ is the reaction cross-section at the beam energy E

μ is the mass absorption co-efficient of BaO for the given gamma-ray

x is the penetration region of the beam in mg/cm^2

and θ is the angle between the beam direction and the normal to the face of the detector.

The attenuation was calculated for a proton beam energy of 7.5 MeV at the surface of the target. The penetration region was estimated by the stopping power data of Northcliff and Schilling (1970). As this table does not give values for barium and oxygen specifically, data for Ag and Eu were interpolated to get an estimate for barium, and carbon and aluminium were used to approximate for oxygen. The stopping power of BaO was then calculated using the following relationship:

$$\left(\frac{dE}{dx}\right)_{target} = \frac{138\left(\frac{dE}{dx}\right)_{Ba} + 16\left(\frac{dE}{dx}\right)_{O}}{154}$$

The mass absorption coefficient μ for the individual gamma-rays was calculated from the photon cross-section data of Storm and Israel (1970) and $\sigma(E)$ at various energies was estimated from the

experimentally measured excitation function of $^{140}Ce(p,n)$ by Furukawa (1967). His curve was adjusted for the different threshold value in the present reaction (2.5 MeV as compared to 4.1 MeV). The expression for f was numerically integrated. The percentage attenuation as a function of γ-ray energy is shown in Fig. 3.3. The attenuation is negligible for $E_\gamma \geq 400$ keV. The finite solid angle subtended by the detectors and the inaccurate estimates of x and σ(E) are major contributors to the uncertainties in absorption which are taken to be about 10% of the correction.

3.2 Gamma-gamma Coincidence Experiment

The (p,n) reaction is expected to populate many more levels than are seen in the particle transfer reactions. The coincidence data are extremely useful in determining the excitation energy of these levels. Also an assignment of γ-rays only on the basis of the energy fits is rather uncertain. The coincidence data provide the information about the cascading γ-rays, and, in many cases, can lead to a very unique level scheme. One can also place an upper limit on the life-time of the intermediate level by observing the time resolution of the system. Thus in order to obtain a better understanding of ^{138}La, we carried out a $^{138}Ba(p,n\gamma\gamma)$ experiment.

3.2a Experimental Set-up

The experiment was carried out twice with slightly different set-ups. The target used in both these experiments was the same as used for the final singles run, i.e. the thick pellet of BaO. The target mounting and the detector arrangement were also essentially identical to the set-up for the singles experiment. A slight variation

Fig. 3.3

The calculated correction for γ-ray absorption in the ^{138}BaO target.

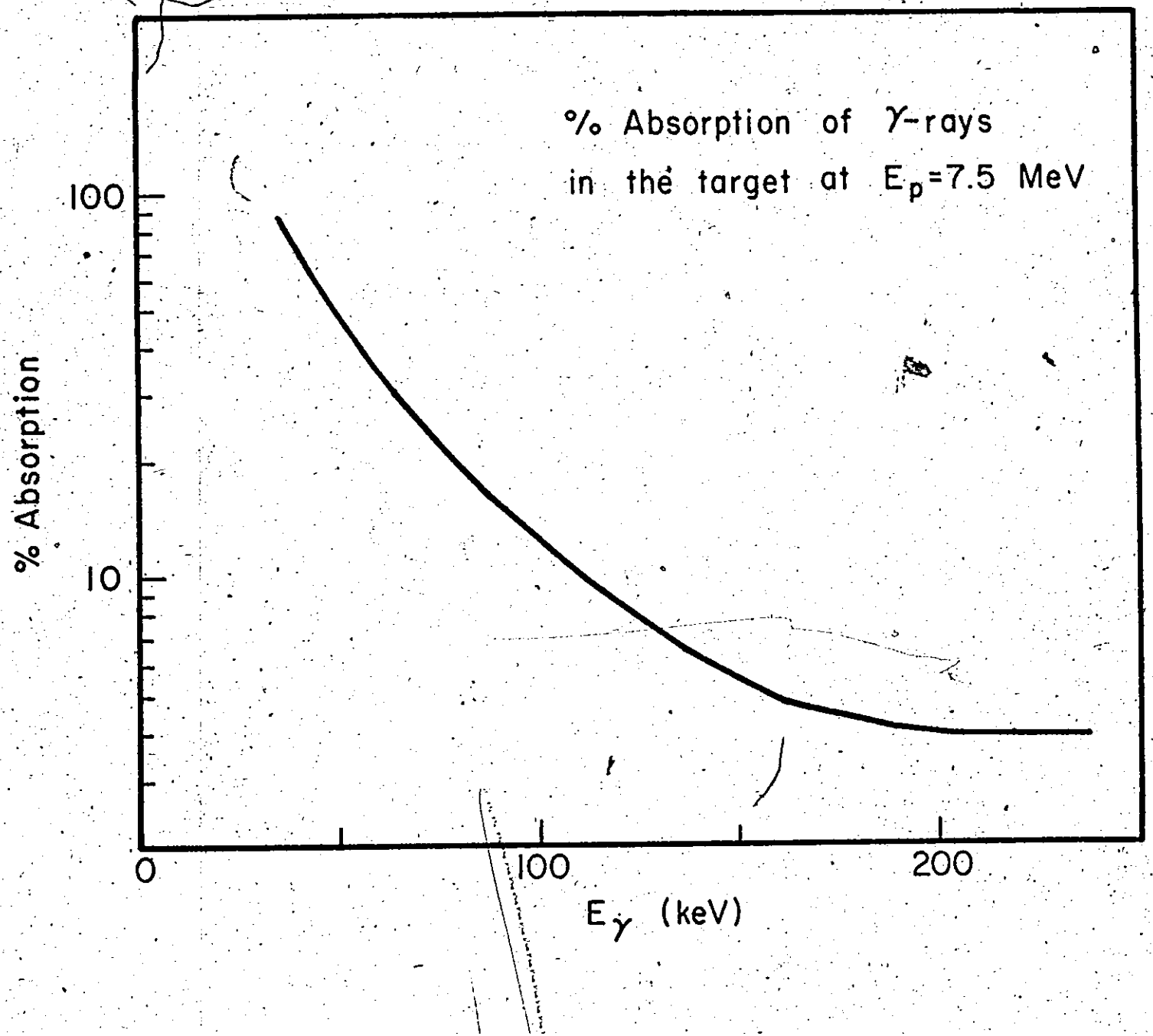
% Absorption of γ-rays
in the target at E_p=7.5 MeV
100
10
% Absorption
0
100
200
E_γ (keV)

was made in the target chamber for the second coincidence run by replacing the pyrex glass tube with a plastic counterpart, to ensure still lower absorption for the low-energy γ-rays. An incident proton beam energy of 7.5 MeV was used for both these runs. Elimination of lead from the vicinity of the detectors and target chamber was not considered necessary in these experiments. In fact the detectors were well shielded from each other by heavy lead jackets and solid lead bricks between them.

For the first set-up a 1 c.c. Ge(Li) was used in conjunction with the 14 c.c. planar detector. A block diagram of the electronics is shown in Fig. 3.4. The pre-amp pulses from the two detectors, suitably shaped by the timing filter amplifier (TFA), were processed by constant fraction timing discriminators (CFTD) to provide fast outputs for the start and stop signals of a time-to-amplitude converter (TAC). The smaller detector started the TAC, whose range was 200 n.s. The width of the logic pulse from the TAC was adjusted using a logic shaper and delay (LSD) and this pulse was then used to gate the inputs to the three ADC's. The shaping and amplification of the energy pulses from the two detectors were done by Tennelec 203 amplifiers in the usual manner. These pulses were suitably delayed to fulfill the coincidence requirement. The outputs from the ADC's were processed by a PDP-9 computer and recorded event-by-event on the magnetic tape. The 3-parameter address recording programme was originally written by L.B. Hughes and later modified by D.T. Kelly. The programme allowed the display of the spectra for the 3 ADCS.

Fig. 3.4

Block diagram of the electronics used in the γ-γ coincidence experiment. The parts are labelled as follows:
LA = linear amplifier, DA = delay amplifier, TFA = timing filter amplifier, CFTD = constant fraction timing discriminator, TAC = time-to-amplitude converter, LSD = logic shaper and delay, ADC = analog-to-digital converter.

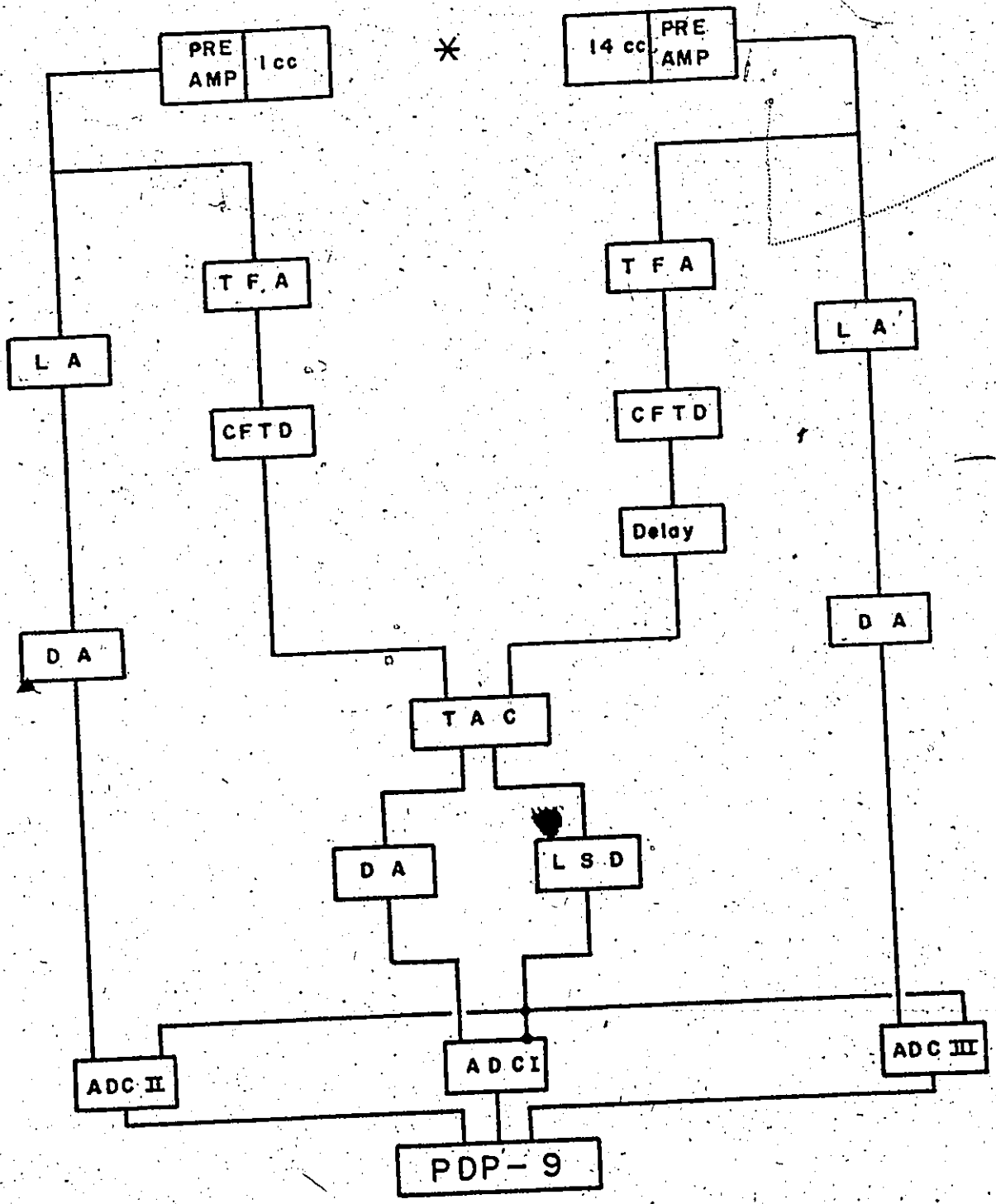
PRE AMP
1 cc
14 cc
PRE AMP
T F A
T F A
L A
L A
CFTD
CFTD
Delay
D A
D A
T A C
D A
L S D
ADC II
ADC I
ADC III
PDP-9

The TAC spectrum consisted of a single peak on a continuous background, the peak-to-background ratio being an index of the true-to-chance ratio of the coincident events. The width of this peak is a measure of the time resolution of the system. In the first set-up we were not able to get a very good time resolution and had to settle for ∿ 64 n.s.

As the relative efficiency of the 14 c.c. detector decreases by an order of magnitude from 100 keV to 1 MeV, the first set-up, labelled as I in the relevant tables and figures, was not very useful in detecting a coincidence with any high energy gamma-ray. So another attempt was made with 14 c.c. and 65 c.c. detectors. The efficiency of the 65 c.c. was about 4 times higher than the 14 c.c. for $E_\gamma \approx 800$ keV, though the resolution was poorer (2.8 keV at 661 keV). In this case an ELSCINT "snap-off" module was used as the time pick-off for the timing output for 65 c.c. Linear gates and stretchers (LGS) were used instead of the delay amplifiers to shape and delay the pulses from the two detectors. The rest of electronics and the experimental details were the same as for the first experiment. Again the TAC was started by the smaller detector.

The true-to-chance ratio and the time resolution were greatly improved in this set-up in spite of the fact that the 6.05 MeV gamma-ray of $^{16}O(p,p')$ generates a high Compton background in the 65 c.c. detector. The time resolution was ∿ 16 nano seconds and the true-to-chance ratio was 30:1 in this set up.

3.2b Analysis of Coincidence Data

The address recorded data were analyzed off-line on a PDP-15 computer using a disk sorting programme made available by D.T. Kelly and H.J. Smith. The programme allowed the subtraction of random events by setting windows of equal width on the time peak and the chance part of the time spectrum. The coincidences due to the Compton events under a photo-peak were eliminated by placing background windows on the two sides of the photo-peak, as close to the peak as possible, and then subtracting the "background" coincidences from those in the "peak" window. Thus the final spectrum represents events in one detector which are in true coincidence with the selected photo-peak in the other detector. The off-line analysis also facilitates gain shift correction.

The sorted spectra from both runs are presented in Fig. 3.5. Spectra which failed to show any interesting features are not included. The fact that subtraction appropriately eliminates Compton and random events is established by the presence of only a very weak 511 keV peak in all the relevant spectra, although it was the strongest peak by far in the singles. It was encouraging to note that the data for the low-energy part of the spectrum obtained from the first set-up were essentially confirmed by the second experiment. The latter also showed some coincidences with higher energy γ-rays not observed in the first set-up. The only remarkable difference in the two sets of data was the absence of any prompt coincidences in the 72 keV gate for the second set-up. Even in the first run the observed coincidences with this γ-ray were too few and far too weak considering that it signifies the

Fig. 3.5

A selection of the Ge(Li)-Ge(Li) coincidence spectra. Each division on the ordinate represents 20 counts per channel. There are 2048 channels in each spectrum. The 72, 76, 86, 89, 101, 120, 177, 183, 221 and 229 keV gates were set on the 1 c.c. detector while the 318, 341, 438, 445 and 545 gates are for the 14 c.c. detector, both from the first set-up. Data from the second experiment include the 227 and 229+230 keV gates set in the 14 c.c. detector and the 576, 670, 717, 765 and 1429 keV gates set in the 65 c.c.

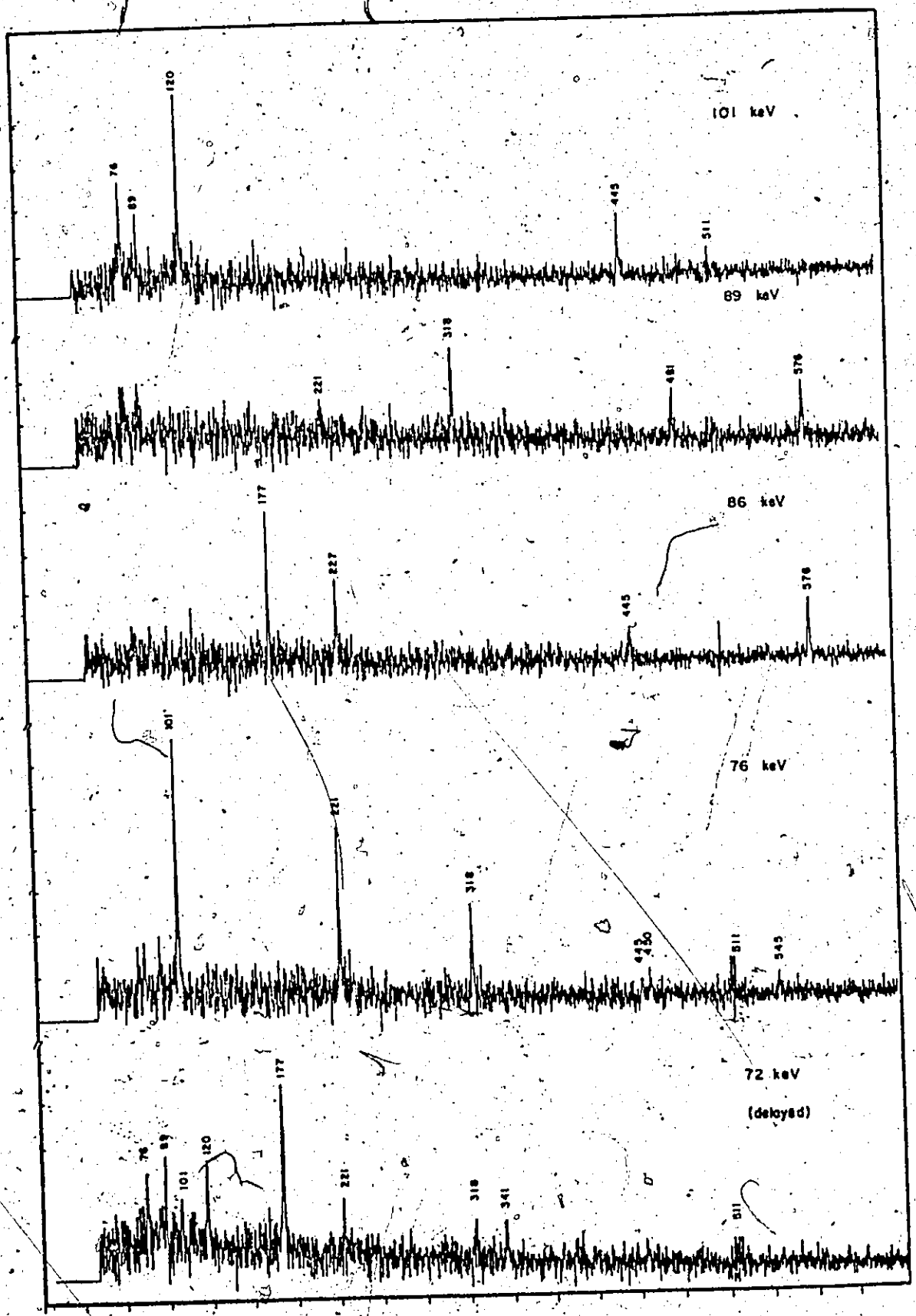
101 keV
76
89
120
443
511
89 keV
221
318
481
576
86 keV
177
227
445
576
76 keV
101
221
318
443
450
511
545
72 keV
(delayed)
177
76
89
120
101
221
318
341
511

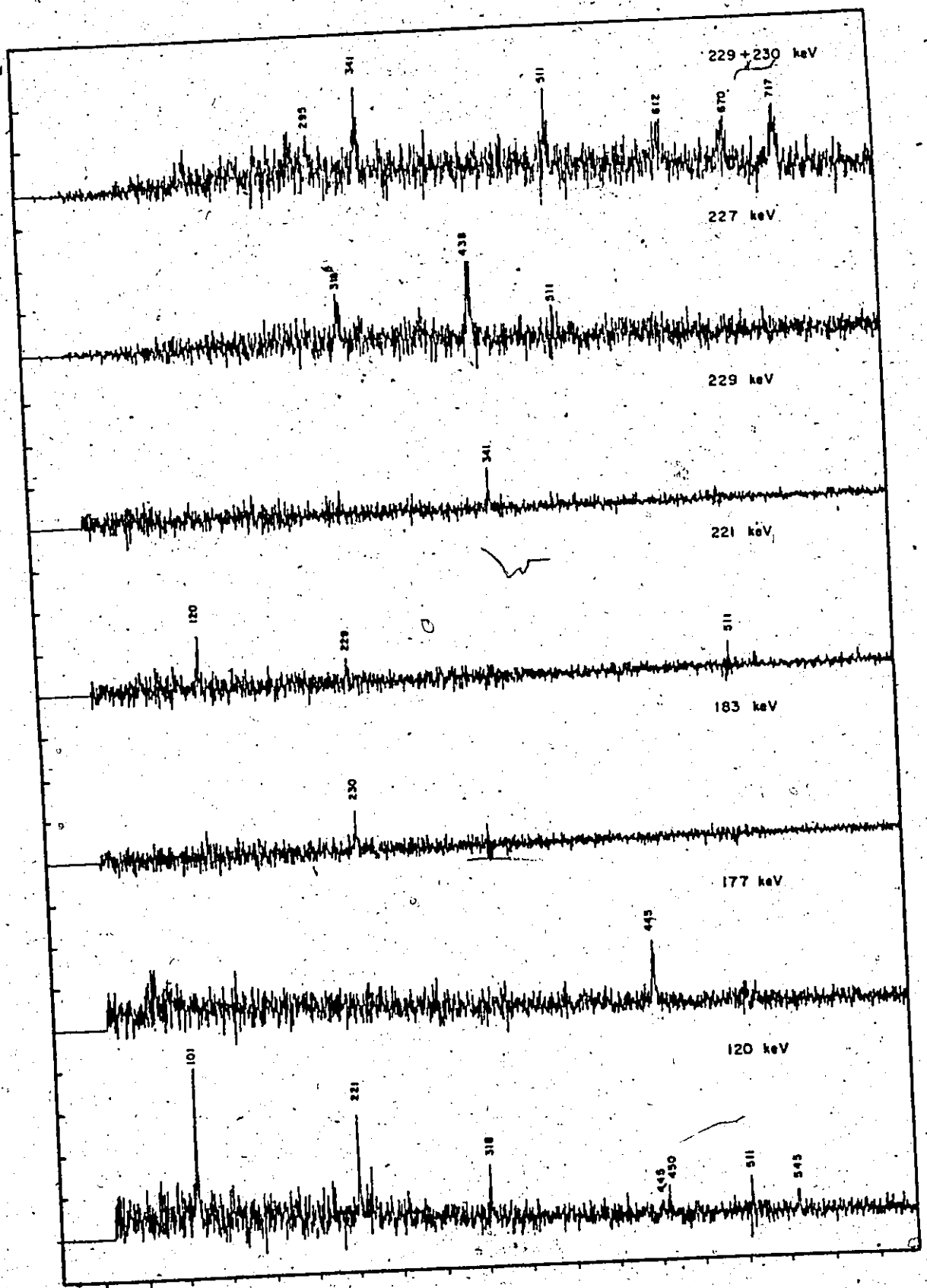
229+230 keV
341
511
295
612
670
717
227 keV
438
511
229 keV
341
221 keV
120
229
511
183 keV
230
177 keV
445
120 keV
101
221
318
446
450
511
545

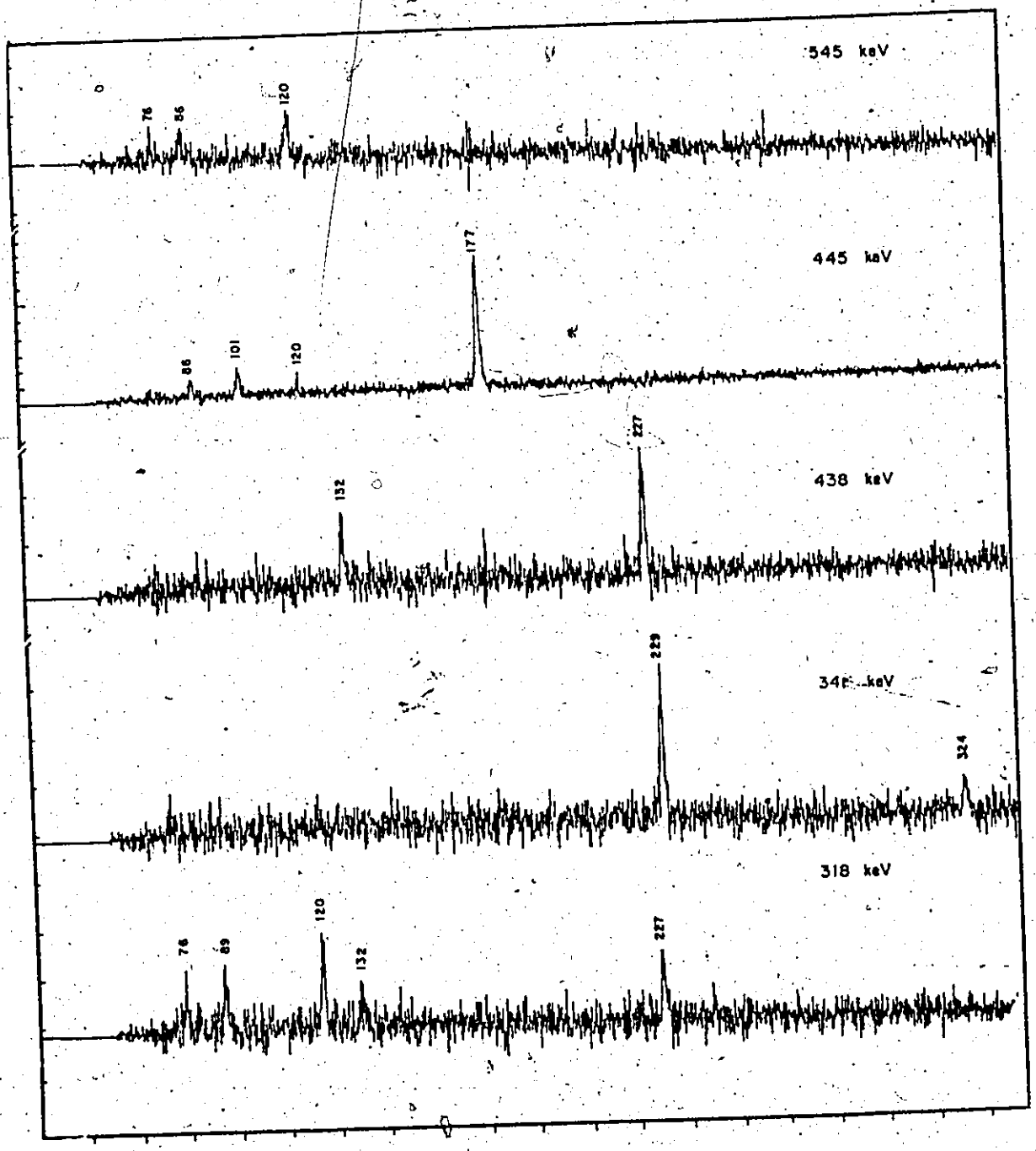
545 keV
76
86
120
445 keV
177
86
101
120
438 keV
227
132
341 keV
229
324
318 keV
76
89
120
132
227

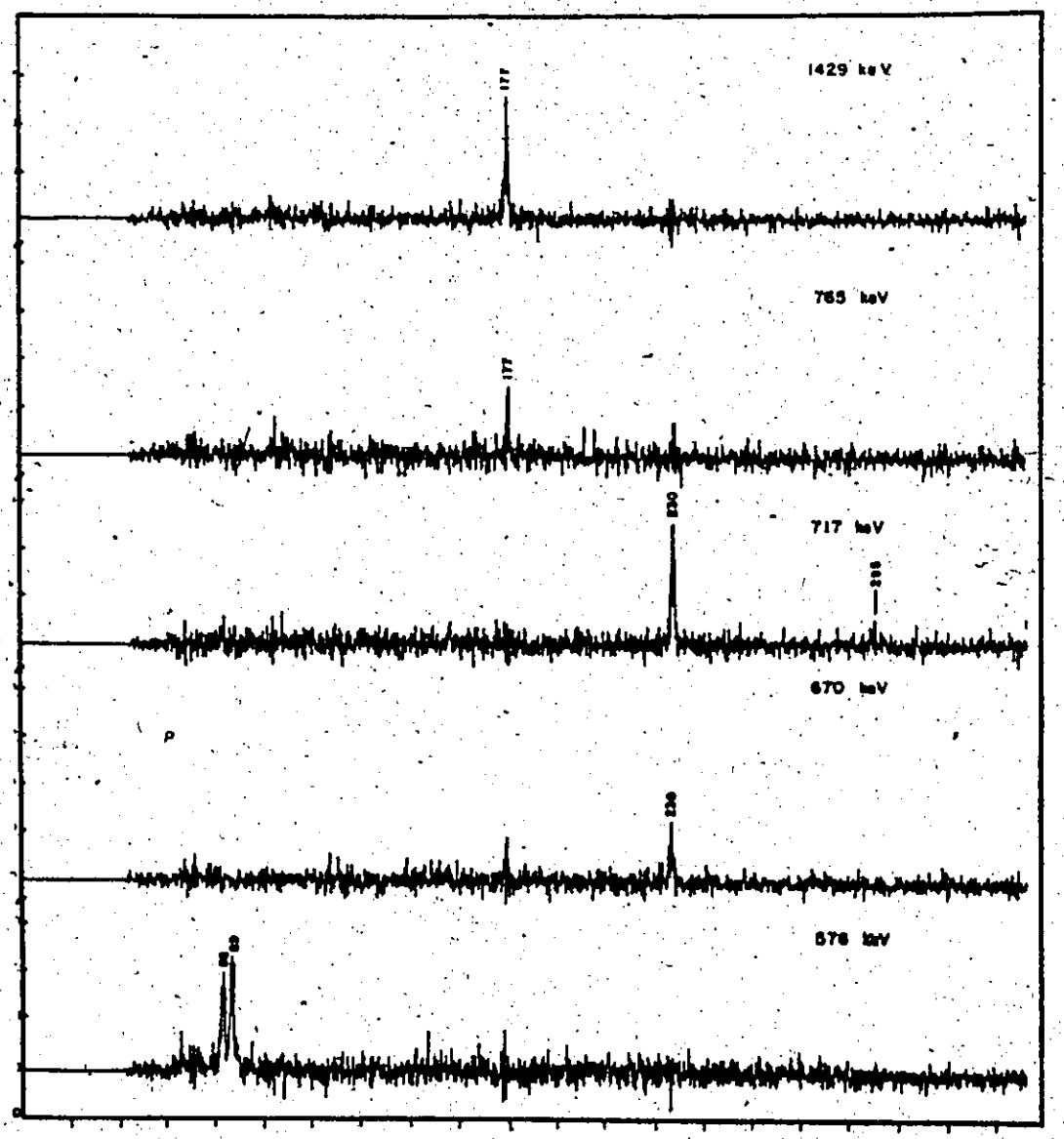
1429 keV
177
765 keV
177
717 keV
330
208
670 keV
330
576 keV
202

decay of the first excited state. Such an observation leads one to believe that the 72 keV level must have a rather long life-time, much larger than the time resolution in the second set-up (16 ns) and perhaps comparable with the time resolution in the first set up (64 ns). The time spectrum for the 72 keV γ-ray alone indicates a life-time of ∿ 100 n.s. The data for the 72 keV gate shown in Fig. 3.5 were obtained by sorting in a wide delayed time window. Table 3.2 gives a summary of the coincidence results.

3.3 Life-time Measurement of 72 keV Level

To get a more quantitative number for the life-time of the 72 keV state we decided to detect the delayed coincidences between the neutrons and γ-rays in $^{138}Ba(p,n\gamma)^{138}La$ reaction. Protons of 7 MeV were employed to populate the levels in ^{138}La. The metallic target, of 99.8% enrichment (Table 2.1), was thick enough to stop the beam. The BaO, obtained in the usual manner from $Ba(NO_3)_2$, was reduced with aluminium and then evaporated on a tantalum backing. A 14 c.c. planar Ge(Li) detector, placed at 90° to the beam direction, recorded the γ-rays while the neutron signal was provided by a 2"×3" plastic scintillator at 0°. The resolution of the Ge(Li) detector was ∿ 1 keV at 122 keV.

The block diagram of the electronics is shown in Fig. 3.6. In the plastic scintillator the neutrons were distinguished from γ-rays by observing the time interval between the fast output from the constant-fraction photomultiplier base and the cross-over obtained from a DDL amplifier. The "shape spectrum" from the neutron counter is presented in Fig. 3.7. For the n-γ coincidences the

Table 3.2

Summary of the Coincidence Data

Gate	γ-rays in Coincidence
72	76, 89, 101, 120, 177, 221, 318, 341, 445
76	86, 89, 101, 221, 318, 445, 450, 545
86	177, 227, 445, 576
89	221, 318, 481, 576, 662
101	76, 89, 120, 445
120	101, 221, 318, 445, 450, 545
132	438
177	445, 765
183	230
221	120,229
227	318, 438
229	341
229+230	280, 295, 341, 612, 670, 717
341	229, 324
438	132, 227
445	86, 101, 120, 177
545	76, 86, 120
576	86, 89
670	230
717	230 ,295
765	717
1429	177

Fig. 3.6

Block diagram of the electronics used to detect n-γ delayed coincidences. The symbols used are: LA = linear amplifier, DDL = double delay-line amplifier, SCA = single channel analyzer, TPC = time pick-off control, TFA = timing filter and amplifier, TAC = time-to-amplitude converter, LGS = linear gate and stretcher, LSD = logic shaper and delay, snap off = time pick-off unit (Elscint), ADC = analog-to-digital converter.

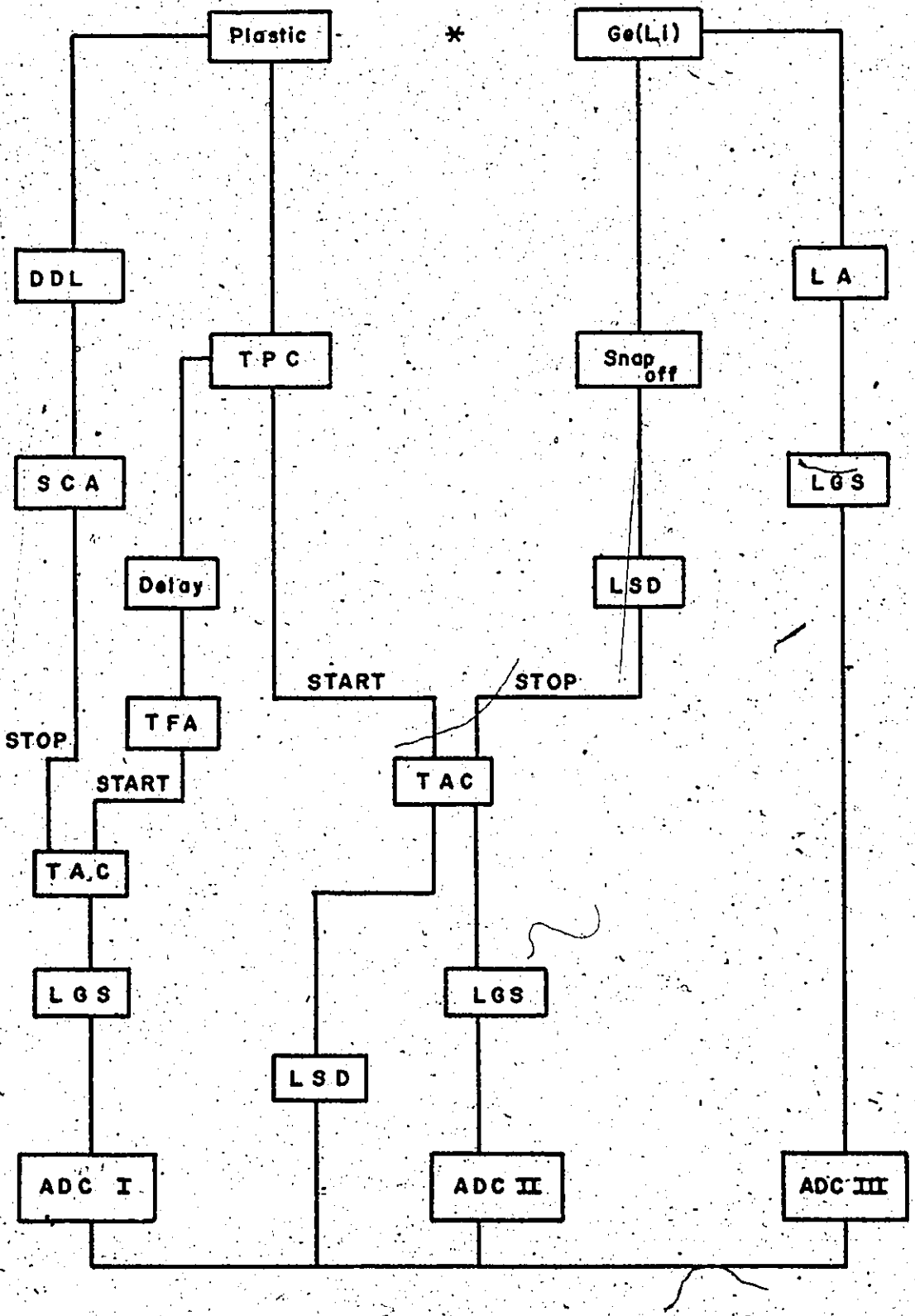
Plastic
Ge(Li)
DDL
L A
T P C
Snap off
S C A
L G S
Delay
L S D
START
STOP
T F A
STOP
START
T A C
T A C
L G S
L G S
L S D
ADC I
ADC II
ADC III

Fig. 3.7

The shape spectrum from the plastic scintillator showing the discrimination between neutrons and γ-rays.

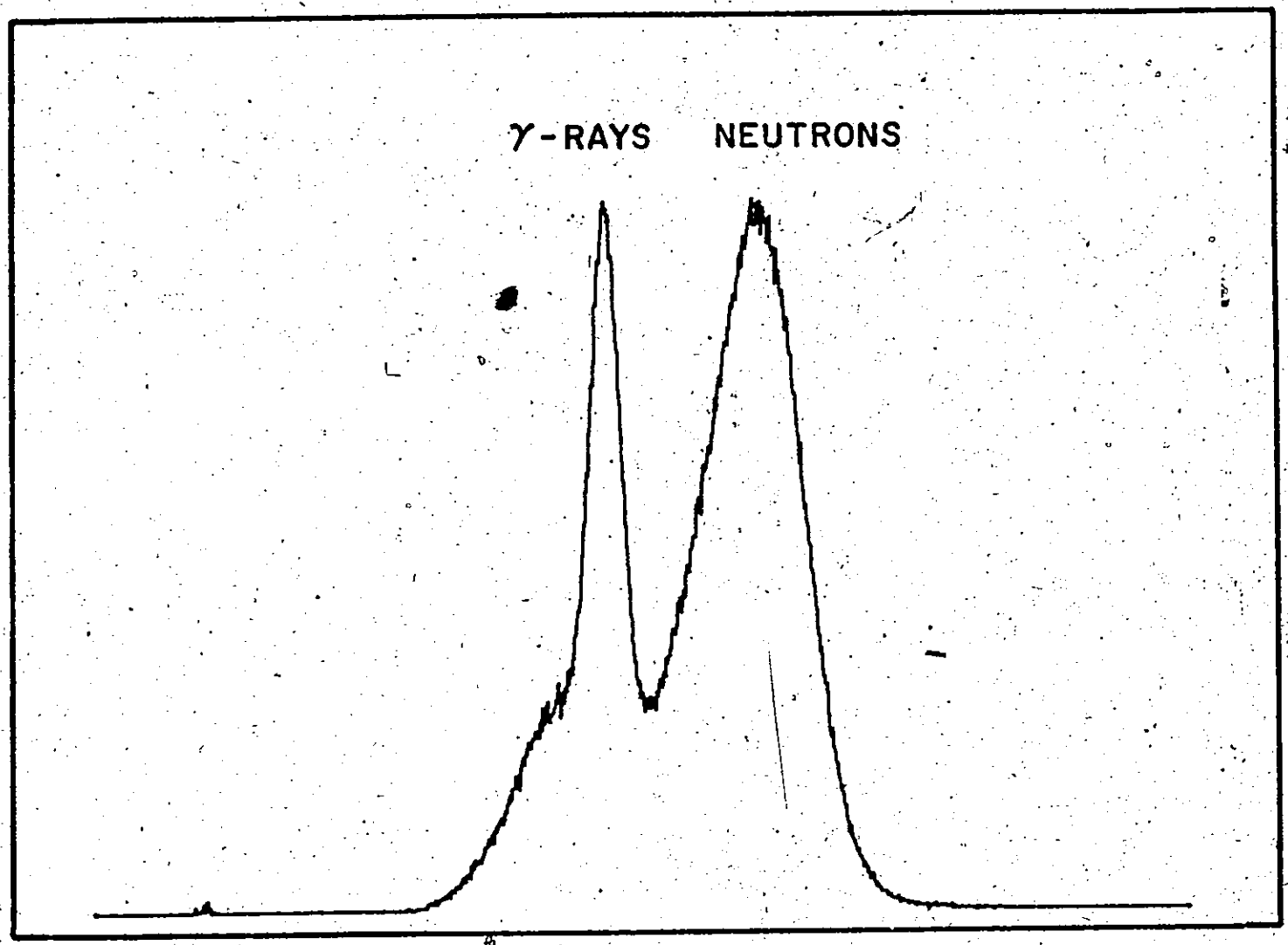
γ-RAYS
NEUTRONS
COUNTS
TIME

TAC was started on the neutron signal and stopped by the Ge(Li) pulse. The TAC range used was 1000 n.s. The data were address recorded on magnetic tape and then sorted off-line. The n-γ time spectra for 72 keV and 76 keV (a prompt γ-ray) were obtained by setting a window on the neutron peak of the shape spectrum and sorting for these energy windows. Figure 3.8 shows these spectra corrected for the Compton background. For 76 keV, the γ-ray region just above the peak was used for Compton subtraction, while for 72 keV the region just below the peak was employed for this purpose. The time resolution for the prompt coincidences was $\sim$ 12 ns full width at half maximum. A least squares fit of the 72 keV time spectrum with an exponential, plus a constant background of accidental events, yields a half-life of 116±5 n.s. Most of the error comes from the uncertainty in the TAC calibration.

By setting a window on the γ-part of the shape spectrum one can obtain a delayed γ-γ coincidence. The half-life of the 72 keV level measured in this manner also comes out to be 116 ns.

Fig. 3.8

The n-γ time spectra (a) the 76 keV (reduced by a factor of ten) and (b) the 72 keV γ-rays. In (b), the dashed line shows the background due to accidentals and the solid line indicates the 116 ns half life; the solid circles show the observed data, the open circles are corrected for accidentals.

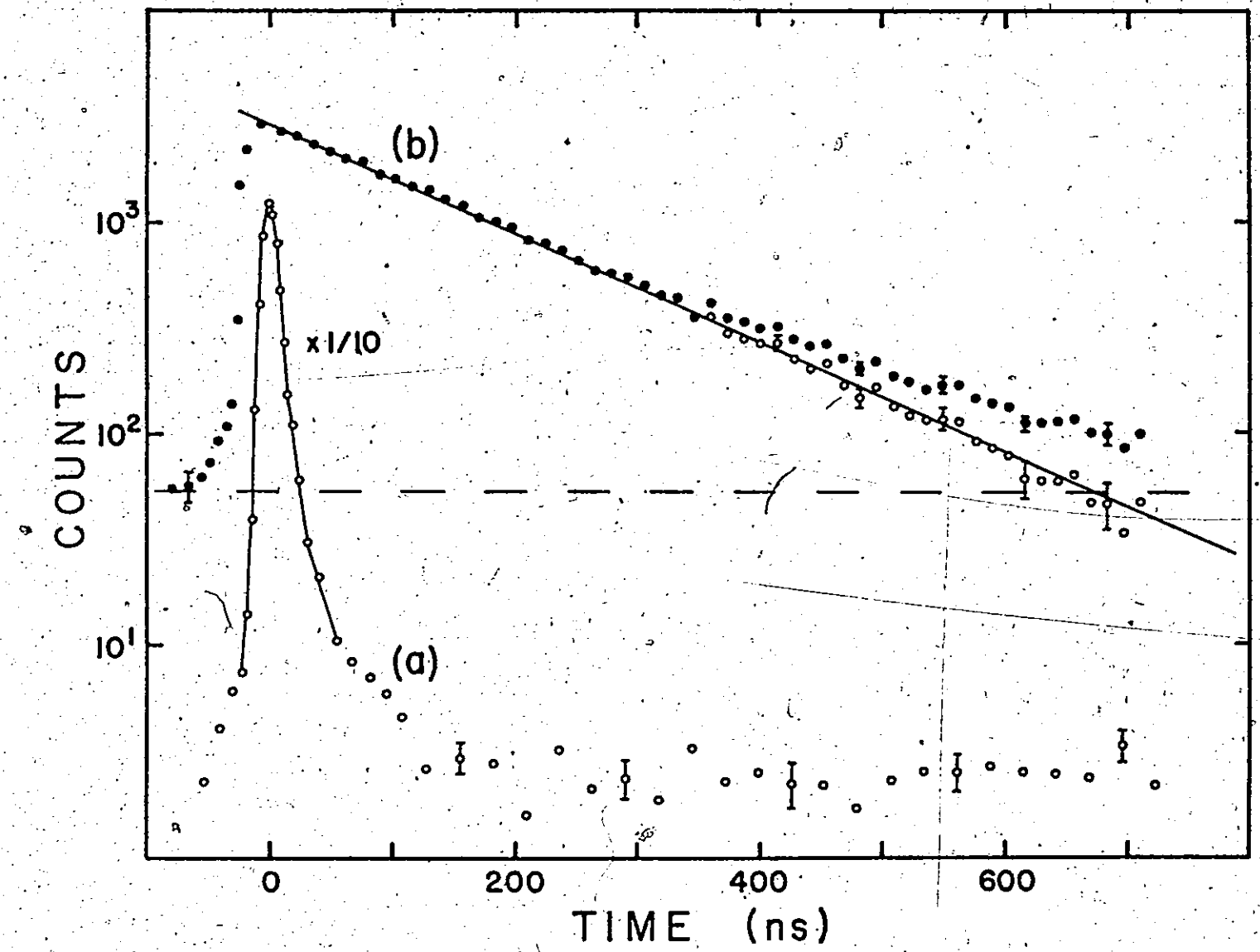
(b)
x1/10
(a)
COUNTS
10^3
10^2
10^1
0
200
400
600
TIME (ns)

CHAPTER IV

DISCUSSION AND INTERPRETATION OF THE RESULTS

Introduction

The experimental data presented in the last two chapters can now be correlated to provide some insight into the nuclear structure of ^{138}La. In this chapter we shall discuss the level scheme of this nucleus proposed on the basis of the particle transfer reactions and γ-ray de-excitation modes. The shell model considerations already discussed in the second chapter seem to be adequate enough for the description of the majority of the states observed up to an excitation of 1.8 MeV. Spin and parity assignments are made on the basis of ℓ-transfers, spectroscopic strengths and the γ-ray transitions. We are very confident about the assignments for the low-lying group of levels. The relevant wave-vectors have been deduced for these levels from their spectroscopic strengths. A lowest seniority shell model calculation is also presented and the spectroscopic factors for proton and neutron transfer are calculated and compared with the experimental findings. Two groups of negative parity states at $E_x > 700$ keV have also been identified and tentative spin assignments are proposed for these levels, mostly on the basis of their spectroscopic strengths. In the higher region of the level scheme there are a number of additional positive parity states

about which little can be said.

4.1 The Level Scheme of ^{138}La

The energies of the various excited states observed in the particle transfer reactions were listed in Table 2.2. Definite parity assignments can be made for the states for which angular distributions are available (Figures 2.8 and 2.11). The γ-rays assigned to ^{138}La in the ^{138}Ba(p,nγ)^{138}La singles and coincidence experiments were listed in Tables 3.1 and 3.2. The level scheme of ^{138}La, constructed on the basis of these findings, is presented in Figures 4.1 and 4.2. Except for the 738.7 keV state, the decay modes of the levels up to an excitation of 823 keV are firmly supported by the coincidence data. The excitation energies of all these levels, from the γ-ray fits, are determined to 0.2 keV. The agreement between these energies and the ones derived from the particle transfer studies is remarkable, the difference being less than 0.5 keV in most cases.

The 43.6 keV γ-ray is assumed to result from the decay of the 116 keV level to the first excited state. As we do not see a γ-ray at 116 keV, it is the only possible mode of decay for this level. One does not expect to detect coincidences with the 43.6 keV γ-ray because low detector efficiency, self-absorption in the target and internal conversion rob it of most of its strength. A 31 keV transition from the 192 keV level was not seen, but a coincidence between the 100.8 and 88.6 keV γ-rays demands the presence of such a transition. The 445 keV peak in the singles spectra is a doublet and the coincidence data only provide definite support

Fig. 4.1

Proposed level scheme for the low-lying states (E_x < 650 keV) of ^{138}La. The notation of Nuclear Data Sheets has been used.

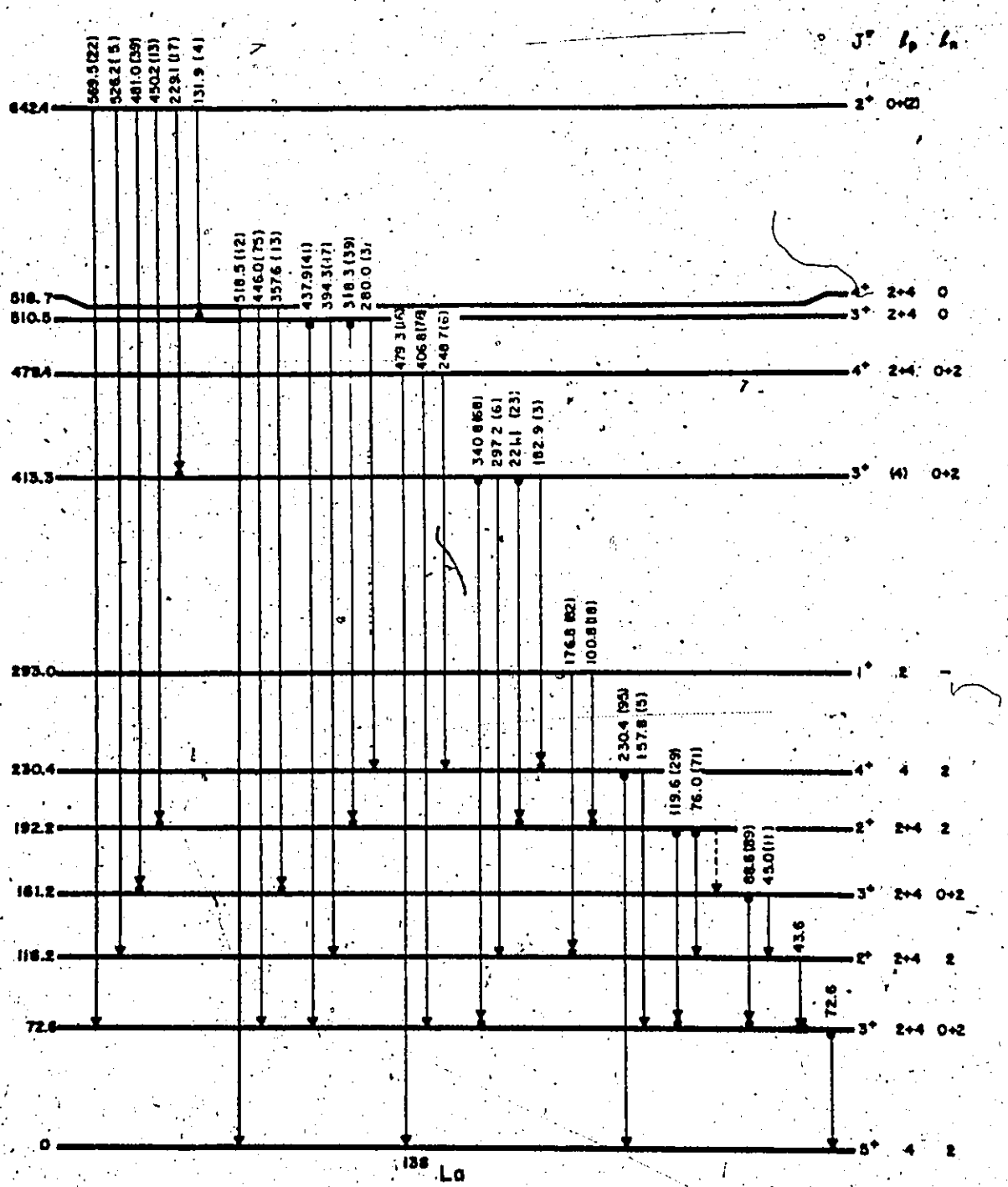
569.5 (22)
526.2 (5)
481.0 (39)
450.2 (13)
223.1 (17)
131.9 (4)
518.5 (12)
446.0 (75)
357.6 (13)
437.9 (41)
394.3 (17)
318.3 (39)
280.0 (3)
479.3 (63)
406.8 (79)
248.7 (6)
340.8 (68)
297.2 (6)
224.1 (23)
182.9 (3)
176.8 (82)
100.8 (18)
230.4 (95)
157.8 (5)
119.6 (29)
76.0 (71)
88.5 (89)
45.0 (11)
43.6
72.6
642.4
518.7
510.5
478.4
413.3
293.0
230.4
192.2
161.2
118.2
72.6
0
J^π l_p l_n
2+ 0+2
4+ 2+4 0
3+ 2+4 0
4+ 2+4 0+2
3+ (4) 0+2
1+ 2 1
4+ 4 2
2+ 2+4 2
3+ 2+4 0+2
4+ 2+4 2
3+ 2+4 0+2
5+ 4 2
^{138}La

Fig. 4.2

Proposed level scheme for ^{138}La showing the γ-ray transitions for the states above 650 keV only. A triangle on the left-hand side of a level indicates that it is populated in the (^{3}He,d) reaction. Levels observed in the (d,t) reaction are designated by triangles on the right. Doubtful levels are shown by dashed lines. The notation of Nuclear Data Sheets is used. Gamma-rays which can be placed in more than one position are indicated by broken lines and are not included in the branching ratio calculations.

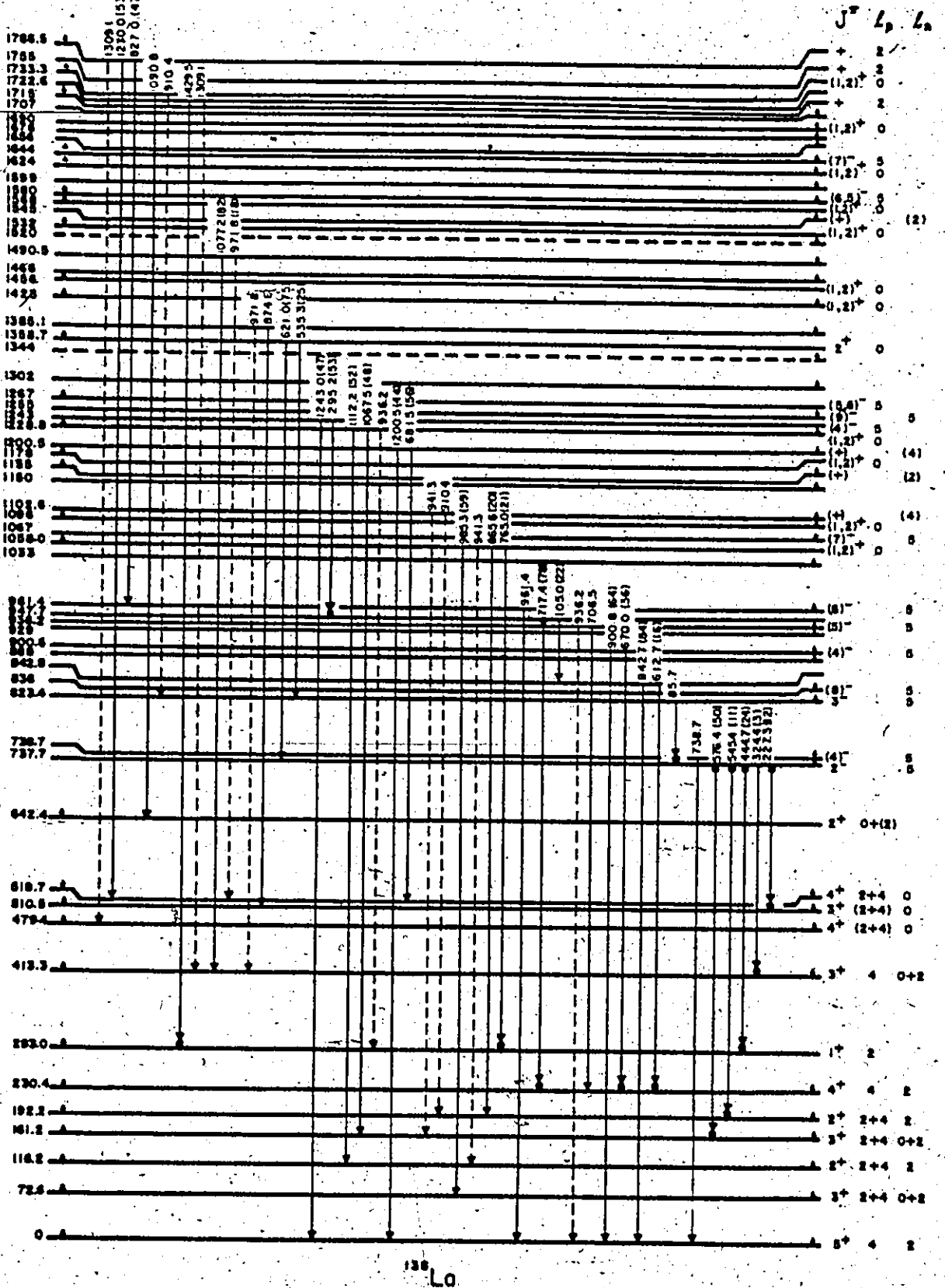
J^π
l_p
l_n
1786.5
1785
1733.3
1722.6
1707
1644
1624
1599
1490.5
1468
1456
1428
1386.1
1358.7
1344
1302
1267
1228.8
1200.5
1178
1155
1160
1103.6
1088
1067
1058.0
1033
961.4
842.8
836
823.4
738.7
737.7
642.4
619.7
610.5
479.4
413.3
293.0
230.4
192.2
161.2
116.2
72.6
0
^{138}La

for the placement of the lower energy component. The higher energy component was assigned to the decay of the 518.7 keV level on the basis of weak evidence for the presence of this doublet in the 72 keV gate and mostly because of a good energy fit.

The two levels at 737 keV deserve a little more attention. The coincidence data require the existence of a level at 737.7 keV. There is also a fairly strong γ-ray at 738.7 keV which is not seen in coincidence with any γ-ray. Three pieces of evidence reject the possibility that this is a ground state transition from the 737.7 keV level:

(i) The energy fit is not within the accuracy of the energy calibration.

(ii) All the stronger γ-rays from the 737.7 keV level are seen in coincidence with the 85.6 keV line feeding it.

(iii) The decay modes of the 737.7 keV level suggest that it has a relatively low spin — its decay to the ground state would be highly improbable.

Considering that a coincidence between the 738.7 keV γ-ray and the 72.6 or 43.6 keV γ-rays could go undetected because of the special problems associated with those gates, one might propose a level at 738.7, 811.3 or 854.9 keV. Since we do not see levels at 811 or 855 keV in the particle reactions and since the peak seen at 737 keV in the (d,t) reaction is stronger than one would expect for a low-spin state we propose that levels at 737.7 keV and 738.7 keV form an unresolved doublet.

The status of the higher part of the level scheme is much less certain. In this region the level density is quite high and it would be too much to hope that all of the levels actually populated in the proton and neutron transfer reactions have been identified. As already discussed in Chapter II only two relatively long (d,t) exposures were carried out (40° and 55°). Several of the levels reported by Lasijo *et al.* have been resolved into doublets. A number of additional states have also been seen. Some of the weakly populated ones, not observed in the (^{3}He,d) reaction as well, may arise from unidentified impurities. These levels are shown by dashed lines in Fig. 4.2.

Only a few γ-rays have been placed in the higher region of the level scheme. Coincidence data provide firm support for some of these assignments. The levels at 842, 947 and 1722 keV are postulated on the basis of this evidence only. The rest of the γ-rays are placed by energy fit, the criterion being that at least two γ-ray energy sums be consistent with one another and correspond to a level seen in a particle reaction. Even so, a number of γ-rays can be placed in alternate ways. These possibilities are indicated in Table 3.1 along with the rest of the assignments, but only the most plausible are illustrated in Fig. 4.2 (with broken lines). One is still left with a number of unplaced γ-rays but this should not be surprising as the (p,n) reaction may populate other levels not seen in the particle experiments, and many of these strong γ-rays might originate from such levels.

It is convenient to discuss the low-lying group of levels first, as the experimental data for this set of levels are more complete and the theoretical interpretation is not so complex. The levels should arise simply from the coupling of the neutron hole to the odd proton. Core excitations and effects due to higher seniority are not expected to contribute at these low excitations. Also we shall feel more confident in using simple shell model considerations for the description of the higher excited states if the low-lying group conforms to the model.

4.2 The Low-lying Positive Parity Levels

The twelve levels observed below 650 keV all have angular distributions in (^{3}He,d) and/or in (d,t) which lead to definite positive parity assignments. Immediately above that group is a series of negative parity states. Since the simple shell model predicts that there should be twelve low-lying positive parity states it is natural to hope that the observed ones correspond to those expected. Their spins do agree with the model. In addition, the observed ℓ-values and spectroscopic strengths of the first eleven states are consistent with the expectation. Although the $\ell_p = 0$ angular distribution of the 642 keV level was a surprise, at first, further consideration reveals that this result is not at all unreasonable.

The general arguments used in establishing the spins are as follows. Purely on the basis of angular momentum conservation

the ℓ values observed in the particle transfer reactions place constraints on the possible spins. In addition, it is not unreasonable, for these low-lying levels, to infer that $\ell_p = 4$ corresponds to $1g_{7/2}$ transfer (not $1g_{9/2}$) and $\ell_n = 2$ corresponds to $2d_{3/2}$ (not $2d_{5/2}$). Since the targets in the (^{3}He,d) and (d,t) reactions have ground state spins of 3/2 and 7/2, respectively, the states populated by the following ℓ values can have spins as shown:

$\ell_p = 4$	$2 \leq J \leq 5$
2	$1 \leq J \leq 4$
0	$1 \leq J \leq 2$
$\ell_n = 2$	$2 \leq J \leq 5$
0	$3 \leq J \leq 4$

Of course these restrictions apply in the case of mixed ℓ values as well as for pure ones. Further constraints on the spins are imposed by the realization that M1 electromagnetic transitions among these low-lying levels should be faster than E2 transitions. Therefore we assume that the observed prompt γ-ray transitions have at least some M1 component and this means that $\Delta J = 0, \pm 1$ for those cases.

4.2a Spin Assignments

If the foregoing considerations are used most advantageously the spins of all the levels in this positive parity group can be determined uniquely. The order in which the levels are discussed is chosen with this in mind. We begin with the ground state for which the spin has been determined by direct measurement.

The ground state: As a result of an n.m.r. experiment, Sogo and Jeffries (1955) reported the ground state spin to be 5. It decays with a half-life of $\sim 10^{11}$ years to the 2^+ states of the neighbouring nuclei ^{138}Ce and ^{138}Ba (Ellis *et al.* (1970)). The log ft values of 19.2 and 18.2, respectively, have been taken to indicate third forbidden transitions and thus a J^π of 5^- but the positive parity assignment is demanded by:

(i) the $\ell_n = 2$ angular distribution observed in ^{138}La(d,p)^{139}La (g.s.) (Dubard *et al.* (1971)),

(ii) the $\ell_n = 2$ values in neutron pick-up reported by Lasijo *et al.* (1972), and Helton *et al.* (1973) as well as in the present studies, and

(iii) the pure $\ell_p = 4$ angular distribution in our ^{137}Ba(^{3}He,d)^{138}La experiments.

The 72 keV state: The admixture of $\ell_n = 0$ in the (d,t) angular distribution limits the spin of this, the first excited state, to 3 or 4. Since the measured half life of 116±5 ns is much too long for an M1 transition the latter possibility is highly unlikely. The Weisskopf estimate for the life time of a 72 keV E2 transition, after correcting for internal conversion, is $\sim$ 420 ns, which would mean an enhancement of 3.6. Thus our measurement leads to a definite assignment of $J^\pi = 3^+$ which agrees with the spin assignment of Helton *et al.* and Lasijo *et al.* extracted from the (2J+1) rules in their neutron pick-up work.

The 293 keV state: The complete absence of this state in the (d,t)

experiments and a relatively strong pure $\ell_p = 2$ angular distribution in the (^{3}He,d) reaction strongly suggest that it is the predicted 1^+ state of the model. There is no observed gamma-ray transition to the ground state (5^+) or to the 72 keV state (3^+). Instead, it decays with considerably less energetic γ-rays to two other low-lying states. This preference is easily understood if the J^π of the 293 keV state is 1^+.

The 230 keV state:. Pure $\ell_n = 2$ and $\ell_p = 4$ angular distributions in the (d,t) and (^{3}He,d) reactions, respectively, suggest that the dominant configuration for this level is $(\pi 1g_{7/2}\nu 2d_{3/2}^{-1})$. Thus a J^π of 2^+, 3^+, 4^+ or 5^+ is possible. Its decay to the 5^+ ground state and 3^+ first excited state fixes the spin as 4^+ if these transitions are at least partly M1. This agrees with the assignment by the earlier workers, made on the basis that the $\ell_n = 2$ strength is the second largest.

The 116 keV state: From the observed angular distributions ($\ell_n = 2$ and $\ell_p = 2+4$), it can have a spin of 2, 3 or 4. It is fed by the 293 keV (1^+) state and decays to the 72 keV (3^+) level, which requires the J^π to be 2^+. This is the same as proposed by Lasijo *et al.* and Helton *et al.*, on the grounds that it is the weakest of the four levels showing an $\ell_n = 2$ angular distribution.

The 192 keV state: Helton *et al.* and Lasijo *et al.* assign it a J^π of 3^+. The former group reports a mixed $\ell_n = 0+2$ angular distribution and hence could only assign 3^+ or 4^+, but the latter authors report a pure $\ell_n = 2$ distribution and suggest 3^+ on the basis of its

spectroscopic strength in (d,t) although the assignment is stated to be very tentative. Our data show ℓ=2 distributions in both neutron pick-up and proton transfer, which means that J^π could be 2^+, 3^+ or 4^+. The level is fed by 293 keV (1^+) state and decays to the 3^+ first excited state, and hence we assign it a J^π of 2^+.

The 161 keV state: This is another level for which our spin assignment differs from that of the earlier workers. Both assigned it as 2^+, though Lasijo *et al.*'s assignment was very tentative. Helton *et al.* did see a slight admixture of $\ell_n = 0$ in its angular distribution, which could rule out their 2^+ assignment. In our (d,t) measurements at small angles the contribution from $\ell_n = 0$ is very obvious and thus it can only be 3^+ or 4^+. The level is observed to decay to the 72 keV (3^+) and 116 keV (2^+) levels. Hence 3^+ is the only choice.

The 413 keV state: The mixed $\ell_n = 0+2$ angular distribution in (d,t) only allows a J^π of 3^+ or 4^+ for this level. It decays to the 192 keV (2^+), 72 keV (3^+) and 230 keV (4^+) states but not to the ground state (5^+) or to the 293 keV (1^+) state. These observations strongly favour a $J^\pi = 3^+$ assignment, in contrast to the 4^+ assignment of the earlier workers.

The 479 keV state: An almost pure $\ell_n = 0$ angular distribution observed in the neutron pick-up reaction also limits the J^π of this level to 3^+ or 4^+. The (p,nγ) singles data suggest that it decays to the ground state (5^+), 72 keV (3^+) and 230 keV (4^+). Hence we

propose J^π is 4^+ for this level which differs from the earlier assignment of 3^+. Both of the previous investigations were led astray because the 510-518 doublet was not resolved and thus the state at 479 keV appeared to be the weaker of two levels populated by pure $\ell_n = 0$.

The 510 and 518 keV states: It was not possible to extract separate angular distributions for these two close-lying levels in the particle experiments. However, they show almost pure $\ell_p = 2$ and $\ell_n = 0$ angular distributions when taken together. In the forward angle (d,t) plates, which were counted in 1/8 mm strips for better resolution, the intensity ratio of the 518 to 510 keV states varies from 2.7 at 7.5° to 1.9 at 14°. This suggests that the lower state might be populated also by a weak admixture of $\ell_n = 2$. In any event these data indicate that both levels must have $J^\pi = 3^+$ or 4^+. The 510-keV state decays to the 230 (4^+), 192 (2^+), 116 (2^+) and 72 keV (3^+) levels. Of course, it is impossible to say whether there is a branch to the ground state or not because of the annihilation peak at that energy. Assuming that there isn't such a branch, we have to assign 3^+ for the 510 keV state. The 518 keV state, on the other hand, feeds the ground state (5^+) and the two lowest 3^+ states (72 and 161 keV). Even for 500 keV γ-rays the M1 rate should still be dominant over non-collective E2's and thus this state is assigned $J^\pi = 4^+$. Since it would be difficult to explain two states of the same spin and configuration only 8 keV apart it is reassuring that the available data for them do lead to different assignments.

The 642 keV state: This state, the last of twelve low-lying positive parity levels, was not observed at all in the previous neutron transfer experiments. In our (d,t) exposures a very weak peak appears at 642 keV although its status is uncertain because the first excited state (29 keV) of ^{140}Pr, due to a possible ^{141}Pr impurity, is expected to interfere at this excitation energy. However, in proton transfer, it is very much evident and shows an essentially pure $\ell_p = 0$ angular distribution which limits J^π to 1^+ or 2^+. This is not to say that an $\ell_p = 2$ contribution can be completely ruled out since it would be easily masked by the lower ℓ_p value. On the basis of shell model systematics this would be an unexpectedly low excitation energy for the $(\pi 3s_{1/2}, \nu d_{3/2}^{-1})$ configuration. It is not surprising, therefore, that this state actually represents < 5% of the total $\ell_p = 0$ strength, which is concentrated mostly above 1055 keV. The question then arises - what is the main component in the wave-function of the 642 keV state? We shall leave this unanswered for a while to follow it up in section 4.2c. The γ-ray decay of this level feeds all four of the lower-lying 3^+ states, one of them by a transition of only 132 keV, and both of the 2^+ states. Thus the possibility of $J^\pi = 1^+$ has to be discounted and we adopt 2^+ for this state.

This completes the description of the twelve low-lying positive parity states. With the adopted spins, all but one of the observed γ-ray transitions between the members of the group are consistent with being at least partly M1. The exception is in the decay of the first excited state, which has no option but to go by E2, and

as a result the level has a life-time of 116 n.s. It should be emphasized that shell model systematics have been invoked in this analysis only to the extent that the $\ell_p = 2$ spectroscopic strength is taken to be $2d_{3/2}$, and $\ell_p = 4$ is limited to $1g_{7/2}$. The resulting spins however are a beautiful confirmation of the model - as we count one 1^+, three 2^+, four 3^+, three 4^+ and one 5^+ level. Before proceeding with a detailed comparison between the model and the observed spectroscopic factors, we discuss a further verification of these spin assignments that can be obtained by examining the excitation functions for the γ-rays that de-excite these levels.

4.2b γ-Ray Excitation Functions and the Spins

Non-selective as compound nucleus reactions may be, the cross-sections for a (p,n) reaction still depend on the spins of the levels being populated. Since protons of low energy do not bring very much angular momentum into the nucleus and with the target being 0^+, higher spin states will be weakly populated. Their relative strength can therefore be improved appreciably by increasing the bombarding energy. Although the intensities of de-exciting γ-rays depend upon indirect feeding as well as direct, the ratios of the intensities of such γ-rays, at two different beam energies, should still be considerably different for different spins.

In Fig. 4.3, intensity ratios for the strongest well-resolved γ-ray de-exciting each low-lying level are plotted against the spins of the levels as deduced in the previous section. A few

Fig. 4.3

A plot *versus* spin of the observed γ-ray intensity ratios . Curve A is I_γ(7.5 MeV)/I_γ(5.5 MeV) and curve B is I_γ(7.5 MeV)/I_γ(6.5 MeV). The solid circles are for the low-lying positive parity levels while the open circles designate more highly excited negative parity states. Spin assignments are definite except for the open circle enclosed in parentheses. The ratio observed for it suggests a spin of 4 for the 738.7 keV level.

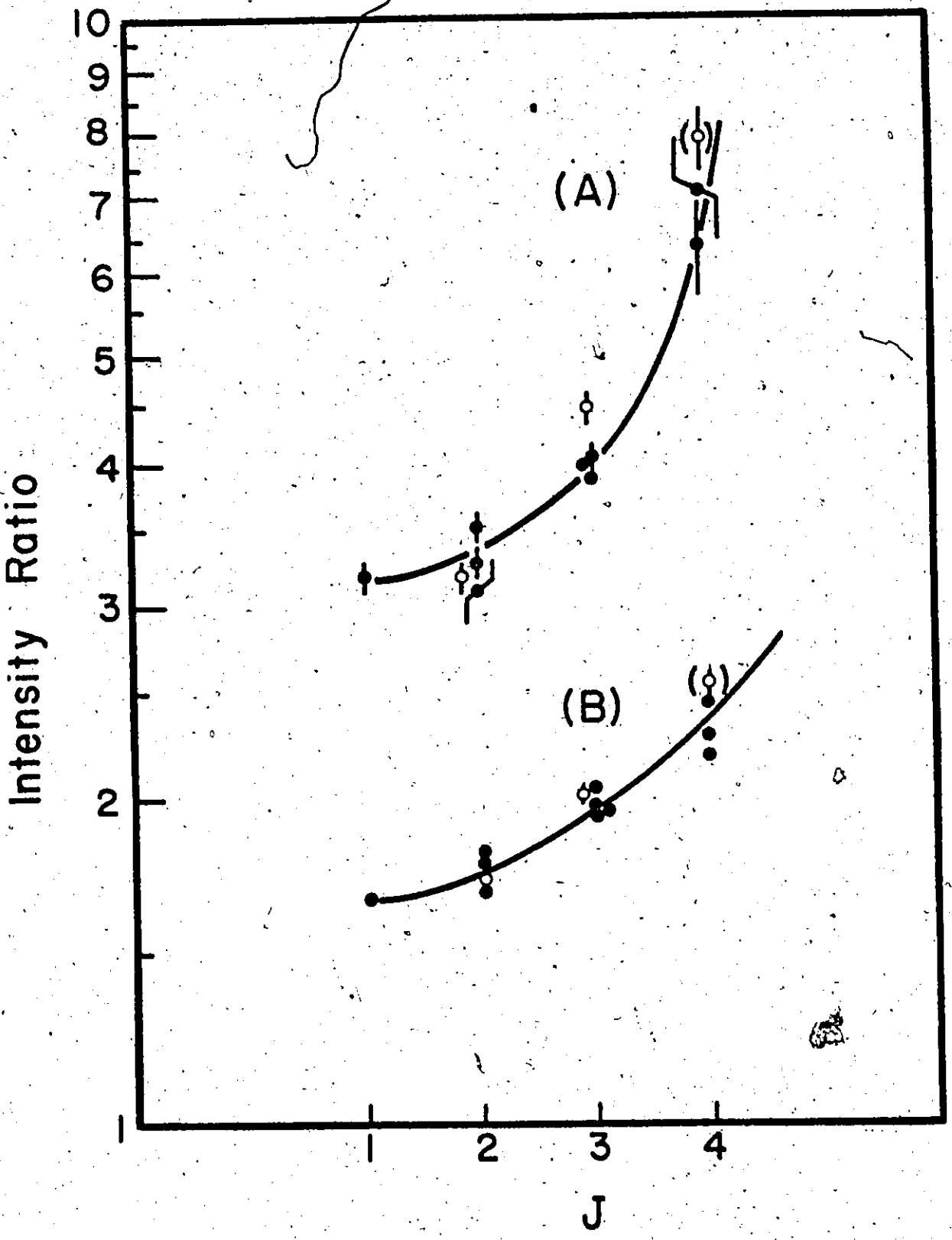
Intensity Ratio
10
9
8
7
6
5
4
3
2
1
(A)
(B)
1
2
3
4
J

points from higher levels are also included where available data allow firm spin assignments. These are indicated by open circles and will be discussed in section 4.3a. The two curves show I_γ(7.5 MeV)/I_γ(6.5 MeV) and I_γ(7.5 MeV)/I_γ(5.5 MeV). Intensities were normalized to the integrated beam current and the same thick target was used throughout. The ratios are independent of the detector efficiency, of course, because the detector geometry was not changed during these experiments. A small correction for the different self-absorption in the target was called for and has been included in the case of γ-rays below 120 keV. Since our spin assignments and intensity ratios generate smooth curves of the anticipated general shape, the results add further support for the correctness of those assignments. Figure 4.3 shows that the method can be used at least to provide tentative spins in the event that other means (threshold angular distributions, for example) are not feasible. Obviously it would be more definitive for high spins rather than low.

It is especially interesting to note that the shape of the 445 keV γ-ray doublet changes remarkably with the change in beam energy, the higher energy component becoming relatively stronger at higher bombarding energy. This is consistent with the placement of the two γ-rays in the level scheme, 446.0 keV de-excites a 4^+ state while 444.7 keV is emitted by the 2^- state at 737.6 keV.

4.2c The 2J+1 Rule and the Wave Functions

The spectroscopic strengths observed in the proton transfer and neutron pick-up reactions have already been listed in Tables 2.5 and 2.9. We shall now investigate the distribution of these strengths as a function of the assigned spins. Figs. 4.4 and 4.5 show the results of such an investigation, for (^{3}He,d) and (d,t) respectively, in the form of separate histograms for $\ell_p = 2$, $\ell_n = 0$ and $\ell_n = 2$. The spectroscopic strengths for $\ell_p = 4$ are not presented because of their large uncertainties. The solid lines are the sum-rule predictions while the dashed lines are normalized to match the observed total strengths. The fact that the 2J+1 rule works so well enhances the degree of confidence in our spin assignments.

As already suggested in Chapter II, one expects the wave vectors of the twelve low-lying positive parity levels, after configuration mixing, to be given as follows:

J^π	Wave Function	No. of Levels
1^+	ϕ_1	1
2^+	$\alpha_{i1}\phi_1+\alpha_{i2}\phi_2+\alpha_{i4}\phi_4$	3
3^+	$\alpha_{i1}\phi_1+\alpha_{i2}\phi_2+\alpha_{i3}\phi_3+\alpha_{i4}\phi_4$	4
4^+	$\alpha_{i1}\phi_1+\alpha_{i2}\phi_2+\alpha_{i3}\phi_3$	3
5^+	ϕ_2	1

where $\phi_1 = |\pi 2d_{5/2}\ \nu 2d_{3/2}^{-1}; J\rangle$

$\phi_2 = |\pi 1g_{7/2}\ \nu 2d_{3/2}^{-1}; J\rangle$

Fig. 4.4

The 2J+1 rule for the $\ell_p = 2$ spectroscopic strengths of the low-lying levels populated in the $^{137}Ba(^3He,d)^{138}La$ reaction. The strength observed for the 510-518 keV doublet has been divided for best agreement. The dashed line shows the expected distribution *versus* spin of the total observed strength. No prediction based on the sum rule is possible because the number of $2d_{5/2}$ protons in ^{137}Ba is unknown.

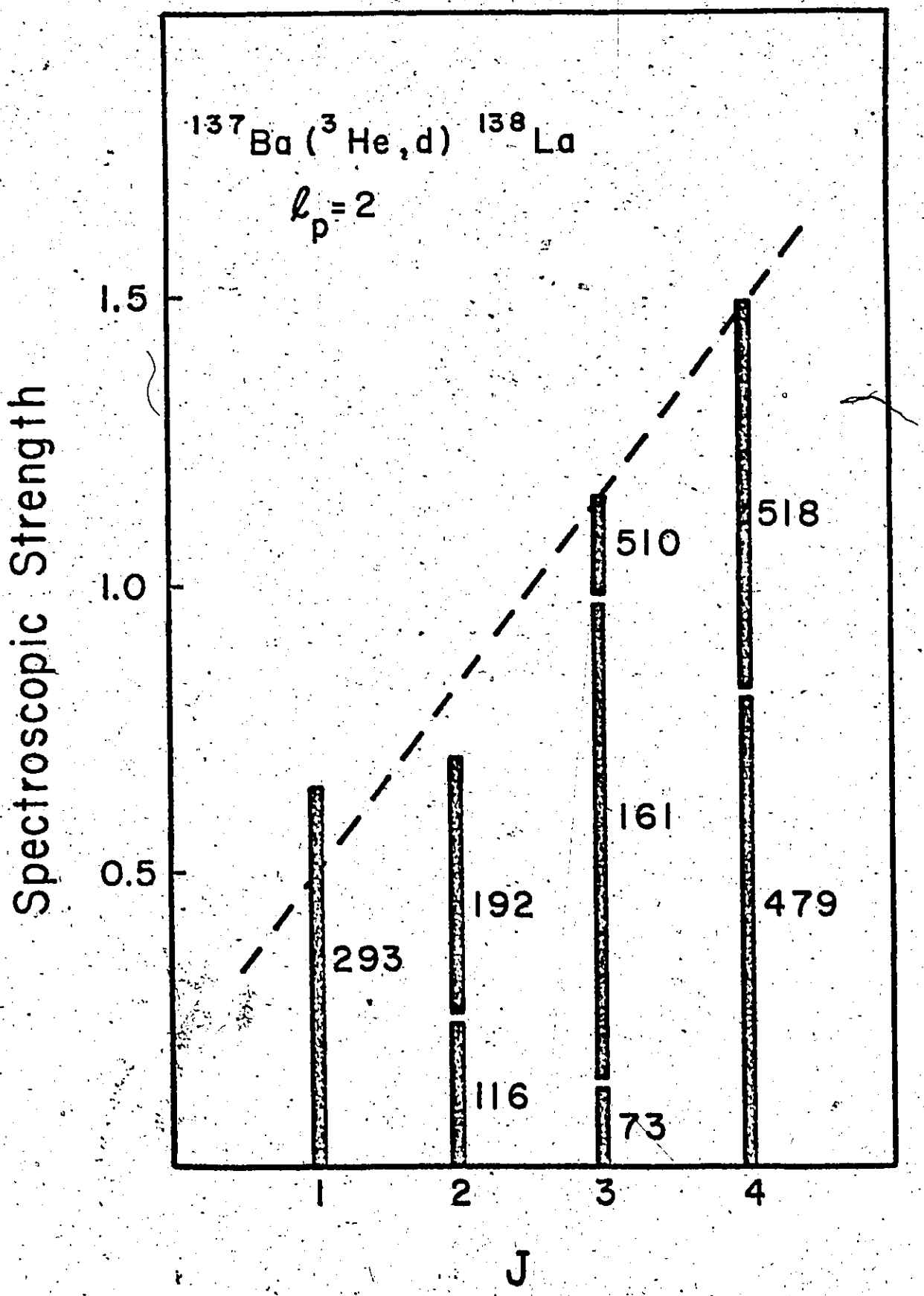
$^{137}Ba(^{3}He,d)\ ^{138}La$
$\ell_p = 2$
Spectroscopic Strength
1.5
1.0
0.5
293
192
116
510
161
73
518
479
1
2
3
4
J

Fig. 4.5

The 2J+1 rule for the ℓ_n = 0 and 2 spectroscopic strengths of the low-lying levels populated in the $^{139}La(d,t)^{138}La$ reaction. The solid lines show the expected distribution *versus* spin of the strengths predicted by the sum rule. The dashed lines are normalized to the total observed strengths.

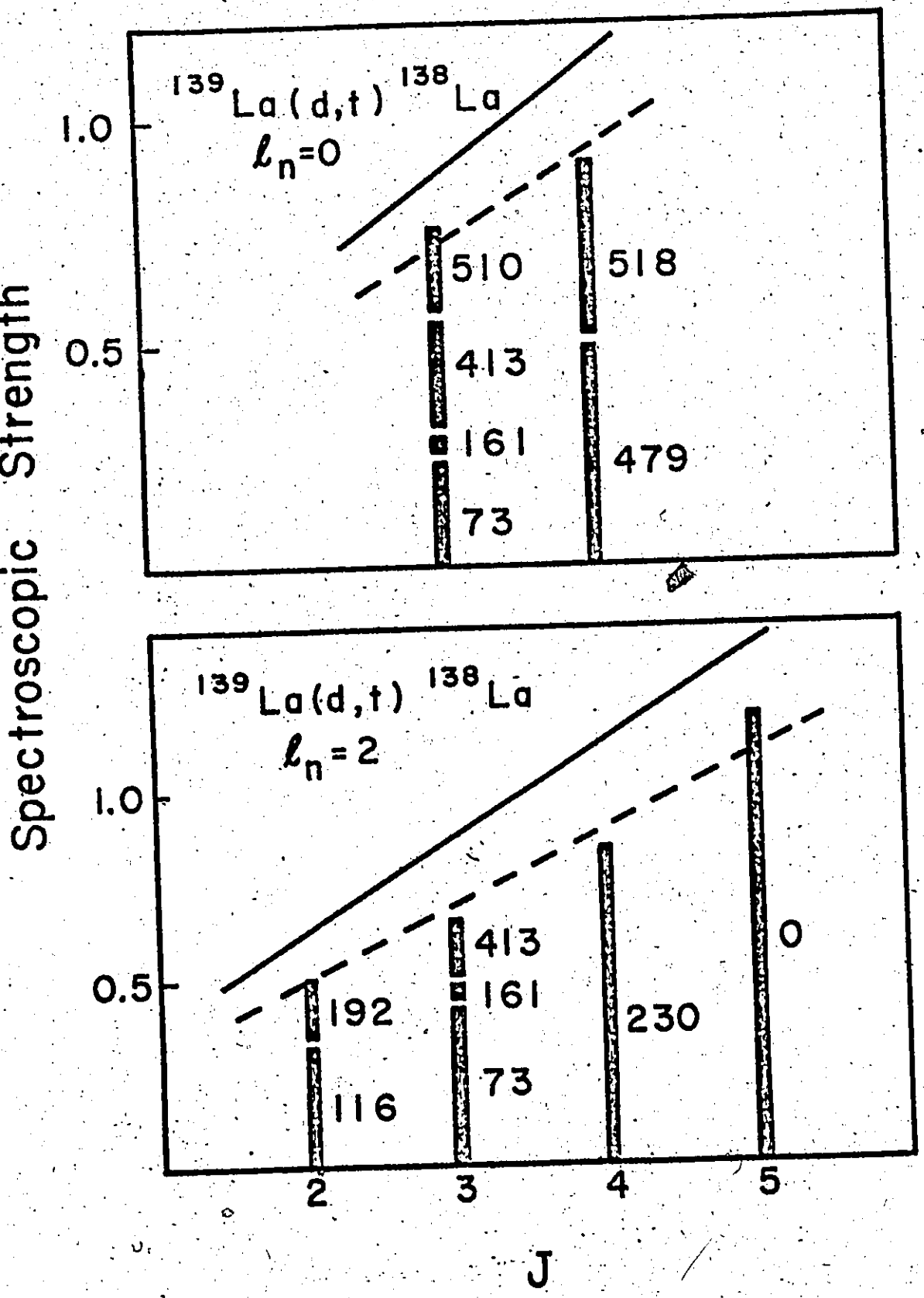
^{139}La(d,t)^{138}La
ℓ_n=0
1.0
0.5
510
518
413
161
479
73
^{139}La(d,t)^{138}La
ℓ_n=2
1.0
0.5
413
192
161
230
0
116
73
2
3
4
5
J
Spectroscopic Strength

$$\phi_3 = |\pi 1g_{7/2}\ \nu 3s_{1/2}^{-1}; J>$$

and

$$\phi_4 = |\pi 2d_{5/2}\ \nu 3s_{1/2}^{-1}; J>.$$

Of course, orthonormality requires that $\sum_j \alpha_{ij}^2 = \sum_i \alpha_{ij}^2 = 1$ for each J value. Knowledge of the three independent spectroscopic factors for each level provides a direct measure of α_{i1}^2, α_{i2}^2 and α_{i3}^2. Even if one had reliable $\ell_p = 4$ strengths they would not add anything because they also measure α_{i2}^2. Unfortunately it is impossible to extract the relative phases of the coefficients since no interference term arises in the calculation of single nucleon spectroscopic factors.

In Table 4.1 we present the α_{ij}^2 for all the low-lying states. These are calculated in the following way. The total observed strength for each given ℓ is partitioned into the shares expected for each J, according to 2J+1 rule. The observed spectroscopic factors for each state, expressed as a fraction of these partial strengths, then give α^2. Thus only the relative strength is actually used. When the observed components of the spin 2^+ and 3^+ states fail to add up to 100%, it is logical to presume that the unseen part arises from configuration 4, which is measured by α_{i4}^2. The 642 keV state requires one additional comment. Since it turned out to have an $\ell_p = 0$ angular distribution, the spectroscopic factor for that contribution (taken as a fraction of the expected sum rule limit of 2) was subtracted from 1 and the remainder equated to α_{i4}^2. As is evident from the table the totals for α^2 in each row and column are pleasantly close to 1, which demonstrates that the low-lying levels can be adequately described

Table 4.1

The Wave Functions of the Low-Lying Group

J^π	E_x	α^2_{i1}	α^2_{i2}	α^2_{i3}	α^2_{i4}	Σ
1^+	293	1.00[a]	-	-	-	1.00
2^+	116	0.29	0.66	-	.05[a]	1.00
	192	0.54	0.32	-	0.14[a]	1.00
	642	0	0	-	0.90[b]	0.90
	Σ	0.83	0.98	-	1.09	
3^+	72	0.11	0.65	0.36	0	1.12
	161	0.73	0.06	0.04	0.17[a]	1.10
	413	0	0.23	0.36	0.41	1.00
	510	0.21	0	0.28	0.51	1.00
	Σ	0.95	0.94	1.04	1.09	
4^+	230	0	0.95	0	-	0.95
	479	0.52	0	0.55	-	1.07
	518	0.44	0	0.44	-	0.88
	Σ	0.96	0.95	0.99	-	
5^+	0	-	1.00[a]	-	-	

a - Adjusted so that the wave function is normalised to unity.

b - The rest of the wave-function consists of $\pi s_{1/2} \nu d^{-1}_{3/2}$.

by the simple shell model.

4.3 Higher Excited States

Above 642 keV, the properties of the observed states are not as clear as was the case for the low-lying ones. Indeed, one cannot even assume that we have identified all the states that exist since many of the observed γ-rays remain unplaced and there could be many excited configurations, including core excitations, that would not be populated in either the neutron or proton transfer investigations.

The levels seen in the (^{3}He,d), (α,t) and (d,t) reactions were listed in Table 2.2. Definite parity assignments can be made for most of the states observed in (^{3}He,d). For (d,t), the negative parity assignments have been taken from Lasijo *et al.* None of the other relatively stronger levels (1102, 1156, 1200 and 1545 keV) seen in (d,t) at 40° and 55° seem to have $\ell_n = 5$ angular distributions, their cross-sections at the forward angles being too large for such an ℓ-value. Since the shell model would suggest $h_{11/2}$ as the only likely origin of negative parity states below at least 1.8 MeV, it seems safe to assign positive parity to all these states. Although it is difficult to fit the angular distributions reported by Lasijo *et al.*, they seem to be consistent with $\ell_n = 2$ or 4. Nothing can be said about the parities of the levels populated only weakly in (d,t).

It is futile to discuss individually all the levels shown in Fig. 4.2. However, a number of spin assignments can be made

and the interpretation of the negative parity states seems definite enough.

4.3a The Negative Parity States

A total of eight negative parity states, with spins ranging from 2 to 9, should be seen in (d,t) arising from the configuration $(\pi 1g_{7/2}\ \nu 1h_{11/2}^{-1})$. In the proton transfer experiments one expects only four states formed by coupling an $h_{11/2}$ proton to the $d_{3/2}$ neutron hole to give $J^\pi = 4^-, 5^-, 6^-$ and 7^-. All of these states, except the 2^- and 9^-, could mix with the states arising from $(\pi 1h_{11/2}\ \nu 3s_{1/2}^{-1})$ and $(\pi 2d_{5/2}\ \nu 1h_{11/2}^{-1})$ and thus give rise to many more observable negative parity levels. In the absence of significant configuration mixing, these may not be identified in the particle transfer work but can still be populated in the (p,nγ) reaction.

Conveniently enough, only 4 levels show the distinctive $\ell_p = 5$ angular distribution in the (^{3}He,d) reaction, and, as already noted, they essentially exhaust the $h_{11/2}$ strength. Tentative spins can be assigned on the basis of the 2J+1 rule and the histogram of their spectroscopic strengths, shown in Figure 4.6, is very encouraging.

Lasijo *et al.* reported seven $\ell_n = 5$ levels in the (d,t) reaction. With the resolution of the doublet at 833 keV we have increased this number to a perfect eight but the γ-ray data have shown that there are actually two levels at ∿ 738 keV, one of these having spin 2 and the other most probably spin 4. Since the (d,t) cross section for the unresolved doublet is consistent

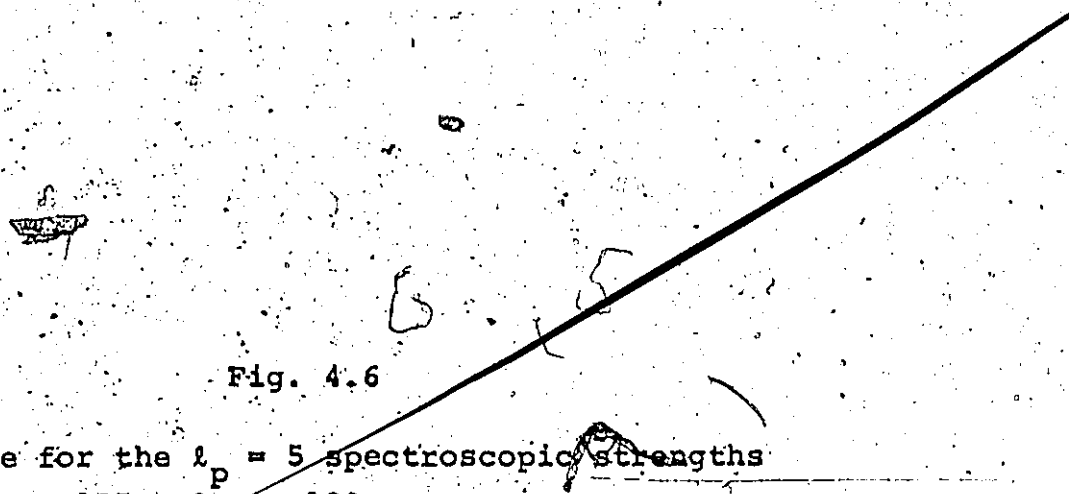

Fig. 4.6

The 2J+1 rule for the $\ell_p = 5$ spectroscopic strengths observed in the $^{137}Ba(^3He,d)^{138}La$ reaction. The solid line shows the expected distribution of the total strength predicted by the sum rule. The dashed line is normalized to the total observed strength and the spins of the states have been tentatively assigned to best fit it.

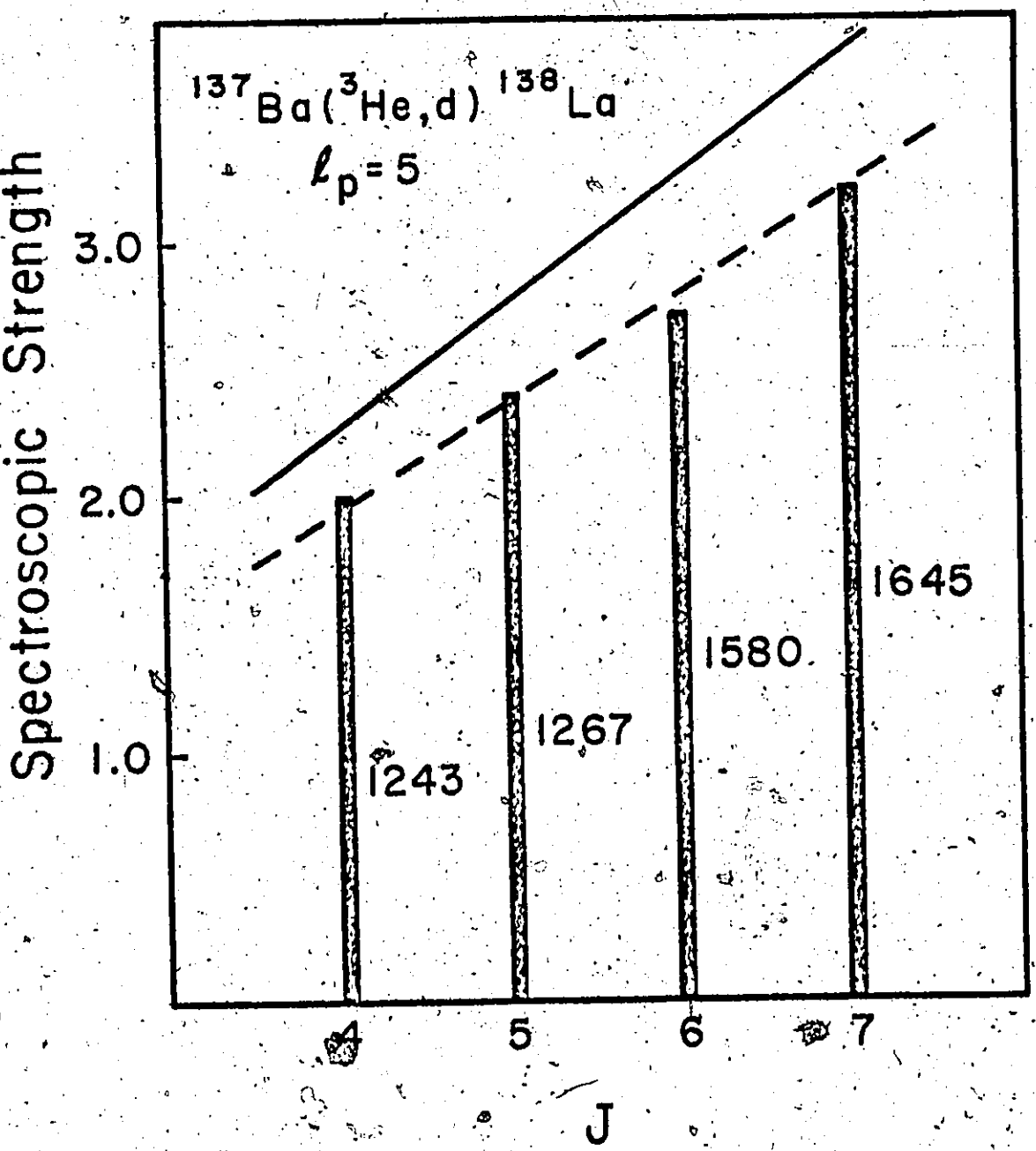
$^{137}Ba(^{3}He,d)^{138}La$
$\ell_p = 5$
Spectroscopic Strength
3.0
2.0
1.0
1243
1267
1580
1645
4
5
6
7
J

with pure $\ell_n = 5$, we have taken the view that both states have odd parity. Thusthere are nine states in all which exhaust the sum rule limit. In the histogram showing the application of the 2J+1 rule, Fig. 4.7, the spectroscopic strength at 738 keV has been divided accordingly. The spin assignments of all the negative parity levels are discussed below.

The 737.7 keV state The decay of this level to 1^+, 2^+ and 3^+ states, established from the coincidence data, requires that its spin be 2. This is confirmed by the intensity ratios for the de-exciting γ-rays (shown as open circles in Fig. 4.3).

The 738.7 keV state The 738.7 keV γ-ray assigned as the ground state decay of this state would suggest a spin of 4, 5, or 6. Its excitation function implies a relatively high spin and the intensity ratios, plotted on Fig. 4.3 in parentheses, are consistent with spin 4.

The 823.4 keV state This state decays by an 85.6 keV transition to the 2^- level at 737.7 keV and so $J^\pi = 1^-$, 2^- or 3^-. Since the model allows only one 2^- state and no 1^-, we propose that it is 3^-. The intensity ratios, at different beam energies, for the 85.6 keV γ-ray are also consistent with a J = 3 assignment.

The 836 keV state The 836 and 1067 keV levels have the second largest $\ell_n = 5$ spectroscopic strengths and are the logical candidates for spins 7 and 8. None of the observed γ-rays could be definitely ascribed to these states which is consistent with the fact that we would not expect to populate such high spins in the

Fig. 4.7

The 2J+1 rule for the $\ell_n = 5$ spectroscopic strengths observed in the $^{139}La(d,t)^{138}La$ reaction. The solid line shows the expected distribution of the total strength predicted by the sum rule. For the 737, 738 and 823 keV levels the spins are fairly firmly determined from the γ-ray data. The tentative spins of the other levels have been chosen to provide a best fit to the 2J+1 rule. Also, the spectroscopic strength of the 738-739 keV doublet has been divided to give optimum agreement with expectation.

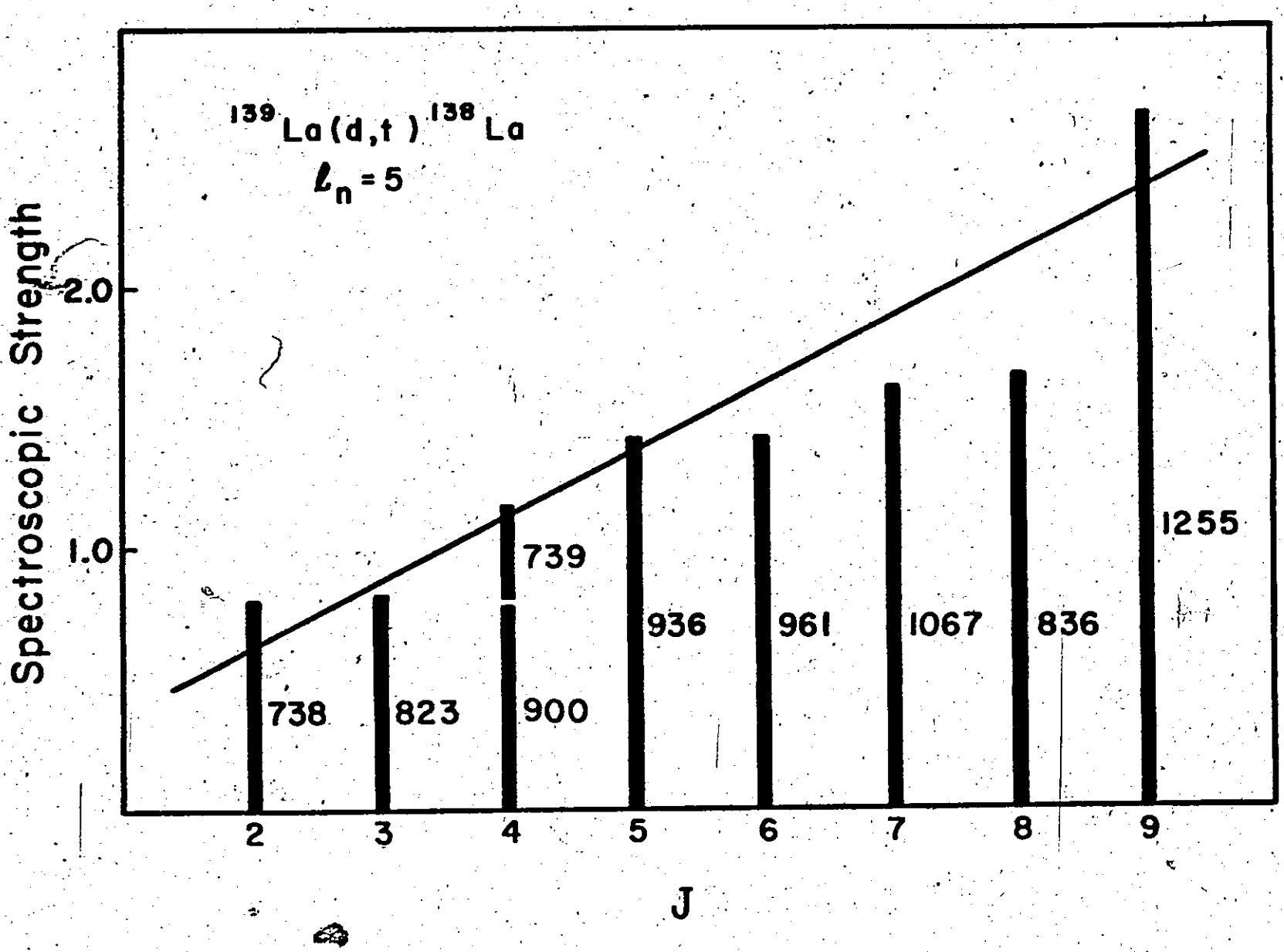
^{139}La(d,t)^{138}La
$\ell_n = 5$
Spectroscopic Strength
2.0
1.0
738
823
739
900
936
961
1067
836
1255
2
3
4
5
6
7
8
9
J

(p,n) reaction. In Fig. 4.2 the 836 and 1067 keV levels are shown as $(8)^-$ and $(7)^-$, respectively. These tentative assignments could easily be reversed.

The 900.6 keV state This negative parity level decays to both the ground state (5^+) and the 230 keV (4^+). Thus J^π can only be 4^- or 5^- if M2 transitions are ruled out as less likely than E1. Since the 739 keV state does not have sufficient (d,t) strength to fit the 2J+1 rule for spin 4, it is proposed that the 900.6 keV level is also 4^-.

The 936.2 keV state The $\ell_n = 5$ spectroscopic strength suggests a J^π of 5^- or 6^- for this level. Its decay to the ground state (5^+) and 230 keV state (4^+) recommends a 5^- assignment.

The 961.4 keV state On the basis of its (d,t) strength, this state, like the preceding one, could have a spin of 5 or 6. The observed decay to the ground state is consistent with either of these values. Since the 5^- assignment has been used up, the J^π of this state is tentatively assumed to be 6^-.

The 1067 keV state This state, which was discussed earlier along with the 836 keV level, is either 7^- or 8^-.

The 1243.0 keV state Since this is the weakest of the negative parity states observed in the proton transfer reactions, we assign it a J^π of 4^- in accordance with the 2J+1 rule. A 1243 keV transition to the 5^+ ground state is not inconsistent with this assignment.

The 1255 keV state This is the strongest $\ell_n = 5$ state observed in (d,t) and hence it is the unchallenged competitor for the 9^- assignment. None of the observed γ-rays can be assigned to it, nor

would one expect a (p,n) reaction to populate a level of such high spin.

The 1267 keV state This state has slightly less $\ell_p = 5$ strength than the 1580 keV level and so it presumably has a J^π of 5^- or 6^-. In Fig. 4.2 it has been shown as $(5)^-$.

The 1580 keV state Second in strength among the negative parity states populated in (^{3}He,d), this state is tentatively assigned as $(6)^-$ but it could be 5^- instead.

The 1645 keV level Being the strongest $\ell_p = 5$ level observed in the proton transfer reactions, this state should be assigned 7^- status. As for the other high spin states, the γ-ray studies provided no information about its decay modes.

4.3b The Others

Not much can be said about most of the remaining higher excited states. Angular momentum conservation limits those populated by $\ell_p = 0$ to $J^\pi = 1^+$ or 2^+ and $\ell_p = 2$ (taken to be $2d_{3/2}$ transfer at this excitation energy) yields $J^\pi = 0^+$, 1^+, 2^+ or 3^+. Since neither sum rule is close to exhaustion, the 2J+1 rule cannot be applied and, in any event, the strengths seem to be greatly fragmented. One cannot even distinguish the parity of the states populated only in (d,t). Below we discuss, in a little more detail, those levels which can be assigned tentative spins on the basis of their γ-ray decay modes.

The 842.7, 947.7 and 1722.6 keV levels owe their existence to the coincidence data alone. Their absence from the particle

spectra leaves their parities in limbo. A sequence of spins can be postulated for each of them:

- 842.7 keV level decays to 230 keV (4^+) and the ground state (5^+) and can have spins of 3, 4, 5 or 6.
- 947.7 keV level decays to 230 keV (4^+) and is fed by the 1243 keV (4^-) level. Can be assigned 3, 4, or 5. Its decay to the above 842.7 keV level places no further constraint.
- 1722.6 keV level decays to 293 keV (1^+) and probably to 3^+ also. Spin 2 would be preferred though it could also be 1 or 3 if the parity is even.

All the levels showing either pure or mixed $\ell_p = 0$ angular distributions have only two choices for their spins, i.e. 1^+ or 2^+, and this is indicated in Fig. 4.2. A definite 2^+ assignment can be made for the level at 1358.7 keV as it has $\ell_p = 0$ and decays to the 737.7 keV (2^-) and 823.4 (3^-) states. For the 1228.8 keV level, though 1^+ or 2^+ are equally good, one would like to favour 2^+ as it decays to the 116 keV (2^+) and 161 keV (3^+) levels.

4.4 The Energy Centroids

If, as our analysis of the data suggests, the levels of ^{138}La can be truly described as simple shell model states then the centroids of the states arising from particular configurations should bear close resemblance to the single particle states observed in the neighbouring odd-A nuclei. For the odd proton states we can best compare and contrast our measurements with ^{139}La which has a magic number of neutrons. In ^{137}La, with only two neutrons less, these states show considerable fragmentation.

The centroids for the various neutron-hole configurations should be analagous with the corresponding states in the N=81 nuclei ^{137}Ba or ^{139}Ce.

In Table 4.2 we present the results of such a comparison. Energies in the odd-A nuclei are taken from the most recent Nuclear Data Sheets. The values for ^{138}La, relative to the ground state in that nucleus, are calculated from the relevant spectroscopic strengths which were given in Tables 2.2 and 2.9. For more direct comparison, the centroids are also given relative to the centroid for the ground configuration $(\pi g_{7/2} \nu d_{3/2}^{-1})$. As one can see, the agreement is really quite satisfying. We have not seen all the strength due to the $(\pi d_{5/2} \nu d_{3/2}^{-1})$ and $(\pi s_{1/2} \nu d_{3/2}^{-1})$ configurations. However it is clear that their centroids must be at least close to or above 1800 keV which is not inconsistent with $1/2^+$ and $3/2^+$ excitations in ^{139}La.

4.5 Shell Model Calculations

At this stage we can confidently proclaim that the levels in ^{138}La, at least the low-lying ones, do appear to arise in a straight forward way from the configurations seen in the odd-A nuclei ^{137}Ba and ^{139}La. Since nuclei near a closed shell are well suited for shell model description, ^{138}La should provide an interesting testing ground to see how well simplified shell model calculations can agree with the observed properties of odd-odd nuclei.

Table 4.2

A Comparison of Energy Centroids in ^{138}La and its Odd-A Neighbours

Odd Proton			^{138}La		Odd Neutron		
	E_x(keV)					E_x(keV)	
Configuration	^{137}La	^{139}La	Configuration		Configuration	^{137}Ba	^{139}Ce
$\pi h_{11/2}$	1005	1418	$\pi h_{11/2}, \nu d_{3/2}^{-1}$	1462(1343)[a]			
			$\pi g_{7/2}, \nu h_{11/2}^{-1}$	987(868)	$\nu h_{11/2}^{-1}$	661	750
			$\pi g_{7/2}, \nu s_{1/2}^{-1}$	412(293)	$\nu s_{1/2}^{-1}$	281	254
$\pi d_{5/2}$	10	166	$\pi d_{5/2}, \nu d_{3/2}^{-1}$	322(203)			
$\pi g_{7/2}$	0	0	$\pi g_{7/2}, \nu d_{3/2}^{-1}$	119(0)	$\nu d_{3/2}^{-1}$	0	0

(a) Energies are given with respect to the ground state. The numbers in parentheses are relative to the centroid of the ground state group.

In section 1.1b we have already discussed the formalism of such calculations. The ingredients are a limited configuration space, the residual interaction and the single particle energies. Wildenthal (1969) has carried out extensive shell model calculations for the N=82 nuclei in the region A=136-145, using the modified surface delta interaction. He treated $^{132}_{50}Sn_{82}$ as an inert core with the extra x protons ($3 \leq x \leq 13$) being distributed in the $1g_{7/2}$ and $2d_{5/2}$ orbits. Excitation of a single proton into $2d_{3/2}$ or $3s_{1/2}$ was also included. Thus the model space consisted of four active shells. The strength of the interaction (only T=1 is involved) and the energy splitting between the different shells were adjusted to give a least squares fit for all the levels of known J^{π} in these nuclei. The monopole term B_1 and the absolute value of the $1g_{7/2}$ single particle energy were also adjusted to reproduce the ground state binding energies of the N=82 nuclei. The best values for A_1 and the $1g_{7/2}$-$2d_{5/2}$ energy splitting, thus obtained, were 383 and 520 keV respectively. Both the ordering of the low-lying levels and their spectroscopic factors compared favourably with the experimental observations. Though the calculations were not limited to the lowest seniority, the contributions of higher seniority were nominal and also the $2d_{3/2}$ and $3s_{1/2}$ shells play a minor role in the low-lying states.

The encouraging results obtained for the N=82 odd-even and even-even nuclei pave the way for a similar exercise in the odd-odd case. This undertaking should be least formidable for

nuclei with N = 82±1, as these can still be described in a limited model space. The energy levels in such nuclei will of course depend upon the parameters already mentioned and also on the relevant single particle energy splittings for the neutron. Most significant, however, is the fact that the p-n interaction brings in the T=0 matrix elements, to which the N=82 calculations are completely insensitive.

The N=83 odd-odd nucleus ^{140}La was the first one in this class of nuclei for which detailed experimental information became available (Kern *et al.* 1967). At that time, Struble (1967) used a quasi-particle model with a finite-range residual interaction to provide a theoretical interpretation of the low-lying levels. A large number of orbitals ($\pi 2d_{5/2}$, $\pi 1g_{7/2}$, $\pi 2d_{3/2}$, $\nu 2f_{7/2}$, $\nu 3p_{3/2}$ and $\nu 2f_{5/2}$) were included in the calculation. Heyde and Brussard (1968) favour the unified model in which the odd proton and neutron are placed in three orbitals ($\pi 2d_{5/2}$, $\pi 1g_{7/2}$ and $\nu 2f_{7/2}$) and coupled to a vibrating ^{138}Ba core. Both these calculations showed somewhat reasonable agreement with the experimental results.

More recently, Hussein (1973) and Macphail (1973) extended the application of the SDI type of interaction to a number of N=83 nuclei including ^{140}La, ^{142}Pr and ^{144}Pm which are now well studied experimentally. Macphail's calculations showed that the best fit is obtained if $A_o = A_1 = 0.383$ MeV. However the agreement between theory and experiment is far from perfect. The

calculations fail to predict the correct ground state spins for both ^{140}La and ^{142}Pr. Also the theoretical predictions for the J=1 states are in serious disagreement with the observed spectroscopic strengths for these states. In spite of these discrepancies the SDI calculations do possess the merit of providing so much qualitative agreement with so few free parameters (just two if $A_o = A_1$).

Helton *et al.* carried out extended SDI calculations for ^{138}La and ^{140}Pr after experimental data became available for these N=81 nuclei. The agreement for ^{140}Pr is not favourable since the calculation produces much more configuration mixing than is observed (Helton *et al.* 1973, Hussein *et al* 1974). On the other hand, the agreement for ^{138}La is really quite good. The ground state spin is correctly predicted, the spacing of the levels is approximately right and the calculated spectroscopic strengths for neutron pick-up are close to the observed ones. Unfortunately their choice of parameters is not evident in the paper and so it was not immediately possible to calculate the proton transfer spectroscopic strengths in order to make the comparison with our experimental results. Through the cooperation of one of the authors (J.B. Ball), their wave functions for ^{137}Ba and ^{138}La were finally obtained. The resulting (^{3}He,d) strengths are given in Table 4.3 together with the previously calculated (d,t) strengths and energies. The correspondence between the observed and calculated levels of a given spin has been chosen for best fit to the spectroscopic factors rather than the energies.

Table 4.3

Comparison of the Calculated and Observed Excitation Energies and Spectroscopic Strengths

J^π	Observed				Helton *et al.*				This Work			
	E_x (keV)	Spectroscopic Strengths $\ell_n=0$	$\ell_n=2$	$\ell_p=2$	E_x (keV)	Spectroscopic Strengths $\ell_n=0$	$\ell_n=2$	$\ell_p=2$	E_x (keV)	Spectroscopic Strengths $\ell_n=0$	$\ell_n=2$	$\ell_p=2$
5^+	0	0	1.18	0	0	0	1.38	0	47	0	1.37	0
3^+	73	0.26	0.45	0.13	37	0	0.71	0.27	89	<0.01	0.85	<0.01
2^+	116	0	0.33	0.24	12	0	0.48	0.23	0	0	0.62	0.01
3^+	161	0.03	0.03	0.84	157	0.17	0.12	0.90	15	<0.01	0.09	1.20
2^+	192	0	0.16	0.45	267	0	0.13	0.76	94	0	<0.01	0.86
4^+	230	0	0.85	0	125	0.02	0.98	0.21	135	0.01	1.08	0.05
1^+	293	0	0	0.65	246	0	0	0.62	204	0	0	0.52
3^+	413	0.26	<0.03	0	535	0.20	0	<0.01	710	0.84	0.02	<0.01
4^+	479	0.49	<0.03	0.77	271	0.32	0.13	1.09	147	<0.01	0.03	1.51
3^+	510	0.20	<0.01	0.89	237	0.57	0.05	0.30	683	<0.01	<0.01	<0.01
4^+	519	0.40	<0.01		373	0.79	0.01	0.53	673	1.18	0.10	<0.01
2^+	642	0	0	0	537	0.00	0.02	<0.01	709	0	<0.01	<0.01

The overall agr ment is still good but it does not justify the unusual parameters used in the calculations. These are given below:

$$E(\pi 2d_{5/2})-E(\pi 1g_{7/2}) = 460 \text{ keV}$$
$$E(\nu 2d_{3/2})-E(\nu 3s_{1/2}) = 250 \text{ keV}$$
$$A_1 \text{ (for p-p)} = 300 \text{ keV}$$
$$A_o \text{ (for p-n)} = 158 \text{ keV}$$
$$A_1 \text{ (for p-n)} = 40 \text{ keV} .$$

Dr. Ball informed us that the three strengths were adjusted for a best fit to the data available at the time, while A_1 (p-p) was kept close to the original value (383 keV) found by Wildenthal *et al.*. A proton-neutron pair interacts half the time in T=0 and half the time in T=1. In the spirit of the iso-spin formalism, the p-n T=1 interaction is intended to be the same as the p-p T=1 interaction. By violating that condition, they have undermined the theoretical significance of SDI and, at the same time, introduced another free parameter.

While awaiting the details of this previous calculation, we decided to carry out our own lowest seniority shell model calculations using the SDI residual interaction. The seven active protons, confined to the $1g_{7/2}$ and $2d_{5/2}$ orbits, were coupled to a neutron hole existing in either the $2d_{3/2}$ or $3s_{1/2}$ shell. Initially A_o and A_1 were both equal to 383 keV and the $d_{5/2}$-$g_{7/2}$ splitting was taken to be 520 keV, the Wildenthal *et al.* value. The observed $d_{3/2}$-$s_{1/2}$ separation varies from 255 keV in ^{139}Ce

to 289 in ^{135}Xe. In the calculation it was varied from 260 to 600 keV. The results were not encouraging at all. The lowest state is always 2^+ and the four states arising from the $s_{1/2}$ neutron hole are virtually unmixed and stay separated from the other group of states. A decrease in the $d_{3/2}$-$s_{1/2}$ splitting reduces the gap but fails to increase the separation between the 3^+ and 2^+ states which remain essentially degenerate. The value of A_o was then varied in an unsuccessful attempt to improve the situation. In Fig. 4.8 we present the results of these calculations along with the experimental findings for comparison. Variations in A_1 and the $g_{7/2}$-$d_{5/2}$ splitting were also investigated but the agreement with experiment remains poor. In Table 4.3, the spectroscopic factors are given for the case $A_1=A_o$ = 383 keV, $E(\pi 2d_{5/2})-E(\pi 1g_{7/2})$ = 520 keV and $E(\nu 2d_{3/2})-E(\nu 3s_{1/2})$ = 330 keV. These reflect the same lack of mixing that is observed in the energy spectrum.

It is hard to understand why the same SDI parameters that gave somewhat reasonable fits for N=83 nuclei prove to be such a total failure in the present case. On the other hand the calculation reported by Helton *et al*, as unconventional as it is, fares much better. This may occur only because of the extra parameter or it could indicate that there is a thus far unrecognized physical reason why the n-p interaction depends upon the orbitals involved. Perhaps the assumption in SDI that all the radial wave functions have the same value at the nuclear surface is seriously at fault. Certainly more test cases are needed to resolve the situation.

Fig. 4.8

SDI shell model calculations for ^{138}La.
The parameters are $A_1 = 383$,
$E(\pi 2d_{5/2}) - E(\pi 1g_{7/2}) = 520$ keV, and
$E(\nu 2d_{3/2}) - E(\nu 3s_{1/2}) = 540$ keV.

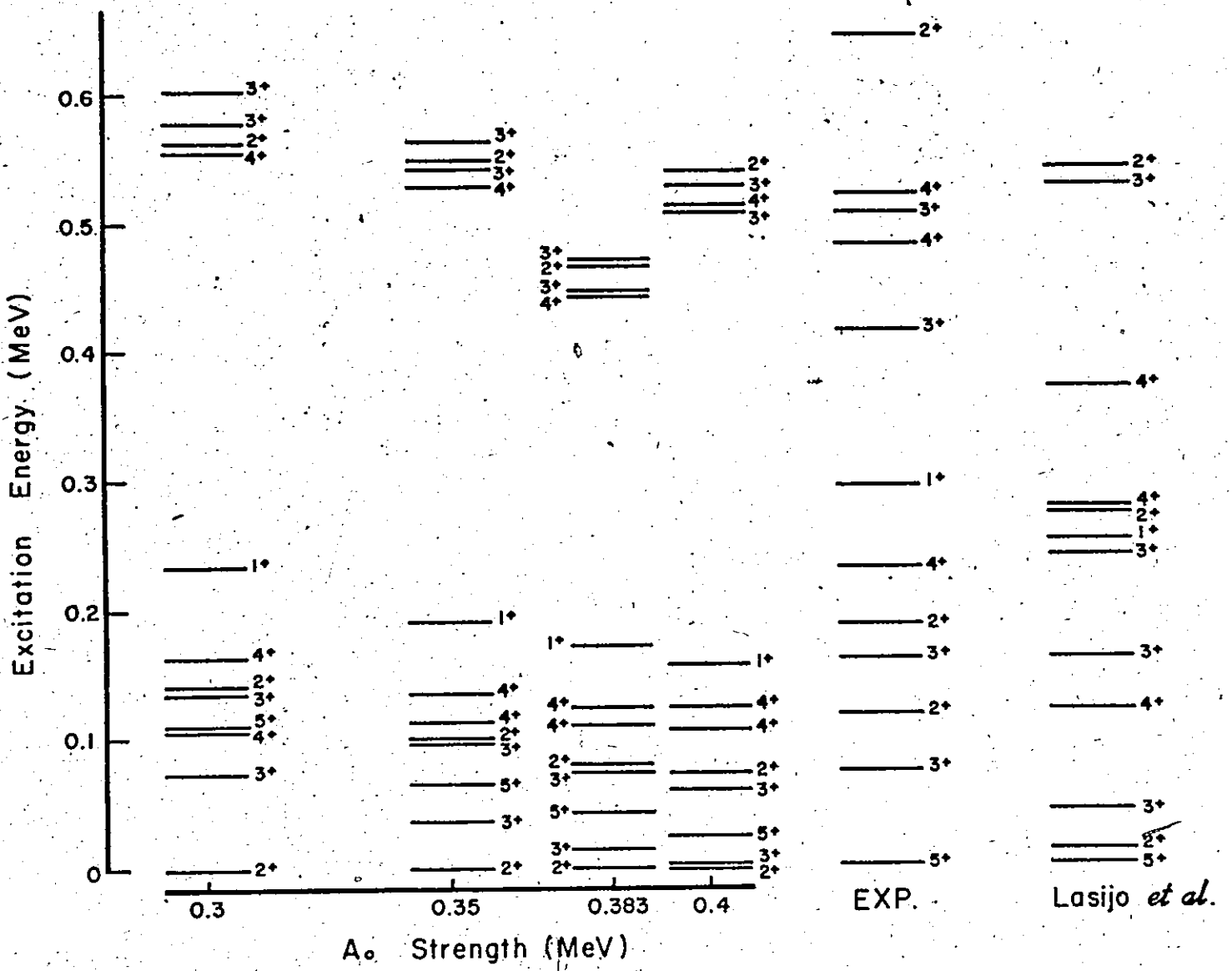
Excitation Energy (MeV)
0
0.1
0.2
0.3
0.4
0.5
0.6
0.3
0.35
0.383
0.4
A₀ Strength (MeV)
EXP.
Lasijo et al.

SUMMARY AND CONCLUSIONS

The particle transfer reactions $^{137}Ba(^{3}He,d)^{138}La$ and $^{139}La(d,t)$ have been used to identify 62 levels of ^{138}La up to an excitation of 1.8 MeV. Definite parity assignments are proposed for most of these levels. The information derived from particle spectroscopy has been complemented and extended with high resolution γ-ray studies employing the $^{138}Ba(p,n\gamma)^{138}La$ reaction. Both the singles spectra and γ-γ coincidences were investigated.

The nuclear structure of the 12 low-lying levels has been studied in great detail. These are found to be simple shell model states arising from the $(\pi 1g_{7/2}, \nu 2d_{3/2}^{-1})$, $(\pi 2d_{5/2}, \nu 2d_{3/2}^{-1})$, $(\pi 1g_{7/2}, \nu 3s_{1/2}^{-1})$ and $(\pi 2d_{5/2}, \nu 3s_{1/2}^{-1})$ configurations. The lifetime of the first excited state, measured by the n-γ delayed coincidence technique, comes out to be 116 ns. This represents a 3.6 times enhancement of the single particle estimate for an E2 transition of 72.6 keV and establishes the spin (3^+) of this level. The unambiguous spin assignments for the other levels in the group are based on the assumption that prompt transitions are predominantly M1 and supported by the spectroscopic strengths observed in proton and neutron transfer.

Parity assignments are proposed for most of the higher excited states observed in the proton transfer reaction. Two

negative parity groups have been positively identified in the (^{3}He,d) and (d,t) reactions. Tentative spin assignments are made for all these levels on the basis of the spectroscopic strengths. Some of these assignments are upheld by the coincidence data and are quite firm.

Further investigation is needed to extract more reliable information about the higher excited states of ^{138}La. It should be worthwhile to try reactions such as ^{134}Xe(^{7}Li,3nγ)^{138}La or ^{130}Te(^{11}B,3nγ)^{138}La to populate levels of high spins. The ratio of the γ-ray intensities in the two reactions can be advantageously used for spin assignments. Even the (p,nγ) reaction at higher beam energies might be useful. The present level scheme suggests the existence of an isomer at 836 keV. Since this $(8)^-$ state will have to decay to the ground state by an E3 transition, a measurement of its life time would verify or disprove the suggestion. An angular distribution of 576.4 keV, 738.7 keV and 85.7 keV γ-rays can be undertaken to establish the spins of 737.7 keV, 738.7 keV and 823.4 keV levels. The threshold for the (p,nγ) reaction is 2.57 MeV and one can run at $\sim$ 4 MeV without indirect feeding. The experiment is difficult as the yield is bound to be very low but at least for 2^- and 3^- states it might prove feasible.

Two general features of nuclear reactions, which are not entirely new, have been utilized as an alternative to more conventional but difficult methods for obtaining ℓ-assignments and spin information.

(i) The $(^3He,d)/(\alpha,t)$ cross-section ratio method has been applied to the odd-odd nucleus to infer ℓ-values of the levels populated in ^{138}La. The ratios for the levels of known J^π in ^{139}La provide the reference point for such an estimate.

(ii) The excitation functions of the γ-rays have been successfully employed for tentative spin assignments.

The investigation of ^{138}La has also produced some interesting results for the neighbouring nuclei. Though the $^{136,138}Ba(\alpha,t)^{137,139}La$ reactions were investigated in order to identify the impurity peaks in the ^{138}La spectrum, these also permit one to determine the Q-value of the $^{136}Ba(\alpha,t)^{137}La$ reaction with respect to the Q-value for $^{138}Ba(\alpha,t)^{139}La$. These precision values (uncertainty in the difference is ± 3 keV only) reveal the presence of an error in the A=138 and 139 data obtained from the most recent mass tabulation. It also allows one to determine the Q-value of the $^{136}Ba(\alpha,t)^{137}La$ reaction for which only an estimate from mass systematics was available earlier.

The other secondary data pertains to the nucleus ^{139}La, specifically to the $^{138}Ba(^3He,d)^{139}La$ reaction. In the course of the experiments carried out to determine the empirical ℓ-shapes the doublet at 1780 keV (Wildenthal *et al.* 1971) was resolved into two distinct levels at 1755 keV and 1786 keV. We were thus able to establish that these states are populated by $\ell_p = 2$ and 0 respectively.

A comparison between ^{138}La and ^{140}Pr, the only other N=81 nucleus studied in some detail, shows that these two nuclei, though similar in their gross features, are still quite different. The 12 low-lying levels in both these nuclei lie below an excitation of 650 keV. The states can be described in a simple shell model framework, and the levels prefer to decay by M1 transitions. The interval between the $\nu d_{3/2}^{-1}$ and $\nu s_{1/2}^{-1}$ energy centroids is also similar (212 keV in ^{140}Pr as compared to 293 keV in ^{138}La) but the addition of 2 protons in ^{140}Pr tends to depress the states. The same is true for the neutron-hole states of negative parity. The two nuclei show a noticeable difference in the amount of configuration mixing. It is interesting to note that in spite of smaller energy gaps the ^{140}Pr levels exhibit almost pure particle-hole configuration whereas the ^{138}La levels show a considerable amount of mixing.

A lowest seniority shell model calculation in a highly truncated space has also been performed using the SDI type of residual interaction. The results are very discouraging. The calculation fails to reproduce the mixing observed experimentally, which is also reflected in the calculated spectroscopic strengths. The spectroscopic factors for proton-transfer are also calculated using the wave-functions made available by Dr. J. Ball, a co-author with Helton *et al* (1973). The agreement is reasonable but the parameters used in their calculations are rather unconventional. As more data become available for N=81 nuclei, it

may be possible to hypothesize a phenomenological interaction by fitting the matrix elements as free parameters to the known energy levels.

TABLE A-1

DIFFRENTIAL CROSS-SECTIONS(COM) FOR 137BA(3HE,D)136LA AT E(LAB)=24MEV.

E (KEV)	10.0	15.0	20.0	22.5	25.0	30.0	32.5	35.0	37.5	40.0	55.0 *
.3 3.0	13 3	17 3	20 5	48 6	56 7	52 6	49 6	45 5	49 6	49 6	28 5
72.6 0.0	34 4	37 6	45 6	38 5	33 5	49 6	50 7	46 6	35 3	40 4	14 3
115.7 .8	66 12	70 8	64 8	57 7	65 6	66 7	96 10	69 6	70 2	70 6	47 6
160.9 .9	232 23	247 14	201 15	171 22	206 22	237 21	225 32	264 26	198 20	208 15	112 13
192.3 .9	104 14	128 12	100 8	95 8	116 12	128 12	129 13	132 10	114 8	108 10	72 7
230 2	2 1	3 1	14 3	13 3	14 5	8 3	13 3	13 3	9 6	17 3	9 3

(CONTINUED NEXT PAGE)

TABLE A-1 (CONTINUED)

E (KEV)	10.0	15.0	20.0	22.0	25.0	30.0	32.5	35.0	37.5	40.0	55.0
293.0 1.0	130 11	151 8	137 14	100 11	116 9	153 12	160 21	145 12	144 14	113 6	52 6
409.0 5.0	~1	2 1	4 2	7 4	7 5	2 2	3 2	3 2	2 2	2 1	~1
479.2 .5	145 12	167 16	147 11	115 11	167 10	168 12	196 19	166 13	145 10	113 6	65 9
517.9 .5	213 19	238 12	196 21	180 11	209 19	305 23	321 31	227 16	167 19	186 9	131 13
642 1	27 5	70 7	77 9	43 5	43 6	58 9	67 6	49 7	51 5	50 5	15 3
1057. 2.	17 3	58 6	60 8	34 8	30 9	56 8	53 7	55 6	42 7	39 5	19 3
1096. 2	***** *****	32 17	44 17	13 6	20 3	26 5	24 3	41 6	27 5	36 3	12 3

(CONTINUED NEXT PAGE)

TABLE A-1 (CONTINUED)

E (KEV)	10.0	15.0	20.0	22.0	25.0	30.0	32.5	35.0	37.5	40.0	55.0
1154	*****	38	42	16	38	53	29	53	29	43	16
2	*****	17	5	3	5	5	5	7	5	15	3
1178	*****	21	16	9	7	*****	15	13	*****	10	9
5	*****	5	3	7	5	*****	5	3	*****	3	3
1230	17	37	35	35	38	17	36	35	34	28	19
2	7	12	9	12	10	6	10	13	9	14	5
1243	9	*****	28	47	65	88	65	87	65	82	57
2	3	*****	13	5	7	10	13	10	10	11	8
1267	19	*****	34	41	59	89	77	70	65	89	55
1	6	*****	5	7	5	9	10	8	7	7	7
1360	17	*****	52	28	39	59	41	48	36	41	23
3	5	*****	6	5	6	7	14	7	6	5	5
1426	9	26	21	20	26	14	26	29	23	23	12
3	3	10	10	5	5	3	6	5	5	3	5

(CONTINUED NEXT PAGE)

TABLE A-1 (CONTINUED)

E (KEV)	10.0	15.0	20.0	22.0	25.0	30.0	32.5	35.0	37.5	40.0	55.0
1455.2	53 12	122 16	102 19	50 10	93 10	100 20	116 12	116 13	106 10	109 7	40 6
1532.2	7 3	19 7	41 16	16 3	27 5	28 5	28 5	26 3	24 3	24 3	10 3
1568.3	46 6	85 10	86 10	61 9	41 6	42 6	44 6	44 7	53 8	42 6	23 3
1580.3	10 3	17 3	42 7	59 7	75 8	92 12	96 12	93 9	86 10	84 9	55 7
1624.4	41 7	99 15	64 13	44 8	46 8	65 8	75 0	72 9	70 12	67 11	41 7
1645.2	21 7	14 3	49 14	48 9	82 16	99 14	111 10	93 10	90 15	97 7	83 9
1665.3	43 5	94 9	114 12	75 8	95 10	103 10	113 12	77 8	78 8	92 9	26 5

(CONTINUED NEXT PAGE)

TABLE A-1 (CONTINUED)

E (KEV)	10.0	15.0	20.0	22.0	25.0	30.0	32.5	35.0	37.5	40.0	55.0
1715	65	122	65	57	93	116	95	81	72	5.	45
4	27	14	27	23	23	20	17	13	13	9	14
1733	78	132	124	81	117	125	122	126	122	96	45
3	38	29	46	17	16	23	17	15	17	21	14
1757	29	35	30	26	21	35	32	32	35	29	24
4	6	7	6	6	5	7	6	6	7	6	5
1766	29	37	35	17	20	41	52	37	32	31	22
4	4	4	4	5	5	7	8	4	4	3	3

*ANGLES ARE GIVEN IN THE LAB SYSTEM.

NUMBERS IN THE SECOND ROW INDICATE UNCERTAINTIES.

***** MEANS THAT THE PEAK WAS OBLITERATED BY AN IMPURITY AT THIS ANGLE.

Table A-2

Observed Cross-sections at 45° for the Reaction $^{137}Ba(\alpha,t)^{138}La$ at 27 MeV

E_x (keV)	$d\sigma/d\Omega$ (μb/sr)
0	68(6)
72.6	40(2)
116.2	53(3)
161.3	109(6)
192.4	59(4)
230.8	37(3)
292.9	52(3)
409	4(1)
479.1*	63(4)
518.1	79(6)
641	9(1)
1058	3(1)
1160	5(1)
1243	82(6)
1268	104(7)
1360	∿4(1)
1426	∿2(1)
1456	5(2)
1530	3(1)
1565	∿5(3)
1579	78(21)
1624	3(1)
1644	90(10)
1686	5(2)
1713	7(2)
1728	5(2)
1755	3(1)
1786	3(1)

Table A-3

Observed Cross-sections for $^{139}La(d,t)^{138}La$ Reaction at 16 MeV

E_x(keV)	$d\sigma/d\Omega$* (μb/sr)	E_x(keV)	$d\sigma/d\Omega$* (μb/sr)
0	874(10)	1200	37(3)
72.0	766(23)	1228	19(7)
115.3	259(10)	1255	80(7)
160.4	80(10)	1302	21(2)
192.0	127(5)	1344	9(2)
229.6	644(15)	1375	19(2)
412.5	554(15)	1386	26(3)
478.4	872(23)	1425	13(2)
508.2	426(17)	1466	30(5)
517.0	640(26)	1490	13(3)
737	24(2)	1520	9(2)
823	28(2)	1545	88(8)
836	41(4)	1571	15(3)
888	5(2)	1583	13(2)
900	19(3)	1599	40(3)
929	7(5)	1646	72(9)
937	32(9)	1656	95(7)
962	38(4)	1676	18(3)
1033	11(2)	1690	22(2)
1067	43(3)	1707	20(3)
1095	12(3)	1726	
1102	27(3)	1739	
1150	18(8)	1783	
1155	18(8)		

*For states up to 518 keV excitation the cross-sections are quoted at θ = 25°. The data taken at 55° are presented for the rest of the levels.

REFERENCES

Agarwal, Y.K., Baba, C.K. and Bhattacherjee, S.K. 1964. Nucl. Phys. 58, 641.

Aniol, K. 1973. M.Sc. Thesis, McMaster University

Austern, N. 1970. "Direct Nuclear Reaction Theories". New Wiley Interscience series.

Bäcklin, A. and Malmskog, S.G. 1967, Arkiv Fysik 34, 531.

Bertsch, F.G. 1972. "The Practioner's Shell Model". North Holland Publishing Company.

Bohr, A. 1952. Kgl. Danske. Videnskab Selskab, Mat-Fys. Medd. 26, 14.

Bohr, A. and Mottelson, B.R. 1952. Kgl Dansker Videnskab Selskab, Mat-Fys. Medd. 25, 14.

Bouley, A.C. and Graetzer, R. 1969. Intern. Conf. Properties of Nuclear States, Montreal, Canada, 106.

Brown, G.E. 1972. "Many Body Problems" Amsterdam, North Holland Publishing Company.

Burde, J., Rakavy, M. and Adam, G. 1965. Nucl. Phys. 68, 561.

Burke, D.G. and Waddington, J.C. 1972. Nucl. Phys. A193, 271.

Cage, M.E., Cole, A.J. and Pyle, G.J. 1973. Nucl. Phys. A201,418.

Cairns, J.E. 1972. M. Sc. Thesis. McMaster University.

Carlson, G.H. and Talbert Jr., W.L. 1972. Bull. Am. Phys. Soc. 17, 898.

Chaumeaux, A., Burge, G., Faraggi, H. and Picard, J. 1971. Nucl. Phys. A164, 176.

Cook, W.B., Waddington, J.C., Burke, D.G. and Nelson, D.E. 1973. Can. J. Phys. 51, 1978.

de-Shalit A. and Talmi, I. 1963. "Nuclear Shell Theory". Academic Press.

DuBard, J.L., Sheline, R.K. and Ball, J.B. 1971. Phys. Rev. C-3, 1391.

Ellis, J.L. and Hall, H.E. Jr. 1970. Bull. Am. Phys. Soc. 15, 1670.

Feshbach, H., Porter, C., and Weisskopf, V.F. 1954, Phys. Rev. 96, 448.

French, J.B., Halbert, E.U., McGrory, J.B. and Wong, S.S.M. 1969. Advances in Nucl. Phys. 3, 193.

Fulmer, R.H., McCarthy, A.L. and Cohen, B.L. 1962. Phys. Rev. 128, 1302.

Funke, L., Fromm, W.D. and Keller, H.J. 1973. Proceedings of International Conference on Nuclear Physics, Munich. North Holland.

Furukawa, M. 1967. Nucl. Phys. A-90, 253.

Geiger, J.S., Graham, R.L. and Ewan, G.T. 1961. Bull. Am. Phys. Soc. 6, 71.

Geiger, J.S., Graham, R.L., Bergstörm, I. and Brown, F. 1965. Nucl. Phys. 68, 352.

Glaudemans, P.W.M., Weichera, G. and Brussard, P.J. 1964. Nucl. Phys. 56, 529.

Glaudemans, P.W.M., Brussard, P.J. and Wildenthal, B.H. 1967. Nucl. Phys. A102, 593.

Gove, N.B. and Wapstra, A.H. 1971. Nucl. Data Tables 9, 265.

_____ 1972. Nucl. Data Tables 11, 127.

Green, I.M. and Moszkowski, S.A. 1965. Phys. Rev. 139, B790.

Greenwood, R.C., Helmer, R.G., Gehrke, R.J. 1970. Nucl. Instr. and Meth. 77, 141.

Guile, J., Goles, R.W., Morgan, C.B., Warner, R.A., McHarris, W.C. and Kelly, W.H. 1973. Bull. Am. Phys. Soc. 18, 99.

Halbert, E.C., McGrory, J.B., Wildenthal, B.H. and Pandya, S.P. 1971. Advances in Nucl. Phys. 4, 315.

Haxel, O., Jensen, J.H.D. and Suess, H.E. 1949. Phys. Rev. 75, 1766.

Helton, V.D., Hiebert, J.C. and Ball, J.B. 1973. Nucl. Phys. A201, 225.

Heyde, K. and Brussard, P.J. 1968. Nucl. Phys. A112, 494.

Hill, J.C. and Widenbeck, M. L. 1968. Nucl. Phys. A119, 53.

Horsch, F. 1970. Proc. Int. Conf. PRop. Nuclei Far from Region of Stability. CERN-70-30.

Hussein, S.G., Sanderson, N.E. and Summers-Gill, R.G. 1973. Nucl. Phys. A219, 407.

Ishimatsu, T., Ohumra, H., Awaya, T., Nakagawa, T., Orihara, H. and Yagi, K. 1969. J. Phys. Soc. Japan 27, 504.

Jackson, D.F. 1970. "Nuclear Reactions". Nederlands Boekdruk Industre N.V.

Jolly, R.K. and Kashy, E. 1971. Phys. Rev. C4, 887, 1398.

Jurney, E.T., Sheline, R.K., Shera, E.B., Koch, H.R., Mair, B.P.K., Gruber, U., Baader, H., Breitig, D., Schult, O.W.B., Kern, J. and Struble, G.L. 1970. Phys. Rev. C2, 2323.

Kern, J., Struble, G.L. and Sheline, R.K. 1967. Phys. Rev. 153, 1331.

Krehbial, H., 1964. Phys.Lett. 13, 65.

Kuo, T.T.S. and Brown, G.E. 1966. Nucl. Phys. 85, 40.

_____ 1967, Nucl. Phys. A103, 71.

Lane, A.M. 1967. "Nuclear Reaction Theory". A.N.U. Monograph.

Lasijo, R., Sheline, R.K., Griffin, R.D. and DuBard, J.L. 1972. Z. Physik 17, 253.

Lederer, C.M., Hollander, J.M. and Perlman, I. 1968. "Table of Isotopes". Wiley and Sons.

Lu, M.T. and Alford, W.P. 1971. Phys. Rev. C3, 1243.

Lucas Jr., G.R., Martin, P., Miller, G.H., Welsh, R.E., Jenkins, D.A., Powers, R.J. and Kunselmen, A.R. 1973. Phys. Rev. C7, 1678.

Macphail, M.R. 1973. Ph.D. Thesis, McMaster University.

Macfarlane, M.H. and French, J.B. 1960. Rev. Mod. Phys. 32, 567.

McIssac, L.D., 1972. ANCR. 387.

Mayer, M.G., 1949. Phys. Rev. 75, 1969.

Monnad, E., Brissot, R., Carray, L.C., Crancen, J., Ristori, C., Schussless, G. and Moussa, A. 1972. Nucl. Phys. A 195, 1972.

Northcliff, L.C. and Schilling, R.F. 1970. Nucl. Data Tables A7, 253.

Norton, G.A., Gearhart, N.L., Hausman, H.J., Morgan, J.F. and Sinclair, J.W.D. 1973. Bull. Am. Phys. Soc. 18, 656.

O'Neil, R.A. 1972. Ph.D. Thesis, McMaster University

Pandya, S.P. 1956. Phys. Rev. 103, 956.

Perey, C.M. and Perey, F.G. 1963. Phys. Rev. 132, 755.

Preston, M.A. 1962. "Physics of the Nucleus", Addison Wesley Publishing Co.

Robertson, R.G.H. 1971. Ph.D. Thesis, McMaster Univ.

Robertson, R.G.H. and Summers-Gill, R.G. 1971. Can. J. Phys. 49, 1186.

Robson, B.A. 1969. "An Introduction to Scattering Theory and Direct Reaction". ANI Monograph.

Rose, M.E., 1965, "Alpha, Beta and Gamma-ray Spectroscopy", ed. K. Siegbahn, North Holland, Amsterdam, 887.

Satchler, G.R. 1966. "Lectures in Theoretical Physics", Vol. VIII C. ed. Kunz, P.D., Lind, D.A. and Britton, W.T., Univ. of Colorado Press, Boulder, 73.

Schmidt, T. 1937. Z. Physik, 106, 358.

Sogo, P.B. and Jeffries, C.D. 1955. Phys. Rev. 99, 613.

Storm, E. and Israel, H.T. 1970. Nucl. Data Tables A7, 565.

Struble, G.L. 1967. Phys. Rev. 153, 147.

Talmi, I. 1962. Rev. Mod. Phys. 34, 704.

Taylor, T. 1974. Ph.D. Thesis, McMaster Univ.

Van-der-Merwe, P., Van Heerden, I.J., McMurray, W.R. and Malam J.G. 1969. Nucl. Phys. A124, 433.

Wapstra, A.H., Nijgh, G.J. and Liesband, R. 1969. "Nucl. Spectroscopy Tables". North Holland Publishing Co., Amsterdam.

White, D.H., Birkett, R.E. and Thomson, T. 1970. Nucl.Inst. and Meth. 77, 261.

Wildenthal, B.H. 1969. Phys. Rev. Lett. 22, 1118.

Wildenthal, B.H., Newman, E. and Auble, R.L. 1971. Phys. Rev. C-3, 1199.

Yoshida, S. and Zamick, L. 1972. Ann. Rev. Nucl. Sci. 22, 121.